ENTROPIC TRAPPING AND POLYMER DYNAMICS IN STATIC, QUASI-PERIODIC ARRAYS OF OBSTACLES IN TWO DIMENSIONAL MEDIA

by

Grant Ian Nixon

A thesis
presented to the University of Ottawa
in fulfillment of the
thesis requirement for the degree of

Doctor of Philosophy
in
Physics

Ottawa, Ontario, Canada, 2003

ProQuest LLC.
789 East Eisenhower Parkway
P.O. Box 1346
Ann Arbor, MI 48106 - 1346

Borrower's Page

The University of Ottawa requires the signatures of all persons using or photocopying this thesis. Please sign below, and provide an address and date.

Acknowledgements

I would like to take this opportunity to express my sincere gratitude to my research supervisor, Dr. Gary W. Slater, for his support, guidance, and example throughout the course of this research.

I would also like to thank the physics graduate students for the many fond memories. Special thanks to Drs. Béla Joős, Emery Fortin, and Brian Logan for the many courtesies extended to me during my graduate studies. To Gary's macromolecular physics group, I wish to thank you all for making academic life so pleasant.

To my wife Dee, I extend my deepest thanks for her continued love, friendship, and support through times thick and thin. I also wish to thank my parents-in-law, Harold and Rita Gregory, for their unwavering support. Lastly, I wish to dedicate this thesis to Katherine Elizabeth Nixon, who I am privileged to have as a daughter: you are most deeply loved.

Fortitudine Vincimus

Publications and Conference Presentations during the Ph.D.

Publications

- Nixon, G. I. and Slater, G. W. 2003, Saturation and entropic trapping of polydisperse polymers in porous media, *J. Chem. Phys.* (to be submitted)
- Nixon, G. I. and Slater, G. W. 2002, Saturation and entropic trapping of monodisperse polymers in porous media, *J, Chem. Phys.* 117(8), 4042-4046.
- Nixon, G. I., Slater, G. W. 1999, The relaxation length of a polymer chain in a quenched disordered medium, *Phys. Rev. E* 60(3), 3170-3173.
- Slater, G. W., Nixon, G. I. 1998. The Size of a polymer chain in an imperfect array of obstacles: Monte Carlo results. *J.Chem.Phys.* 108, 3310-3312.
- Slater, G. W., Nixon, G. I. 1997. Polymer Dynamics in Random Media. Physics in Canada Sept./Oct. Issue, 177-183.
- Slater, G. W., Guo, H. L., Nixon, G. I. 1997. Bidirectional Transport of Polyelectrolytes Using Self-Modulating Entropic Ratchets, *Phys.Rev. Lett.* 78, 1170-1173.
- Nixon, G. I. and Slater 1996, G. W., Entropic trapping and electrophoretic drift of a polyelectrolyte down a channel with a periodically oscillating width, *Phys. Rev. E* 53(5), 4969-4980.

Oral Presentations

- Nixon, G. I., A cursory survey of applied radiation physics at MDS Nordion, Oral Presentation at the Ottawa Medical Physics Institute (OMPI) Physics Seminar Series, Carleton University, Ottawa, January 21, 2002.
- Slater, G. W., and Nixon, G. I., Entropic Trapping at Finite Polymer Concentrations, Oral Presentation at the Meeting of the American Physical Society, Centennial Meeting Program, Atlanta, GA., March 24, 1999.
- Nixon, G. I. and Slater, G. W., Conformational Relaxation of Polymers in Quenched Disordered Media, Oral presentation at the Annual Congress of the Canadian Association of Physicists (CAP), Waterloo, June, 1998.
- Nixon, G. I. and Slater, G. W., Entropic trapping of Polymers in Disordered Systems, Oral Presentation at the Ottawa-Carleton Institute of Physics (OCPI) Graduate Student Seminar Series, Carleton University, Ottawa, May 1996.

Poster Sessions

- Slater, G. W., and Nixon, G. I., Diffusion and Relaxation of a Polymer Chain in a Disordered Medium, Poster presentation at the XXth IUPAP International conference on Statistical Physics (StatPhys20), Paris, July, 1998.

Preface

The selection of material to be included in the thesis concerns the dynamics of linear polymer chains diffusing inside systems characterized by fixed random disorder. Particular attention was devoted to the issue of the phenomenon of entropic trapping, which characterizes many such systems. As the objective was to render a cohesive document, in accordance with this objective, some results, of a somewhat disjointed nature (i.e., those involving electric fields), have been excluded. In particular, we omitted those studies on electrophoretic entropic trapping (Nixon and Slater 1996) which made use of the Brownian dynamics algorithm developed by the author during his M.Sc. degree (Nixon 1994). Similarly, the topic of a later collaborative study (Slater, Guo, and Nixon 1997) on entropic ratchets was also omitted.

The subject of polymer dynamics in disordered systems is truly multi-faceted. One cannot help but be struck with the sober realization that there is a rather large pool of important works, in various research domains, whose direct pertinence is not fully appreciated. In this regard, some references have been made to some conclusions derived using state-of-the-art theoretical physics at the frontiers of modern research. Fully appreciating the significance of such works often requires a high level of specialization in the field of theoretical statistical mechanics of disordered systems. Such sophisticated "machinery" of theoretical physics falls beyond the scope of this largely "experimental" work. Yet, this does not necessarily preclude the use of such works when they can be brought to bear on a problem. It is hoped that this philosophy will not detract from the main thrust of the thesis.

Although much effort went into citing relevant works and in putting these within the context of the work at hand, serious omissions are inevitable, particularly so in areas outside one's domain of expertise. Yet, it is sincerely hoped that the approach taken will provide a useful compendium, provoke some interest, build upon the current understanding, and possibly serve to stimulate further investigation into the nature of disordered polymeric systems.

Summary

Using the bond fluctuation algorithm of Carmesin and Kremer (Carmesin and Kremer 1988), we investigate the static and dynamic properties of self-avoiding linear polymers embedded in static, two-dimensional (d=2), quasi-periodic arrays of obstacles with entropic traps.

The phenomenon of polymer collapse, the closely related enrichment and depletion of polymer configurations, the conformational relaxation, and the diffusive behaviour are all investigated within the framework of the lattice Monte Carlo method. Several distinct dynamical regimes are encountered: the (obstacle-free) Rouse-like regime (obstacle sub-array concentration c=0), the reptation regime for chains in perfectly periodic obstacle sub-arrays (c=1), and, in the presence of disorder and entropic traps (0<c<1), the anomalous regimes where the scaling properties differ from those predicted by the Rouse and reptation theories.

Prior to the onset of normal diffusion, even systems characterized by very slight disorder (i.e., the existence of random isolated void spaces) are shown to lead to long, transient, subdiffusive regimes where the mean square displacement of the centre of mass scales as $R_{CM}^2 \sim D^* t^\beta$ where $0.5<\beta<1$ is the anomalous diffusion exponent and D^* is the anomalous diffusion coefficient.

In such disordered systems, conformational relaxation is shown to be coupled with centre of mass subdiffusion, resulting in long, time-stretched, exponential relaxation of the Rouse coordinates, viz. $\exp[-(t/\tau)^\alpha]$. The stretching exponents $0.5<\alpha<1$ are shown to be closely related to the anomalous diffusion exponents β and where the α, for a given chain, are shown to decrease with increasing mode number and with strong disorder.

The molecular size–dependence of the steady-state diffusion coefficient, as well as that of the conformational relaxation time, is shown to be greatest when the concentration of obstacles is large and when that of the voids is non-vanishing ($c \lesssim 1$). Thus, the dynamical scaling in entropic trapping systems is non-monotonic with respect to the concentration of obstacles. Polymer reptation dynamics thus appears to be intrinsically unstable with respect to static disordered systems of obstacles.

Having demonstrated the coupling of centre of mass subdiffusion and conformational relaxation, we introduce a new relaxation length scale, $\lambda=(2dD^* t^\alpha)^{1/2}$, that is more appropriate for characterizing disordered systems than is the ubiquitous radius of gyration used in both the Rouse and reptation

theories. However, λ could not be distinguished from the radius of gyration in terms of the molecular size scaling given the uncertainty in our data.

Finally, having proposed a theoretical dynamic model of entropic trapping for dilute polymer solutions in embedded mesoscopic voids, we investigate the effect of polymer solution concentration on the dynamics for both monodisperse and polydisperse polymer solutions. New, unexplored dynamical behaviours are manifest as the conformational and translational entropies compete to minimize the system free energy.

Table of Contents

List of Figures

List of Tables

Chapter 1
Introduction to the literature and to our model system

1.1 Introduction

The science of macromolecules has played a prominent role in chemical technology, biology, physics, and engineering for well over half a century (de Gennes 1990). But for all their rich properties, however, the physical description of the molecules is often given in simple form. Consider the random walk (RW) model. This construct of a featureless line object most economically characterizes the basic conformational features of linear polymer chains. As such, the RW chain is often invoked as a minimal model for linear polymer chains. The microscopic physics (details of the chemical structure, side group, backbone composition, etc.) are subsumed into as few *phenomenological* parameters or constraints, as possible [see, e.g., (Flory 1969)]. The classical Rouse model, which describes polymer chain dynamics with localized interactions, is based entirely on the idea of a RW chain, which is composed of nearest-neighbour-coupled oscillators undergoing Brownian motion in a heat bath (Doi 1986). The Rouse model is important not only in its own right as a tractable mathematical description forming the basis of the dynamics of dilute polymer solutions [for recent experimental relevance of the Rouse model, see, e.g., (Lee and Loring 2001)], but also as a stepping stone towards another highly-successful model description of the mean-field type for polymer dynamics in highly-concentrated solutions (e.g., melts): the reptation model. Moreover, the Rouse model also applies in the case of an un-entangled melt of polymer chains where hydrodynamic and excluded volume effects may also be ignored.

As alluded to, polymer chains can thus be thought of as being made up of a great many molecular segments whose spatial directions are statistically uncorrelated in space[1]. The large size of macromolecules enables a statistical description, encapsulating the microscopic details, and achieving a macroscopic theory of the global properties. An all-encompassing polymer model, however, remains elusive, and is likely to remain so for a variety of reasons.

The effect of excluded volume (EV) interactions on the dynamic properties of polymer chains is known to be particularly difficult to treat analytically (Kranbuehl, Eichinger et al. 1991). The steric

[1] The minimum such statistical length is known as the Kuhn segment length.

repulsive interactions between chain segments, which act as hard-core EV "beads", lead to chain dimension expansion as well as to the lengthening of relaxation times. The EV effect also requires that a topological constraint, known as chain connectivity (CC) (de Gennes 1979), prevent the chain backbone from passing through any other part of the chain (or other parts of the system). This is also known as the entanglement effect. Therefore, topological constraints can seriously affect the dynamical properties. A polymer melt is a perfect example of a highly entangled polymer system for which the topological constraints strongly affect the dynamics (e.g., we may compare the reptation theory of melts with the Rouse dynamical model).

Of course, the true physical properties of polymers depend also on the solvent, the environment, the temperature, and the polymer concentration. For the discussions contained herein, we focus on the dynamics of polymer chains in "good-solvents". Solvents that dissolve polymers over a broad range of temperatures, while remaining chemically neutral, are deemed "good" solvents. In a good solvent, the polymer segments are (sterically) self-avoiding. In particular, real chains in good solvents have the same universal features as self-avoiding-walks (SAWs) on a lattice [p. 43 of (de Gennes 1979)]. For a given good-solvent solution, we may loosely classify the solution density according to three regimes: dilute, semidilute, and concentrated.

In a dilute solution, the concentration is sufficiently low to allow polymers to be separated with negligible polymer-polymer interaction, each polymer occupying its own spatial region, which may be characterized by its end-to-end distance and its radius of gyration. A simplified dynamical model, known as the Rouse model, applies in dilute solution if one ignores EV, CC, and hydrodynamic interactions. In the dilute regime, polymer solutions are also expected to fractionate according to molecular weight (size) when placed inside porous media where the mean pore size is comparable with the radius of gyration of the chains. As first shown by Casassa (Casassa 1967), the conformational entropy loss associated with the confinement of polymer chains is such that the longer chains will be preferentially excluded from pores because of the larger entropic cost associated with their confinement. Dilute solutions are thus important in the characterization of polymers such as in determining their molecular weight (or size).

In the semidilute regime, the polymer concentration has increased to the point where polymer coils begin to overlap while still occupying a small volume fraction. Several mechanical properties become quite conspicuous above the overlap concentration, notably the viscosity of polymer solutions increases steeply with molecular size. Similarly, in response to external forces, polymeric liquids

(e.g., melts) exhibit elasticity with a restoring force that decreases with time as molecular conformations relax. In fact, the relaxation time of molecular conformations is a strong function of M, the polymer's molecular weight (Doi and Edwards 1986). According to experimental data, in the melt (or in the case of a highly-entangled semidilute solution), the characteristic relaxation time τ_R for elastic behaviour, as well as the viscosity η, scale (in 3 dimensional physical space) as $\tau_D \sim \eta \sim M^{m_\eta} \approx M^{3.4}$ at constant solution concentration, irrespective of temperature, solvent, and molecular species for linear flexible polymer chains.

For sufficiently large concentrations, the solution is deemed a "concentrated" solution and mathematical treatment using mean field theory becomes possible[2] for thermodynamic properties. In particular, a polymer melt represents the high concentration limit with a zero volume fraction for the solvent. Flory was the first to conjecture that the conformation of polymers in concentrated solutions and melts become *ideal* or Gaussian (Doi and Edwards 1986). In the highly entangled state (concentrated solution regime), the dynamical description reverts to that of a random walk (RW) chain whose topological constraints (i.e., the entanglements) confine the chain's motion within an effective "tube". The chain may then be redefined in terms of a *primitive chain* or one that follows the shortest curvilinear tube-like pathway connecting the two ends of the chain. The "tube concept", first proposed by Edwards for the problem of rubbers, forms the basis for the dynamics of chains in a network, as first derived by de Gennes, and which has proven to be quite successful in explaining the dynamical properties of entangled polymers. This dynamical model is known as the reptation model, after the Latin *reptare*, to creep (Doi and Edwards 1986). The reptation model is built upon the foundation of the Rouse model through the addition of constraints to the polymer motion and, in the end, essentially provides a mean-field description of the dynamics of polymer melts.

It is to be noted, however, that reptation was originally developed with the concept of a single chain migrating in a network of fixed, or frozen, points (e.g., cross-links or fixed obstacles) and, as such, is only believed to be rigorously correct for the case of a fixed system of obstacles. It remains a matter of debate whether or not the reptation concept holds for semi-dilute or concentrated polymer solutions or melts (Doi and Edwards 1986).

Arguably, it is also debatable whether the reptation concept, as developed in the case of melts, holds in the case of fixed systems of obstacles. Fixed obstacles are required for a fixed reptation tube.

[2] This situation pertains to the highly-entangled semi-dilute case as well.

However, as revealed in computer simulations such as ours, fixed obstacles do not lead to self-excluded-volume (SEV) screening for the chains, as they would in a melt (whose entanglements are "obstacles" of finite lifespan). Moreover, as we will also show, even slight disorder, in an otherwise perfectly periodic system, is enough to ruin the reptation picture. The reptation concept has been touted to be "rigorously correct" in the case of a single chain in a fixed obstacle network and self-consistent[3] in the highly entangled state (e.g., a concentrated polymer solution or even a melt) of topologically interacting chains (Doi and Edwards 1986).

The behaviour of EV polymer chains in random media controls a wide variety of phenomena and is relevant to experimental situations such as filtration, gel permeation or exclusion chromatography, and the transport of polymers through microporous membranes. For decades, the problem of disorder and disordered systems has been one of the hottest topics in condensed matter physics and statistical mechanics.

There has also been considerable interest in the dynamics of SAW polymers in random lattices. Many analogies have been made between a Gaussian chain in a random environment and an electron in a disordered medium. In the latter case, electron localization is known to occur, regardless the strength of the disorder [see (de Gennes 1978) and (de Gennes 1979)]. Similarly, Sommer and Blumen investigated the localization effects of ($M\rightarrow\infty$) polymers in periodic and aperiodic potentials by using an attractive 1D Kronig-Penney model (Sommer and Blumen 1996). They found that a low number of isolated defect sites of the periodic structure might localize polymers.

The early mean-field theory (MFT) approaches, as exemplified by the pioneering works of Flory (Flory 1953; Flory 1969; de Gennes 1979) have made, and continue to make, valuable contributions to our understanding of polymer properties and have helped elucidate some of the power law scaling forms, such as simple conformation molecular size scaling of the Flory type (Pereira 1996). More recently, de Gennes' scaling theories (de Gennes 1979) have provided deeper insight into ensemble averages of polymers (in the thermodynamic limit) and the associated critical exponents.

But despite great strides, the statistical mechanics of polymers with intrinsic disorder, such as chains in fixed porous media, remains ill understood (Baumgärtner and Muthukumar 1996). The

[3] The description of the single-chain dynamics occurs in an effective medium that includes the effects of the other chains. The properties of the effective medium are then determined self-consistently from that of the single chain.

physical and mathematical ideas are often obscured by technical details and, often, by general disagreement among the experts.

1.2 Simulation models and methods

One highly effective means for simulating and studying the static and dynamic properties of polymeric systems is through the application of Monte Carlo (MC) algorithms. In particular, efficient lattice MC methods have enjoyed considerable success because they are readily amenable to the introduction of EV and CC (self-entanglement) effects.

As in the case of analytical models, however, to render as simple a system as possible, some potentially important physical effects may be neglected; in this regard, hydrodynamic interactions being the most noteworthy (except when screened, as in a gel). It is known that the motion of chain elements through the surrounding solvent induce velocity-dependent forces upon other chain elements. Models which ignore hydrodynamic interactions are referred to as *free-draining* systems.

It is important to realize that the method by which polymer motions are implemented in a model may affect the rate of conformational relaxation and, consequently, the dynamic properties as a whole. Care is required in the implementation of any model in order to ensure that the system is ergodic or at least to ensure that those regions of phase space, which are inaccessible, have negligible contribution to the properties of interest. There are no general rules governing the manifestation of ergodicity breaking, a possible artifact of the particulars of the algorithm (Binder 1988).

Various simulation approaches have appeared over the years, including a very early bead-stick model (VS) developed by Verdier and Stockmayer (Verdier and Stockmayer 1962). It took many years before the inherent difficulties of the VS model were sorted out. Successive studies yielded conflicting results, raising concerns about the possibility of anomalous effects due to lattice constraints and the particular choice of bead movement rules (Hilhorst and Deutch 1975; Naghizadeh and Kovac 1985; Verdier and Kranbuehl 1987; Crabb, Hoffman Jr. et al. 1988). In particular, the problem of the proper definition of the time scale in Monte Carlo simulations has been a topic of intense debate (Downey, Crabb et al. 1986; Kranbuehl, Eichinger et al. 1991). Also, the appropriateness of choosing move types on a contingent basis (i.e., by attempting one type of move if the other is found to be blocked), for example, as exemplified by the models employed by Kovac et al., has been questioned by some (Romiszowski and Stockmayer 1984) on the grounds that such moves could distort the time scale. Kranbuehl et al. (Verdier and Kranbuehl 1987; Kranbuehl,

Eichinger et al. 1991) have concluded that the dynamical behaviour depends upon the bead movement rules chosen and also the presence or absence of a lattice but is essentially independent of type of lattice, or lattice coordination number. In particular, they claim that the selection of bead movement rules predetermines the effect of excluded volume on the time scale. These claims are contrary to those made in earlier studies that advocated the use of certain lattice models over others (Downey, Crabb et al. 1986; Crabb, Hoffman Jr. et al. 1988). The off-lattice model known as the "pearl-necklace model" exemplifies a particularly straightforward implementation of EV effects. This model is an adaptation of the bead-stick model in which bead diameter is adjusted above a certain fraction of the stick length [e.g., at least $\sqrt{(3)}/2$ in 3D]. This choice automatically prevents illegal moves such as chain crossing (Kranbuehl and Verdier 1996).

But of the many Monte Carlo models for lattice chains with excluded volume in existence, one has gained particular prominence: the bond fluctuation algorithm (BFA) of Carmesin and Kremer (Carmesin and Kremer 1988). Whereas some models employ contingent rules that can distort the time scale, the BFA has the advantage of yielding the correct Rouse dynamical behaviour, even in 2D where EV (and CC) effects are very strong. Moreover, the model is also ergodic. Consequently, the BFA has enjoyed widespread use since its inception and we have made extensive use of our own implementations of this model throughout.

1.3 Entropic trapping and disordered systems

Within the last fifteen years, the phenomenon of entropic trapping has emerged onto the scene as a particularly active area of research within the broader context of disordered polymer systems. Muthukumar and Baumgärtner (Baumgärtner and Muthukumar 1987; Baumgärtner and Moon 1989; Muthukumar and Baumgärtner 1989; Muthukumar and Baumgärtner 1989; Baumgärtner and Muthukumar 1996; Baumgärtner 1998) have shown that both ideal and self-avoiding polymer chains can be entropically trapped in fixed "random" environments. Under these conditions, the diffusion coefficient D was found to decrease strongly with molecular size M, in qualitative agreement with their model which predicted that diffusion is then governed by the conformational entropic costs associated with the diffusion between open pore spaces and narrow passages. This phenomenon was observed in computer simulations of the dynamics of random-walk (RW) (Baumgärtner and Muthukumar 1987) as well as self-avoiding walk (SAW) (Muthukumar and Baumgärtner 1989) chains in "random" environments composed of monomer-sized obstacles (placed randomly in space

at a concentration well-below the percolation threshold), and for environments composed of large empty boxes connected by narrow channels (Baumgärtner and Chakrabarti 1990). In an experimental study, Rotstein and Lodge (Rotstein and Lodge 1992) have reported that, for linear polystyrenes diffusing in poly(vinyl methyl ether) gels, D scales roughly as $1/M^{2.7}$, in qualitative agreement with the predictions of entropic trapping, since one would normally expect reptation with an exponent between 9/5 (for a self-avoiding chain in a fixed obstacle gel) and 2 (for a chain in a melt).

Hoagland and Muthukumar's electrophoretic studies on linear, star, and ring macromolecules, have yielded dynamical results whose explanation cannot be described by standard models (i.e. the Rouse and reptation models). This is an indication that polyelectrolytes such as DNA can get entropically trapped in the larger pores of the sieving gel (Hoagland 1992).

It must be admitted that many simulation studies (such as ours) are restricted to d=2 dimensions (2D). There are two main reasons for this: i) in 2D, the effects of excluded volume are much stronger and, hence, more readily identified; and ii) finite-size effects are very strong in disordered systems because the system needs to be much larger than the correlation length of the disorder, and require very large systems (with periodic boundary conditions) which increase rapidly with the molecular size M, rendering simulation studies computationally too demanding for 3D.

However, the limitations inherent in restricting our studies to 2D should not be overstated. There has been growing attention paid to the dynamics of linear polymer chains in 2D systems, not only for the physical insight they provide, but also for their experimental relevance. Many qualitative features of 2D systems also remain relevant in 3D and, perhaps as importantly, many of the resulting dynamics of 2D systems are directly pertinent to many realizable *layer systems*. For example, the 2D case may physically correspond to quasi-two-dimensional systems in which interplanar interactions are much greater than the intraplanar ones, as in the case of chains adsorbed at an interface (Maier and Rädler 2001) or as a simple theoretical model of a broad class of collapse phase transitions (e.g., adsorption collapse driven by an external field, attracting the chains to the absorbing surface). Also, the group of Austin and Duke has performed several pioneering separation studies using microlithographic arrays of micron-sized posts in silicon devices. Recently, along with others, they explored the possibility of using microfabricated hexagonal arrays of posts to separate DNAs using an entropic trap and pulsed field electrophoresis in a quasi-two-dimensional flow channel (Bakajin, Duke et al. 1998). Van Oudenaarden and Boxer, on the other hand, have explored microstructured membrane-coated surfaces as a possible means of separating proteins (Van Oudenaarden and Boxer

1999). Maier and Rädler (Maier and Rädler 1999; Maier and Rädler 2000) performed a 2D dynamical study by using cationic lipid membranes to electrostatically bind DNA molecules onto the lipid surface (Maier and Rädler 2000).

It is now well known that the diffusion of polymers in a disordered or random matrix of obstacles cannot be completely described by classical reptation theory, which is a mean field theory that assumes all spaces in the medium to be energetically equivalent (Doi and Edwards 1986). But how the behaviour changes from classical reptation to entropic trapping with increasing disorder strength is an issue that is not well-understood. While some contend that the reptation model, as applied to a fixed obstacle medium, such as a gel, is self-consistent[4], even in the presence of disorder, the centre of mass (CM) diffusion for a homopolymer is predicted to be exponentially small (Cule and Hwa 1998). Briber, Liu, and Bauer, using neutron scattering, have shown that the radius of gyration of linear chains collapse for a high density of cross-links (fixed disorder), suggesting that the dynamics may therefore differ from what would be expected for reptation (Briber, Liu et al. 1995). Moreover, Sommer and Blumen (Sommer and Blumen 1996) have recently predicted the existence of collapsed polymer conformations for random walk (RW) polymers for a system exhibiting a small degree of disorder.

Our primary goal is to provide a better understanding of the relation between the structure of a fixed, disordered obstacle medium, and the dynamics of polymer chains. But in order to understand how disorder affects the two main models of polymer physics (i.e., the Rouse and the reptation models), we need a system that converges towards these models in the appropriate limits. Therefore, it proved particularly interesting to explore these various phenomena using an elegant 2D MC model system, first introduced in an earlier, preliminary study by Slater and Wu (Slater 1995). This model exhibits this desired convergence while allowing for the introduction of a controlled degree of disorder. We will now discuss the model system.

1.4 Our model system

We employ the model of Slater and Wu, consisting of a particular implementation of the bond fluctuation algorithm (BFA) of Carmesin and Kremer (Carmesin and Kremer 1988), and designed to simulate the dynamics of a single chain in a 2D square lattice of obstacles where a fraction (1-c) of the obstacles, on a periodic array, are removed at random (c=the remaining obstacle fraction).

Slater and Wu's model of a fixed quasi-periodic obstacle array exhibits the expected Rouse and reptation dynamics as limiting behaviours when c=0 and c=1, respectively, while providing for the introduction of a controlled degree of disorder in an otherwise perfectly periodic system. This controlled disorder allows for a systematic study of spatial disorder effects. Slater and Wu found that the steady-state diffusion coefficient of the centre of mass D could be a non-monotonic function of the concentration of obstacles c on the lattice. Moreover, their work supported the notion of a broad intermediate regime existing between the Rouse and reptation limits, corresponding with the entropic trapping regime. First, let us explain the BFA before describing the special features of the model.

Briefly, monomers (and obstacles) are represented by square plaquettes comprised of four lattice sites (vertices) of a unit cell (see Figure 1) and the rules that take into account the excluded volume effects are identical for monomer-monomer and monomer-obstacle interactions. Our d=2 (2D) square lattice system is of size 1260×1260 and periodic boundary conditions apply. Accordingly, Carmesin and Kremer refer to this model as the 'four-site model' (Carmesin and Kremer 1988). Self-avoiding-walk (SAW) statistics and excluded volume (EV) effects are imparted on the system by forbidding the double occupancy of lattice sites. In other words, each lattice site can only form part of one monomer or obstacle. The bond lengths are restricted and, by virtue of the lack of double occupancy and only allowing moves of a single lattice spacing for each monomer at a time, the model ensures that there are no chain crossings. For the 2D square lattice, the lengths of all the bond vectors linking 2 monomers must be restricted to the range $u \in [2,16^{1/2})$ which can be represented as the set of bond lengths $\{2, 5^{1/2}, 8^{1/2}, 3, 10^{1/2}, 13^{1/2}\}$. This implies that there are 36 possible bond vectors for our 2D lattice: 4 of length 2, 8 of length $5^{1/2}$, 4 of length $8^{1/2}$, 4 of length 3, 8 of length $10^{1/2}$, and 8 of length $13^{1/2}$.

Local monomer (bead) moves are simple: given a (valid) realization of a polymer conformation, one chooses a particular monomer at random and a step (jump) size of one lattice spacing is attempted in a random direction (i.e., the ±x or ±y direction for our 2D implementation) with the lattice constant, or unit lattice spacing, being the natural unit of length in the system. Bond length and lattice site occupancy restrictions are then applied and the move is either rejected or accepted accordingly.

[4] That is, under "special" conditions which allow for the use of theory for a directed SAW (DSAW).

I hereby declare that I am the sole author of this thesis.
I authorize the University of Ottawa to lend this thesis to other institutions or individuals for the purpose of scholarly research

Signature

I further authorize the University of Ottawa to reproduce this thesis by photocopying or by other means, in total or in part, at the request of other institutions or individuals for the purpose of scholarly research.

Signature

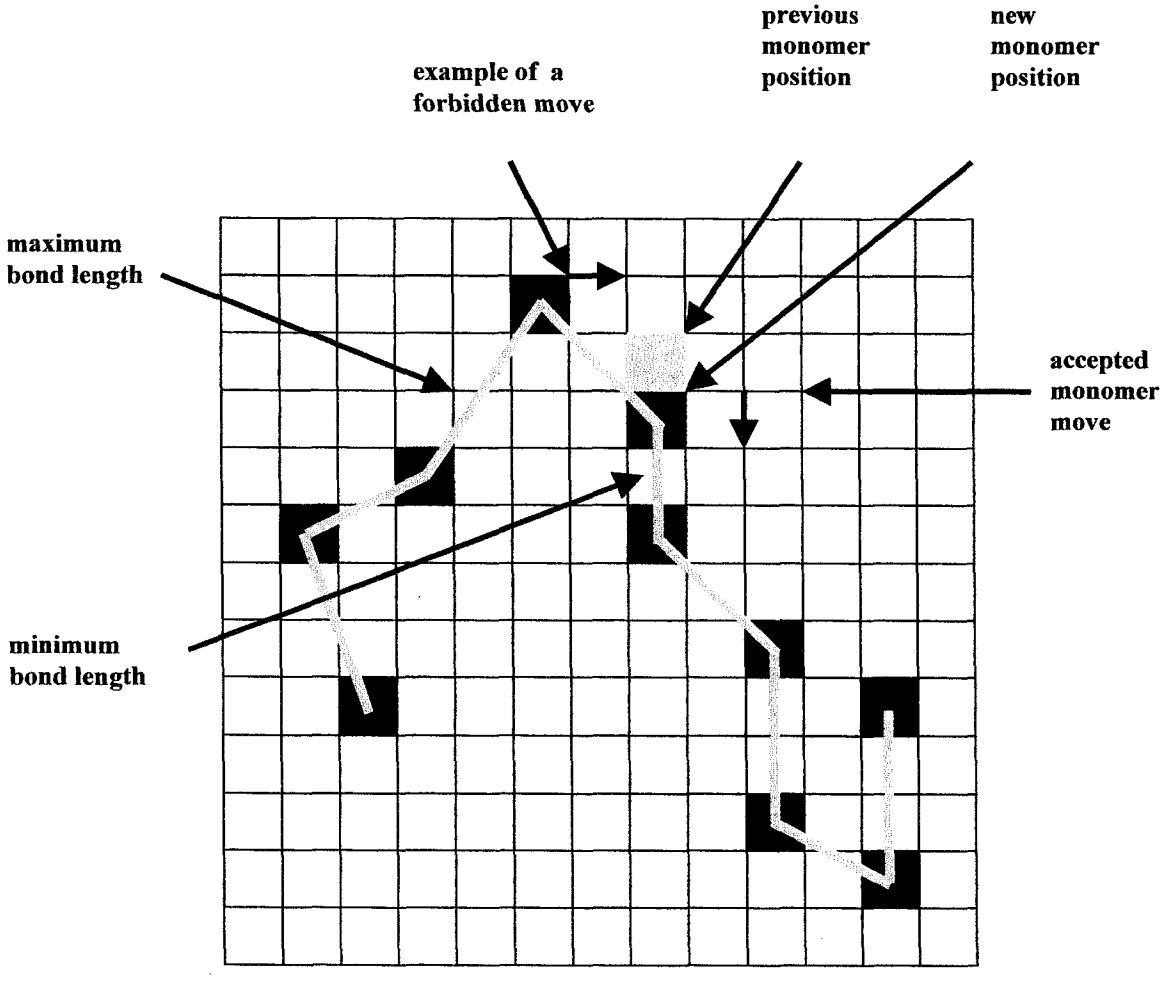

Figure 1. Pictorial representation of the bond-fluctuation algorithm.

A 14×14 cross-section of our 1260×1260 model system is shown for the obstacle-free case. Each of the M=10 monomers occupies 4 lattice sites (vertices) of a unit cell with no lattice site being occupied by more than one monomer (i.e., the excluded volume effect). Rows and columns are shown for clarity. Bond lengths are greater than or equal to 2 and smaller than or equal to $13^{1/2}$ in order to prevent bond crossings and preserve chain-connectivity.

It is clear that the limited set of bond vectors ensures that EV and CC properties are maintained for all subsequent times (moves) if one starts from an initial, permitted conformation. For instance, increasing the maximum bond lengths to 4 would permit bond crossings as monomer or obstacle plaquettes could then be placed on the bond segment linking two monomers without necessitating double occupancy and forcing EV interaction effects.

In Figure 1, the single shaded plaquette represents an initial monomer position that has just been (randomly) moved "downward" by a step of one lattice unit. The move is accepted because, for the new configuration, all the bond vectors have lengths within the defined limits and there is no double occupancy of lattice sites. Conversely, we also depict an example of a "forbidden" move where a monomer jump is attempted to the "right" and the "new" monomer position results in a bond, already at the maximum permissible length of $13^{1/2}$, to extend to $18^{1/2}$ which no longer complies with the bond length restrictions of the model. The attempted monomer move is thus rejected. In both cases, however, the move for the monomer was attempted and one Monte Carlo time Step (MCS) is accumulated after all monomers (the monomer sequence being random) in the system have attempted their random single moves (i.e., it is not dependent on the outcome of individual attempts). As such, MC time measures the number of attempted moves per monomer.

The reptation media are formed by perfectly periodic obstacles on sub-lattice arrays of obstacles with periodicity p=4 and with sub-lattice obstacle concentration c=1 (see Figure 2). There are a total of $(1260/4)^2=315^2\approx10^5$ obstacles. With the convenient definition for the obstacle concentration, the Rouse obstacle concentration limit (no obstacles) corresponds to $c=c_{min}=0$ (see Figure 1) and the reptation limit corresponds with $c=c_{max}=1$ (315^2 obstacles).

The entropic trapping media are formed by imperfect obstacle arrays, i.e. by periodic systems of periodicity p=4 where a fraction (1-c) of the obstacles have been randomly deleted (see Figure 3). As we will see, a few defects[5] in an otherwise perfectly periodic array of obstacles are enough to destabilize reptation because of the onset of entropic trapping (ET).

We have greatly extended the preliminary study of Slater and Wu by considering many dynamical properties. Steady-state diffusion is preceded by long anomalous diffusion regimes whose time exponent can exhibit a broad minimum as a function of obstacle concentration.

[5] It is perhaps more conventional to think in terms of the concentration of random defects (1-c) introduced in the quasi-periodic array of obstacles rather than the concentration of the quasi-periodic obstacles themselves.

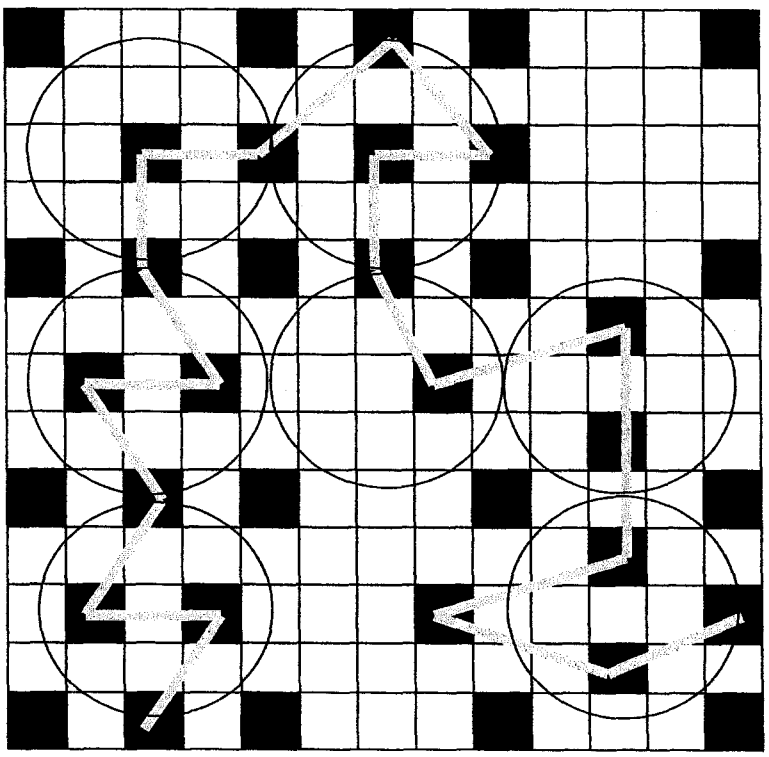

Figure 2. Pictorial snapshot of an M=20 monomer chain reptating in a system of perfectly periodic obstacles with sub-lattice obstacle concentration c=1 (and sub-lattice constant p=4).

Monomers and obstacles are equivalent and each must occupy individual four-site plaquettes. Bonds are drawn as gray segments in order to help distinguish the polymer monomers from the obstacles (both are depicted as black squares). Excluded volume effects are fully in evidence by the lack of double occupancy of sites (and the lack of adjacent plaquettes). There is no excluded volume screening and, for long enough chains, the motion may effectively be described as a string of subchain segments (of size $M_p \approx p-1$) or reptation blobs (encircled) which migrate in an effective tube whose diameter is governed by the topology of the environment (i.e., the constant p). The obstacle sub-lattice, with periodicity p=4, has concentration c=1 which is the tightest obstacle sub-lattice possible for this 2D model. Because the obstacles are perfectly-periodic, long linear chains are expected to exhibit reptative motion in such a system.

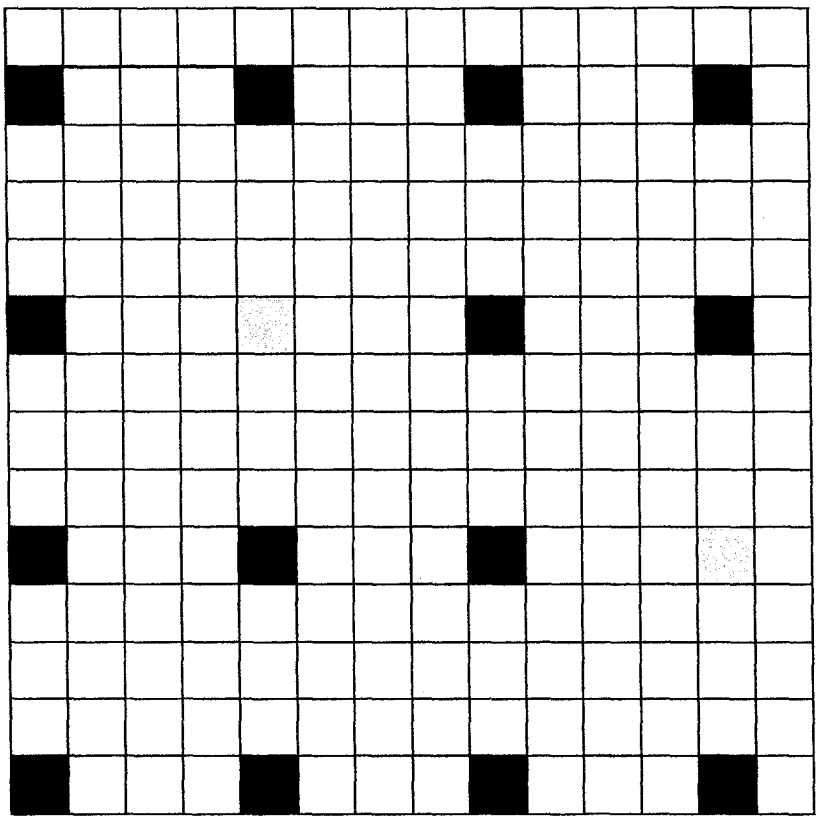

Figure 3. A disordered system of voids is introduced in an otherwise perfectly-periodic (p=4) array of obstacles by randomly removing a fraction (1-c) of the obstacles from the obstacle sub-lattice.

In the depicted view of a model system, there is a 4×4 obstacle sub-lattice where two obstacles have been removed at random (and gray-shaded for clarity). The obstacle concentration depicted in this view is c=(16-2)/16=0.875 whereas, for a perfectly periodic system of obstacles, one would have c=1 and, in the case of a Rouse-like (free-chain) system, one would have no obstacles and thus c=0. Such a system amounts to an entropic trapping system where monomers preferentially occupy porous regions.

Indeed, in ET systems, the displacement of the centre-of-mass may be characterized by long, anomalous, diffusion regimes (Baumgärtner and Moon 1989) before attaining the steady state. This we found engenders a coupling of the polymer conformational relaxation to anomalous diffusion processes, resulting in stretched-exponential behaviour for the conformational relaxation for all intermediate concentrations c.

We show conformational relaxation to be characterized by a newly-defined relaxation length scale, λ, that seems to be distinct from the polymer's radius of gyration, but whose molecular size scaling exponent differs little from that given by the well-known Flory exponent ν for the SAW chain, even under strong entropic trapping conditions.

Moreover, the corresponding relaxation times exhibit an apparent scaling which can be a strong function of molecular size and mode number in the strong ET regime. This apparent scaling behaviour yields effective exponents, which are stronger than those, predicted on the basis of reptation, in the limit where the concentration of obstacles is greatest for the system (c=1).

The onset of steady-state diffusion following anomalous diffusive also allowed us to define steady-state time and length scales. These also serve to better characterize disordered media.

A common feature of the previous studies is that they apply to the case of a single migrating polymer chain in an infinite medium whereas, in many important experimental systems, one is generally interested in finite concentrations in both the diffusing species *and* entropic traps. This naturally begs the question as to the consequences of these heretofore ignored finite-concentration effects (e.g., trap saturation). Recently, Liu, Li, and Asher (Liu, Li et al. 1999; Liu, Li et al. 1999) designed an elegant model experimental system where linear polymers migrate in a hydrogel patterned with mesoscopic voids (or pores), perhaps the first experimental system to be designed exclusively for the study of the ET mechanism. Their study clearly demonstrated non-trivial ET effects at finite polymer concentrations. However, such studies on the effects of finite concentrations and on many chain interactions have focused primarily on the simple problem of the partitioning of polymer chains between, e.g., a fluid phase and a porous material (or similar situations). The resulting dynamics and the pore saturation effects have not been investigated.

To our knowledge, the literature has been devoid of studies concerning concentration effects in entropic trapping systems. As ET is known to be strongest when the polymer radius-of-gyration R_g is comparable to the mean pore radius (a) in a disordered medium, and inspired in part by the

experimental system of Asher et al., we modified the Slater-Wu model system, specifically, to investigate "patterned" or "imprinted" gels whose large (mesoscopic) pores are, in fact, perfectly periodic as well as being comparable in size to the polymers ($a \cong R_g$) we study. In particular, we investigate the effects of polymer concentration and trap saturation on the pore site occupation probability (a measure of the trapping or localization of the polymer chains) as well as on the diffusion properties of a monodisperse solution of polymer chains. Our goal here is to help characterize some of the interplay between trapping, pore saturation, and crowding on the bulk transport of polymer. For monodisperse solutions, we show that at high concentration, the saturation of entropic traps can led to the masking of entropic trapping signatures. We will show that the commonly held notions about entropic trapping systems leading to slower dynamics must be tempered with finite size effects in mind, especially for non-negligible polymer concentrations.

After first characterizing the mesoscopic pore system for monodisperse solutions, we then characterize the concentration-dependence of the trapping behaviour as well as the diffusion for a polydisperse (bimodal) polymer solution. In the dilute concentration regime (when the number of polymers is less than the number voids), we find that the smaller molecular sizes have a higher affinity for the voids (entropic traps). For intermediate concentrations, above the pore saturation threshold, we find that the larger chains have a slightly higher affinity to void trapping. Finally, in the crowding concentration regime, steric effects finally overwhelm the entropic potentials and both of the polymer species then have the same affinity for pore-site occupation because of crowding.

Chapter 2
Static and dynamic properties of polymer chains

We will now describe the static and dynamic properties that are most pertinent to the analysis of our polymeric EV chains in systems with varying degrees of disorder. We will review the expected results in the obstacle-free concentration limit (Figure 1), the perfectly-periodic (and dense) obstacle lattice regime (reptation limit) where there are no isolated point (void) defects (Figure 2), and the intermediate, disordered regimes created by the random deletion of obstacles amid the otherwise perfectly-periodic lattice of obstacles (Figure 3). The latter cases can be referred to as deletion or void disorder. We note that the classical Rouse model applies to RW chains (no EV) and the classical reptation model applies for systems where the EV effects have been screened (as in the melt) (Doi 1986). Therefore, due accounting for EV effects will be in order in both these limit cases as well.

For the intermediate disordered regimes, there has been little in the way of characterization, particularly in the case of dynamic properties. This situation is unlike that for the Rouse or reptation regimes where scaling forms are more readily established. In order to accomplish our characterization of disordered polymer dynamics, we have borrowed from the results of our analysis of disordered systems (Chapter 3) and propose the effective scaling forms up-front. This helps to give the desired impression that the obstacle-free (c.f., Rouse with EV) and perfectly-periodic (reptation with no EV screening) systems are but special limiting cases within the context of the much more general case of disordered systems (see section 1.4).

Therefore, for the disordered systems shown in Figure 3, we characterize the conformational relaxation process using parsimonious stretched exponentials. We also characterize the diffusion as anomalous sub-diffusion during the conformational relaxation process. We relate these two processes directly by proposing length and time scales characterizing the relaxation process as a whole.

Finally, we develop a simple analytical ET model that helps characterize systems in which the size of the periodic void spaces nearly matches that of the diffusing polymers (the voids are then referred to as mesoscopic). We characterize the resulting expression for the diffusion coefficient in terms of the strength of the ET disorder. Specifically, we relate ET to effective coordination numbers that characterize the (lattice) space. As such, ET within the context of a lattice system can be related to an effective *attrition factor*, which characterizes the conformation of SAWs within the (heterogeneous) reptative, gel-like regions and the large void spaces of the system.

Let us begin with a description of the static properties of interest and then follow with the above-mentioned presentation of the dynamical properties under study.

2.1 Static Properties

The conformation of a polymer chains can be described as a self-avoiding random walk with M beads connected through M-1 monomer segments. The two properties commonly used to describe the conformation of polymers are the end-to-end vector $\vec{h}$ and the radius of gyration R_g. The mean square end-to-end distance is defined as:

$$\left\langle h^2(M)\right\rangle = \left\langle \vec{h} \bullet \vec{h} \right\rangle = \left\langle \left(\vec{r}_M - \vec{r}_1\right)^2 \right\rangle \tag{1}$$

where $\vec{h} = \vec{r}_M - \vec{r}_1$ is the end-to-end vector and $\vec{r}_M$ and $\vec{r}_1$ are the vector positions of the last and first monomers of the M-monomer chain, respectively (see Figure 4). Here and in all subsequent sections, the angled brackets $\langle \ldots \rangle$ signify that we are dealing with an ensemble average, although we will allow ourselves the notational convenience of dropping the angled bracket notation when there is no danger of confusion.

The mean-square radius of gyration is defined by

$$\left\langle {R_g}^2(M)\right\rangle = \left\langle \frac{1}{M}\sum_{j=1}^{M}\left(\vec{r}_j - \vec{R}_{CM}\right)^2 \right\rangle \tag{2}$$

where the position of the centre-of-mass (CM) is given by

$$\vec{R}_{CM} = \frac{1}{M}\sum_{j=1}^{M}\vec{r}_j \tag{3}$$

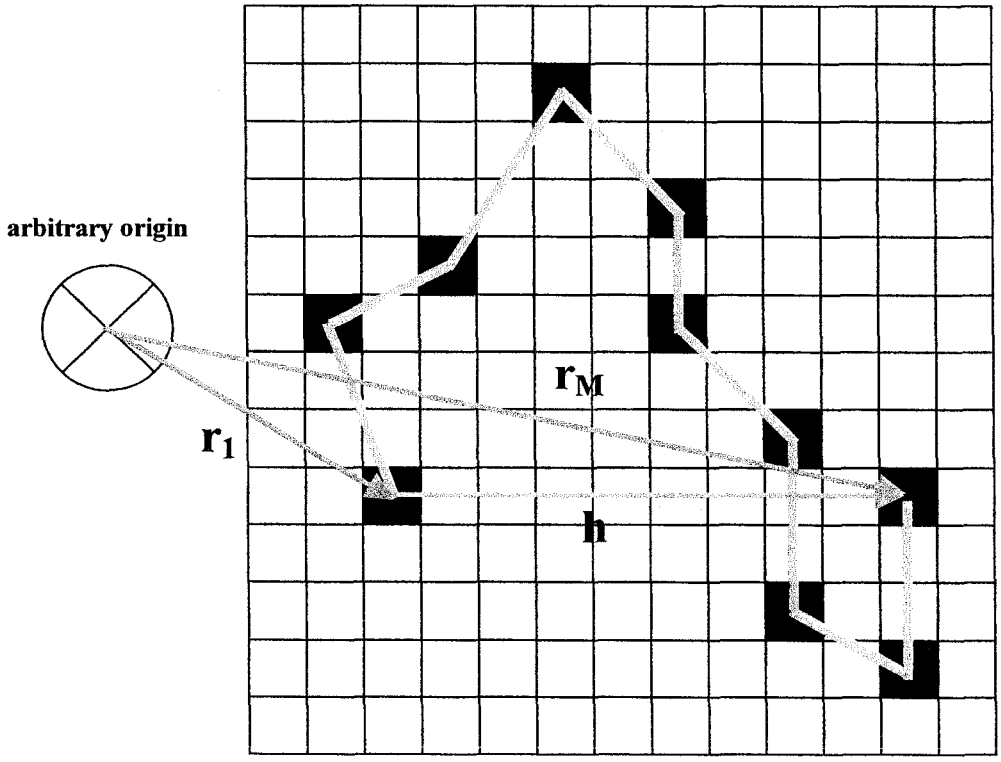

Figure 4. Pictorial representation of the polymer end-to-end vector $\vec{h} = \vec{r}_M - \vec{r}_1$ of Eq. (1) within the context of our model system implementation of the BFA.

In the diagram of an M=10 monomer chain, the end-to-end distance (h) is 9 lattice spacings whereas the minimum possible value would be h_{min}=2 (no double occupancy permitted) while the maximum value, corresponding to a maximally extended straight chain, would be $h_{max}=9\times13^{1/2}$ because there are 9 bonds and the maximum bond length for the BFA is $13^{1/2}$.

For an unperturbed[6] self-avoiding-walk (SAW), scaling theory predicts that these mean square values obey

$$\left\langle h_0^2 \right\rangle \cong \left\langle R_{g0}^2 \right\rangle \cong a^2 M^{2\nu} \tag{4}$$

where ν is a universal exponent for which Flory's theoretical result ν_F (Flory 1953), as generalized to arbitrary dimensionality d by Fisher (Fisher 1969), is given by

$$\nu \approx \nu_F = \frac{3}{2+d}, \quad \text{(Flory - Fisher excluded - volume exponent)} \tag{5}$$

The dimensional dependence of ν_F is quantitatively inaccurate in the case d=3, although, for d=1, d=2 dimensions (ν_F =3/4), and d=4 dimensions, ν_F is known to be exact for unperturbed SAW chains.

The probability distribution function (PDF) for the end-to-end distance (amplitude) $h \equiv \left|\vec{h}\right|$ depends only on the scaled ratio

$$p(h) = \frac{1}{h_0^d} f_p\left(\frac{h}{h_0}\right), \quad (a << h << Ma) \tag{6}$$

where a is the root mean square bond length, h_0 is the root mean square end-to-end distance of Eq. (4), and $f_p(x)$ is the reduced PDF which obeys [the p subscript is only used here to remind us of p(h)]

$$\begin{aligned} \lim_{x\to 0} f_p(x) &= cx^g \\ \lim_{x\to\infty} f_p(x) &= e^{-x^\kappa} f_1(x) \end{aligned} \tag{7}$$

where f_1 varies as a power of x [$f_1(x) \sim x^{1/(2\nu)} \sim x^{2/3}$ in 2D], $g_{2D} \approx 4/9$ [using $\gamma_{2D} \approx 4/3$ and Eq.(12)] and $g_{3D} \approx 1/3$ (de Gennes 1979). The exponent κ is responsible for most of the chain properties for large extensions and is simply given by: (de Gennes 1979)

$$\kappa = (1-\nu)^{-1} \tag{8}$$

For convenience, we define the reduced end-to-end amplitude H, viz.

[6] Within the context of our system, we mean a free EV chain in an obstacle-free system.

$$H = \frac{h}{h_0} \tag{9}$$

where $h \equiv |\vec{h}|$ is the end-to-end distance (amplitude). We may then implicitly define the probability distribution function $p_M(H,c)$ of H via the moment ratio (de Gennes 1979)

$$\frac{\langle h^n \rangle}{h_0^n} = \int_0^\infty H^n p_M(H,c)\, 2\pi H\, dH \tag{10}$$

where H possesses planar rotational symmetry. Using the scaling forms found in Eq. (7), we expect $p(H<1) \sim H^{4/9}$ and $p(H>1) \sim H^{2/3} \exp[-\lambda H^4]$ in the case of no obstacles for d=2 dimensions.

The study of SAWs on a lattice has also provided us with an expression for the total number of available conformations, Ω_M, for M steps in the limit $M \to \infty$. For a lattice devoid of obstacles, Ω_M should obey the asymptotic form (des Cloizeaux 1976)

$$\Omega_M^{SAW} \underset{M\to\infty}{\to} M^{\gamma-1} z_{eff}^M, \quad (z_{eff} \le z-1) \tag{11}$$

where the factor $M^{\gamma-1}$ is the *enhancement factor* (de Gennes 1979), γ is a *universal* critical exponent that depends only on the dimensionality [$\gamma_{2D}=43/32\approx4/3$ (Nienhuis 1984 and de Gennes 1979, respectively); $\gamma_{3D}\approx1.16\approx7/6$ (Sokal 1995 and de Gennes 1979, respectively)], and the effective chain or lattice coordination number z_{eff} [a.k.a. the connectivity constant (Baumgärtner and Muthukumar 1996)] is, in general, noninteger. It is known that $z_{eff}=z-1=1$ only in 1D where $\Omega^{SAW}=2$, independent of M; it thus also follows that $\gamma_{1D}=1$. The effective lattice coordination number is known to obey $z_{eff}\approx4.68$ for the 3D simple cubic (SC) lattice where z=6 (de Gennes 1979) and $z_{eff}=2.880(2)$ for the 3D diamond lattice (Kremer, Baumgartner et al. 1981).

The scaling relationship among the three critical exponents is well known (de Gennes 1979):

$$g = \frac{\gamma - 1}{\nu} \tag{12}$$

Thus, the general static features of isolated, pure SAWs on a lattice, or equivalently, that of single real chains in good solvents, may be described using any two of these three critical exponents

(typically ν and γ). It also proves useful to make use the Flory-Fisher excluded-volume exponent [Eq. (5)] in order to express g via the hyperscaling[7] relation

$$g \approx \frac{(\gamma - 1)(2 + d)}{3} \tag{13}$$

where the symbol ($\approx$) acknowledges the quantitatively inaccurate dimensional dependence so-introduced (i.e., for d=3). We may also express another dimensionless quantity, the conformational compactness, expressed by the ratio

$$S^2 \equiv \langle h^2 \rangle / \langle R_g^2 \rangle \tag{14}$$

which provides a measure of the *span* of the conformation.

2.2 Dynamic properties

It is interesting to note that, for many physical systems, the PDFs are characterized by "heavy tails" where there are larger probabilities for large events compared to the prediction of, say, a Gaussian PDF using the variance estimated from the data. Even if less frequent, it is known that these large events can play an important, if not leading, role. Let us, therefore, introduce the (un-normalized) simple stretched-exponential distribution (SED) function

$$f(x)dx = e^{-\left(\frac{x}{x_0}\right)^{\alpha}} dx, \quad (\mathrm{x} > 0) \quad \mathrm{SED} \tag{15}$$

which, when integrated[8], yields the (normalization) constant

$$\int_0^{\infty} e^{-\left(\frac{x}{x_0}\right)^{\alpha}} dx = \frac{1}{\alpha}\Gamma\left(\frac{1}{\alpha}\right) \tag{16}$$

and the moments

[7] A scaling relation that involves an explicit dependence on the spatial dimensionality is known as a hyperscaling relation.

[8] CRC Standard Mathematical Tables, 28th Edition, Eq. (662).

$$\left\langle \left(\frac{x}{x_0} \right)^n \right\rangle = \Gamma\left(\frac{n+1}{\alpha} \right) \Big/ \Gamma\left(\frac{1}{\alpha} \right) \tag{17}$$

From these relations, we can derive the relative width of the SED to its mean

$$\begin{aligned} \Delta_\alpha &= \frac{\sigma_x(\alpha)}{\langle x/x_0 \rangle} = \frac{\Delta(x/x_0)}{\langle x/x_0 \rangle} = \sqrt{\Gamma(3/\alpha)\Gamma(1/\alpha)/\Gamma^2(2/\alpha) - 1}, \ (0 < \alpha \le 1) \\ &\approx \frac{-185690.5 + 1201549 \times \alpha + 1748316 \times \alpha^2 - 24009.62 \times \alpha^3}{1 - 516552.5 \times \alpha + 3256728 \times \alpha^2}, \ (0.5 \le \alpha \le 1) \end{aligned} \tag{18}$$

where the rational polynomial fitting function approximates Δ_α within a relative uncertainty of the order of $\pm 4 \times 10^{-6}$. We note that Δ_α is a monotonically decreasing function of α with $\Delta_{\alpha=1}=1$, $\Delta_{\alpha=1/2} \approx 1.52753$, and $\Delta_{\alpha \to 0} \to \infty$ (see Figure 5).

The smaller is α, the larger is the probability to observe large event values. Similarly, the larger the probability to observe large values of the event x, the smaller is the stretching exponent α.

We should also mention, that it is a non-trivial matter to accurately determine the parameters of phenomena that follow such distributions. For a finite set of observations, maximum likelihood methods are known to provide a useful scheme for estimating the parameters of stretched exponentials. We will not delve into such issues of robust estimation, choosing instead to obtain estimate for such quantities, based on rudimentary least squares fitting techniques on log-transformed data (which is, admittedly, a special case of the maximum likelihood method). The interested reader should consult Sornette for a fairly comprehensive discussion on this subject (see pp. 151-162, (Sornette 2000)).

As the polymer explores its conformational phase space, we can characterize the change in the end-to-end vector $\vec{h}(t)$ via the decay of the auto-correlation function

$$C_h(t) = \frac{\left\langle \vec{h}(t) \bullet \vec{h}(0) \right\rangle}{\left\langle h^2 \right\rangle} \tag{19}$$

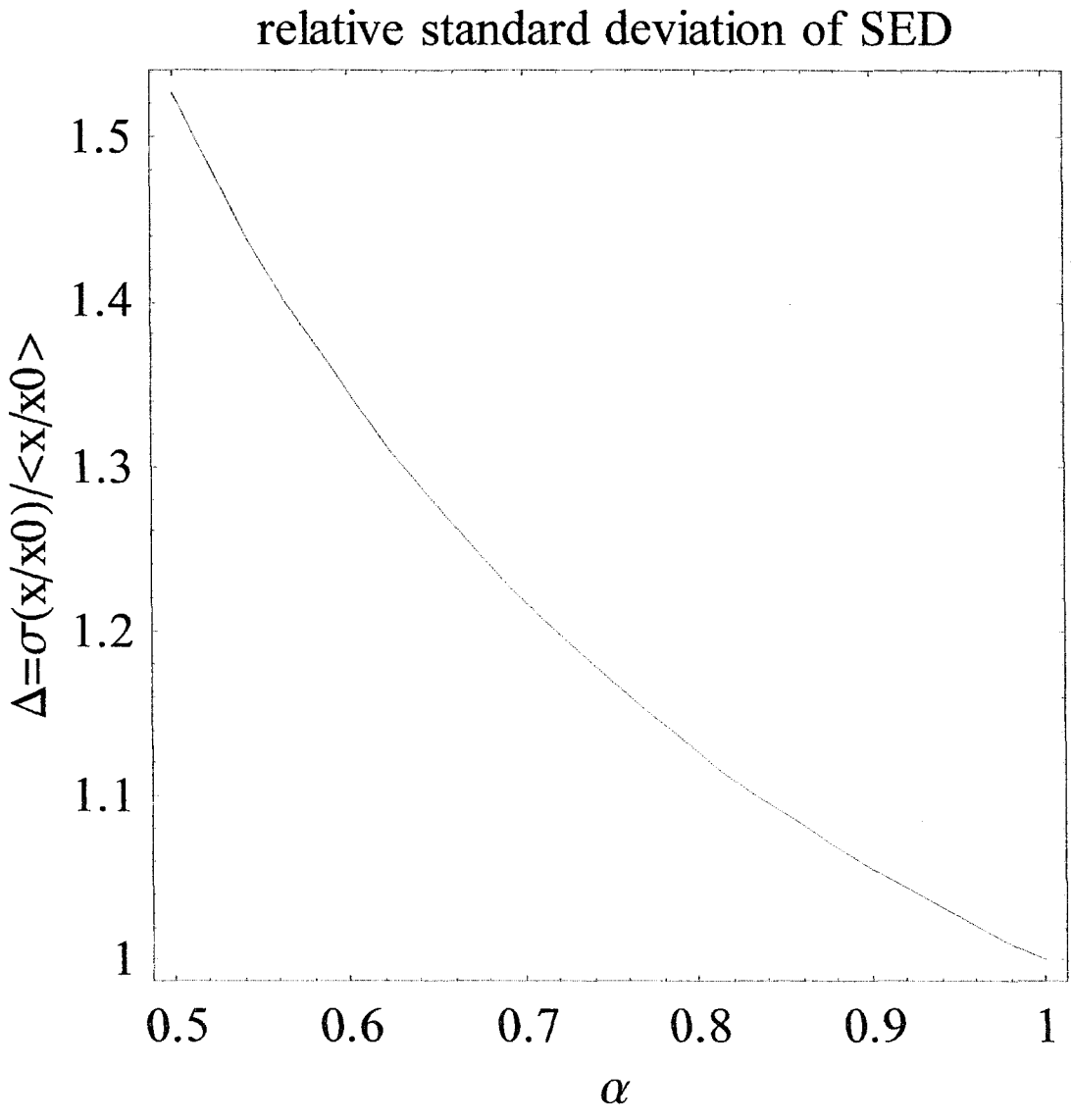

Figure 5. The relative width, Δ_α, as per Eq. (18), of the stretched-exponential distribution function (SED).

In our disordered lattice systems, we found it convenient to express the long-time dependence of $C_h(t)$ via the stretched-exponential form

$$C_h(t) \approx e^{-(t/\tau_h)^{\alpha_h}} \tag{20}$$

where τ_h is the characteristic internal relaxation time and the stretching exponent obeys $\alpha_h=1$ for simple, Rouse-like or reptation-like, exponential relaxation.

In a similar vein, we found it useful to study the Fourier coordinates $\vec{X}_k$ defined by

$$\vec{X}_k(t) \equiv \sqrt{\frac{2-\delta_{k,0}}{M}} \sum_{j=1}^{M} \cos\left(\frac{k\pi\,(j-1/2)}{M}\right) \vec{r}_j(t) \tag{21}$$

(with modes k=0, 1, 2,...), which correspond with the normal modes of the classical Rouse (and reptation) model of RW chains (Verdier 1966; Doi and Edwards 1986)). Note that the zeroth-mode, k=0, corresponds to the motion of the centre-of-mass, R_{CM}, of Eq. (3). However, these coordinates are expected to be subject to mode mixing (for short times) when excluded volume effects are taken into account (Downey 1994). Yet, these coordinates are still useful for examining the relaxation of polymer conformations through the autocorrelation function

$$C_k(t) = \frac{\left\langle \vec{X}_k(t) \bullet \vec{X}_k(0) \right\rangle}{\left\langle X_k^{\,2} \right\rangle} \tag{22}$$

which, in the classical Rouse and reptation models, describes the exponential relaxation of the chain over mode wavelengths M/k. In the case of SAW chains in disordered media, it is more useful to express the autocorrelation function as a stretched-exponential function viz.

$$C_k(t) \approx e^{-(t/\tau_k)^{\alpha_k}} \tag{23}$$

where $\alpha_k=1$ in the classical Rouse and reptation limits. For reasons that will become clear later, the scaling exponents for the characteristic relaxation times may be implicitly defined via the (effective) scaling expression

$$\tau_k = \tau_{k=1} / k^{b_k} \sim \frac{M^{1+b_M}}{k^{b_k}} \tag{24}$$

where M is the molecular size, k is the mode number, and we have introduced generic exponents for both the molecular size M via $(1+b_M)$ and the mode number k via b_k.

In general, the decay of $C_h(t) \approx C_{k=1}(t)$ is due to two processes: i) the rotation of the polymer chain which renders the vector $\vec{h}(t)$ uncorrelated to $\vec{h}(0)$, and ii), the vibrational amplitude of the end-to-end vector $\vec{h}(t)$ which fluctuates in time. It is the first process that typically leads to the long time decay of $C_h(t)$. In particular, the long-time behaviour of $C_h(t)$ is governed primarily by the longest internal relaxation time of the chain, the Rouse (or reptation) time, via

$$\tau_R \equiv \tau_{k=1} \approx \tau_h \tag{25}$$

where, in the case of reptation, we require the notational substitution $\tau_R \to \tau_D$. Alternatively, we may introduce an essentially equivalent relaxation time using the integral

$$\tau_k^* = \int_0^\infty C_k(t)\,\mathrm{d}t \approx \Gamma(1+1/\alpha_k)\tau_k = \frac{\Gamma(1/\alpha_k)}{\alpha_k}\tau_k \tag{26}$$

where $\Gamma(x)$ is the gamma function and where this result corresponds with Eq. (16). The time τ_k^* has the slight advantage of being a less subjective quantity than τ_k, the latter quantity requiring fitting the decay of the correlation function data. When dealing with conformational relaxation, we will be making use of Eq. (26) exclusively and, for notational expedience, we will drop the asterisk that distinguishes between the two relaxation time definitions. This is further justified on the grounds that the distinction is unimportant insofar as the scaling predictions are concerned and, even quantitatively, the two times are often barely distinguishable because the proportionality constant is a typically of the order of unity.

Over short time scales $t \lesssim \tau_{k=1}$, the diffusive process in random systems is frequently characterized by subdiffusion via

$$g_3(t) = \left\langle [\vec{R}_{CM}(t) - \vec{R}_{CM}(0)]^2 \right\rangle = \left\langle \left(\Delta \vec{R}_{CM}\right)^2 \right\rangle = 2dD^* t^{\beta}, \quad (t \ll \tau_{SS}) \tag{27}$$

where d=2 is the spatial dimension and where $0<\beta<1$. For normal, steady-state (SS) diffusion processes, one observes $\beta=1$ and $D^*=D$ is then given by the diffusion coefficient.

The question may arise as to the degree of correspondence between the conformational relaxation process and the (possibly anomalous) diffusion process. Therefore, using Eqs. (20) and (23), along with Eq. (27), let us establish the following ratios upfront

$$\begin{aligned} \lambda_h(t) &= \sqrt{\frac{\left\langle (\Delta R_{CM})^2 \right\rangle}{-\ln C_h(t)}} = \sqrt{2dD^* \tau_h^{\alpha_h} t^{\beta-\alpha_h}} \equiv \lambda_h, \ (\beta = \alpha_h) \\ \lambda_{k=1}(t) &= \sqrt{\frac{\left\langle (\Delta R_{CM})^2 \right\rangle}{-\ln C_{k-1}(t)}} = \sqrt{2dD^* \tau_{k=1}^{\alpha_{k=1}} t^{\beta-\alpha_{k=1}}} \equiv \lambda_{k=1}, \ (\beta = \alpha_{k=1}) \end{aligned} \tag{28}$$

where, for vanishing time-dependence, the final equalities define the two conformational relaxation length scales λ_h and $\lambda_{k=1}$ such that $C_{h \text{ or } k}(t)=C_{h \text{ or } k}[\langle(\Delta R_{CM})^2\rangle]\sim\exp[-\langle(\Delta R_{CM})^2\rangle/\lambda^2_{h \text{ or } k}]$ expresses the conformational autocorrelation in terms of the mean square diffused distance $\langle(\Delta R_{CM})^2\rangle$. The first, λ_h, corresponds with the relaxation length scale of the end-to-end distance while the latter, $\lambda_{k=1}$, to that of the first Fourier coordinate of Eq. (21). Note that, for c=0 and c=1, $\beta=\alpha=1$ and one expects to recover a relaxation length scale of the order of the radius of gyration R_g.

The long-term, $t \gg \tau_{SS}$, steady state diffusion coefficient of the centre-of-mass (CM) is defined by

$$D = \lim_{t \to \infty} g_3(t)/(2dt), \quad (t >> \tau_{SS}) \tag{29}$$

The molecular-size scaling of the steady-state diffusion coefficient D of a polymer chain may be characterized via an "effective" power-law[9]

$$D \sim M^{-\delta} \tag{30}$$

where δ is implicitly defined as the molecular size scaling exponent for terminal CM diffusion.

[9] We note, however, that in the case of entropic trapping, Muthukumar predicts that D is an exponential function of M. We will derive a functional form confirming this assertion later in 2.5.2.

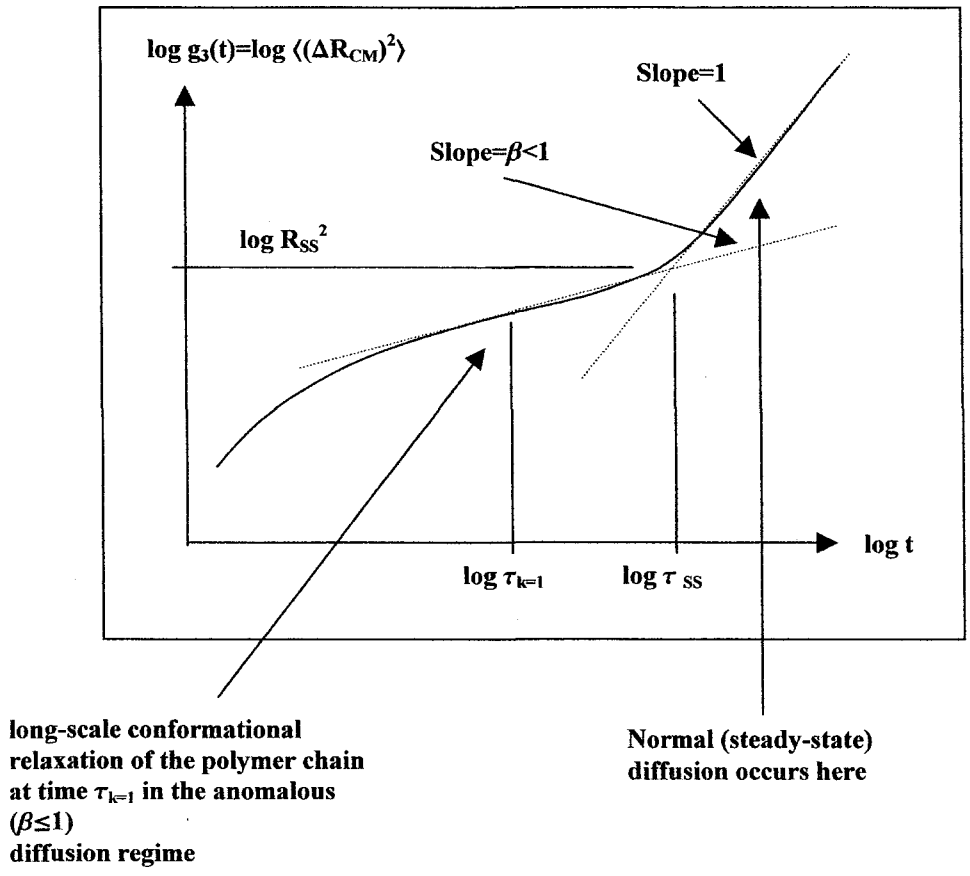

Figure 6. Schematic diagram detailing the relevant length and time scales characterizing anomalous and normal diffusion of polymers in entropic-trapping systems.

The steady state time τ_{SS} and length R_{SS} scales are defined at the crossing point between the anomalous diffusion regime and that of normal (steady-state) diffusion. The time and length scales are indicative of the scales for which the system becomes homogeneous and normal diffusion may take place.

As defined implicitly in Figure 6, the crossover from subdiffusion to normal, steady-state (terminal) diffusion defines the steady-state distance

$$R_{SS} = \sqrt{4D\tau_{SS}} = \sqrt{4D^{*}\tau_{SS}^{\beta}} \tag{31}$$

and the steady-state time

$$\tau_{SS} = (D^{*}/D)^{1/(1-\beta)}, \quad (0<\beta<1) \tag{32}$$

These length and time scales are important parameters for defining disordered media. For time and length scales larger than these characteristic times, the system is said to become homogeneous and normal diffusive behaviour occurs (Baumgärtner 1996). The β-exponent will be important in future sections concerning disorder effects.

The mean square displacement of the central monomer (or centre bead CB)

$$g_1(t) \equiv \left\langle [\vec{r}_{CB}(t) - \vec{r}_{CB}(0)]^2 \right\rangle \tag{33}$$

is also a useful physical quantity, characterizing the monomer dynamics and providing an indicator of the time scale for which diffusion of the central monomers are affected by the topology of the surrounding environment and time scales for which monomer motion becomes coupled with the diffusion of the chain's CM.

2.3 Free (Rouse) chains in d=2 dimensions

The classical Rouse model provides a theoretical description for the dynamics (e.g., viscous flow) of dilute polymer solutions. The polymer molecule is subdivided into M submolecules. The end-to-end distance of each submolecule is described by Gaussian statistics and the mass of, and friction on, each submolecule is thought of as being concentrated in a solid "bead". Brownian motion acts on each bead that is coupled by an entropy-elastic recovery force that can be assigned an effective entropic "spring constant" k. The Rouse model thus represents the simplified dynamics of a connected object in which the interactions among segments is localized (i.e., nearest-neighbour entropic spring interactions). The conformational properties are ubiquitous due to the universal applicability of RW statistics in many areas of science. The beads interact only locally with (connected) nearest neighbours (through an entropic spring constant k). In the classical treatment of

the model, EV, self-entanglement, and hydrodynamic effects are ignored. The Rouse model thus describes the properties of an ideal, free polymer chain (the Rouse limit is the c=0 limit).

The simple obstacle-free (c=0) situation has been studied extensively. The primary complication arises from the EV interactions, which effectively add constraints that complicate any analysis through the normal modes used for the classical Rouse chain model.

The mean square radius-of-gyration $\langle R_g^2 \rangle$ and mean square end-to-end distance $\langle h^2 \rangle$ of a polymer molecule with M»1 monomers [Eq. (4)] scale like

$$\begin{aligned} \left\langle h^2 \right\rangle \sim \left\langle R_g^2 \right\rangle \sim (M-1)^{2\nu} &= (M-1)^1, \quad \text{RW} \\ &= (M-1)^{3/2}, \ \text{SAW (2D)} \end{aligned} \tag{34}$$

where the molecular size exponent, as per Eq. (5), obeys $\nu=½$ for random walk chains (RW), i.e. when there is no excluded volume effect. In two-dimensions, our self-avoiding walk chains (SAW) are characterized by the (exact) Flory exponent $\nu=¾$.

As for the compactness of free chains [see Eq. (14)], we know that (des Cloizeaux and Jannink 1990):

$$\begin{aligned} S^2 &\equiv \left\langle h^2 \right\rangle / \left\langle R_g^2 \right\rangle \\ &= 6, \quad \text{RW} \qquad\qquad (\text{d} = 2) \\ &= 12, \quad \text{rigid rod} \qquad (\text{d} = 2) \\ &= 7.1296(56), \ \text{SAW} \quad (\text{d} = 2) \end{aligned} \tag{35}$$

where the results of Sokal et al. (Sokal 1995) were used for the SAW in d=2 dimensions. As for the diffusion coefficient [see Eq. (30)], the molecular-size scaling parameter $\delta=1$ for both RW and SAW free chains in the Rouse limit (and for no hydrodynamic interactions). Moreover, for a free-chain, there exists no anomalous diffusion regime and $\beta=1$ for the anomalous time exponent of Eq. (27), and the motion of the center-of-mass is normal for <u>all</u> time scales

$$g_3(t) = \left\langle \left(\Delta \vec{R}_{CM} \right)^2 \right\rangle = 2dD^* t^{\beta} = 2dDt \sim M^{-1} \tag{36}$$

In the absence of excluded volume effects, the decay of the autocorrelation function of the Fourier coordinates is purely exponential

$$C_h(t) \approx e^{-(t/\tau_h)^{\alpha_h}} = e^{-(t/\tau_h)}$$
$$C_k(t) \approx e^{-(t/\tau_k)^{\alpha_k}} = e^{-(t/\tau_k)} \tag{37}$$

where the exponents $\alpha_k=\alpha_h=1$ in Eqs. (20) and (23). Because of the SAW statistics, however, there exists some degree of mode-coupling that is more prevalent for small times of the order of the coarse-grained time scale of single moves, although we expect to recover exponential relaxation for long enough times.

As there is but a single characteristic length scale for free chains, the size of the polymer conformation ($\approx R_g$ or h) describes the molecular size scaling for both diffusion and conformational relaxation. Consequently, both conformational relaxation and steady state diffusion are related through the scaling relation $\tau \sim R_g^2/D$. Thus, the relaxation time scaling of the Fourier coordinates, as per Eq. (24), is expected to scale as

$$\tau_k(M) \sim (M/k)^{2\upsilon+1} \sim \tau_h(M) \sim M^{2\upsilon+1} \tag{38}$$

where we have equated $1+b_M=b_k=2\nu+1$. For our 2D SAW polymers, we expect $1+b_M=b_k=2\nu+1=5/2$ whereas, for the special case of a Rouse chain without excluded volume effects ($\nu=1/2$), one would expect $1+b_M=b_k=2$.

2.4 Reptation

The classical reptation model provides a theoretical description for the dynamics of polymer chains in the concentrated solution regime where fluctuations in solution concentration are damped-out and a mean-field approach is possible. The motion of an individual chain is then said to reptate inside a hypothetical "reptation tube" which is effectively born out of the topological constraints imposed on this chain by its (mean field) environment. However, for the classical reptation theory, polymers chains are in the melt where screening of EV effects takes place. Within a system of fixed obstacles, however, this EV screening is absent and SAW statistics apply (see Figure 2), a point often neglected in the literature.

The curvilinear motion of the chain in its tube is Rouse-like, with a diffusion coefficient $D_T \sim 1/M$, as per Eq. (36), with M representing the number of monomers. Since the curvilinear reptation tube length scales as the number of monomer segments viz. $L \sim M-1$, the tube disengagement time is expected to scale as

$$\tau_D \approx \frac{L^2}{D_T} \sim M(M-1)^2 \approx M^3 \tag{39}$$

As the radius of gyration, R_g, is expected to be the only length scale of relevance, and since the EV effects are not screened in the presence of fixed obstacles as they are in the melt (and in the classical reptation model), we have

$$\left\langle h^2 \right\rangle \sim \left\langle R_g^2 \right\rangle \sim (M-1)^{2\nu} = (M-1)^{3/2}, \text{ SAW} \tag{40}$$

and we would thus expect the scaling form

$$D \approx \frac{R_g^2}{\tau_D} \sim \frac{M^{2\nu-1}}{(M-1)^2} \approx M^{-\delta} = M^{-(3-2\nu)}, \text{ (fixed obstacles)} \tag{41}$$

with $\delta=3-2\nu=3/2$ for d=2 for long enough chains to eliminate finite-size effects. We expect a very-short anomalous diffusion regime, due to the variation in the exploration time of the CM before it experiences the effective tube constraints. We also expect the bead movement rules and the "graininess" of the model to become more apparent at very short time scales $1 \le t \ll \tau_R < \tau_D$. This brief anomalous diffusion regime is expected to be quickly followed by normal diffusion regime $\langle [R_{CM}(t)]^2 \rangle = 2dDt$.

The reptation model can also be solved using normal-mode analysis but excluded volume leads to mode-mode coupling for short times $t \ll \tau_D$. The situation is further complicated by the appearance of a second length scale, the obstacle spacing p=4, which is analogous to the entanglement spacing, or tube diameter, d_T, in the theory of polymer melts (Doi and Edwards 1986). However, the terminal relaxation of the functions $C_k(t)$ remains exponential (i.e., the exponents $\alpha_k=1$). Reptation theory predicts that $\tau_k(M) \sim M(M/k)^2$. However, this scaling relationship is strictly valid only for $(M/k) \gg M_p$ where M_p is the size of a reptation blob (see Figure 2). Strong finite-size correction factors are known to exist for τ_k for finite sizes M due to tube length fluctuations scaling as $(k/M)^{1/2}$ to first-order [i.e., the so-called contour-length fluctuations (Doi and Edwards 1986)]. Therefore, we expect the conformational relaxation time to follow the theory-motivated functional form

$$\tau_k = \frac{\mathrm{M}}{\mathrm{M}_p}\left(\frac{M}{k}\right)^2 \times B_1\left[1-\frac{B_2}{(M/k)^{1/2}}\right]^2 \qquad (42)$$

where B_1 is a model-dependent proportionality time constant and B_2 is a model-dependent topological constant or metric accounting for tube length fluctuations (Doi and Edwards 1986). The constant M_p ($\approx$2 for our p=4 system of obstacles, see Figure 2) is the average number of monomers between consecutive obstacles (c.f. entanglements in the case of melts).

According to the reptation model, there are four different characteristic time scales (Doi and Edwards 1986). For short times such that $g_1<a^2$ ($a\approx p$, is the effective "tube" width), the SAW chain does not yet feel the tube constraints; the motion is then described by the Rouse model for a free chain, and $g_1(t)\sim t^{1/(1+1/2\nu))}\sim t^{3/5}$. This is valid for times $t<\tau_R(M_p)$, where $\tau_R(M_p)$ is the relaxation time of a reptation blob or subchain of size M_p (see Figure 2), between two constraints (i.e., fixed obstacles). When the chain begins to "feel" the lateral constraints of the effective tube, i.e. for times $t>\tau_R(M_p)$, the chain's motion is unimpeded along the tube axis. In other words, the motion of polymer segments is directed along a random-walk tube, and a displacement of length s along the curvilinear 1D tube leads to a net displacement of length s^ν in the d-dimensional space. We thus have $g_1(t)\sim t^{\nu/2}$ up to $t\approx\tau_R(M)$, i.e. until complete Rouse relaxation. For $\tau_R(M)<t<\tau_D$, the central monomer follows the diffusion of the CM into the random-walk tube and we obtain $g_1(t)\sim t^\nu$. Finally, we expect the terminal diffusion limit $g_1(t)\sim t^1$ for $t>\tau_D$. This sequence of regimes is uniquely characteristic of reptation.

2.5 Entropic trapping and disorder effects

2.5.1 Introduction

The dynamical scaling laws for polymers in disordered fixed obstacle systems do not simply interpolate between those of the Rouse and reptation limits. As we will show, the chain properties do not even vary monotonically with the concentration of fixed obstacles.

One special concentration c of obstacles deserves mention and may be of some relevance. For the obstacle sub-lattice (see Figure 3), the percolation threshold concentration is c*=0.4072, above which

the missing obstacles cease to form a connected[10] cluster (Stauffer and Aharony 1992) and the chains must diffuse through very dense areas in order to migrate over macroscopic distances (Slater and Wu 1995).

Let us now formulate a simplified, idealized model for ET in which the pore size is large enough to fully accommodate polymer chains, such as in a mesoscopic void system (see the M=10 chain in Figure 7).

[10] That is, connected in sublattice spacing units of p=4 in our model.

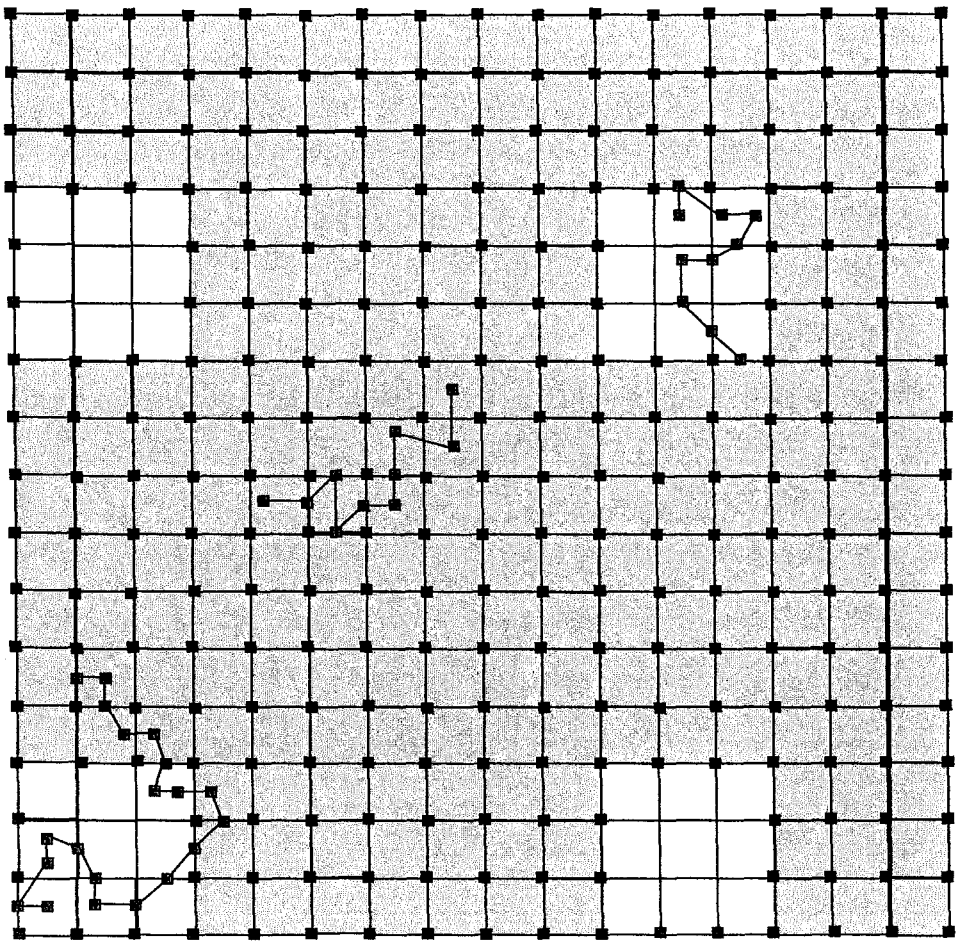

Figure 7. Pictorial representation of a 65×65 mesoscopic void system. The black square plaquettes represent fixed obstacles in the otherwise perfectly-periodic (p=4 lattice spacing) obstacle array whereas the periodic (P=40) white spaces represent mesoscopic voids created by the removal of integral 2×2 sections of obstacles. Also appearing are one chain with M=20 and two chains with M=10 monomers.

Two chains appear entropically trapped inside the (white) mesoscopic voids, which act as entropic traps. One M=10 chain appears in the denser (gel-like) region which has been grayed in order to highlight the voids. We note that, in the case of the M=20 chain, monomer spill-out occurs whereas, in the case of the M=10 chains, the voids are of sufficient size to fully accommodate the chain's monomers.

2.5.2 Strong entropic trapping (ET) in mesoscopic void systems (hydrogels)

If we designate P(x,y) to be the centre-of-mass (CM) site occupation probability in our lattice system, we may, in principle, calculate for each site (x,y) an effective local potential energy, U'(x,y), or the dimensionless version U(x,y), implicitly defined by the relation

$$P(x,y) \sim e^{-U'(x,y)/k_BT} \sim e^{-U} \tag{43}$$

whose form asserts a hopping-like motion of the CM on the potential landscape U(x,y). In analogy with the diffusion of a point-like particle, let us assume that we are observing a homogeneous Poisson process whose mean hopping time, as derived by Kramers (Kramers 1940), is given by

$$\langle \tau_K \rangle = \tau_{relax} e^{|\Delta U'|/k_BT} = \tau_{SS} = \tau_{relax} e^{|\Delta U|} \tag{44}$$

where τ_{SS} is the steady-state (SS) time defined in Eq. (32), $|\Delta U'| \approx T|\Delta S|$ is the entropic barrier height for hopping between the voids and the dense, gel-like regions shown in Figure 7, τ_{relax} is an effective relaxation time within the well, and $|\Delta U(x,y)| = U_{gel}(x,y) - U_{pore}(x,y)$ is the dimensionless (units of k_BT) barrier height for jumping between voids. We assume that the time scale for SS hopping is given by

$$\langle \tau_K \rangle = \tau_{SS} = \frac{R_{SS}^{\ 2}}{2dD} \tag{45}$$

where d is the dimensionality (in this case, d=2), R_{SS}^2 is the mean square distance characterizing large-scale disorder [as defined in Eq. (31)], governed by the distribution of the voids, and D is the steady-state diffusion coefficient characterizing the void-to-void hopping of the center of mass.

Using the analogy of the escape of a Brownian particle from a potential trap [see, e.g., (Simon and Libchaber 1992)], we expect, for steady-state (SS) diffusion, that the (normalized) hopping time probability distribution should have an exponential density of the form

$$p(\tau_K) = Exp(-\tau_K / \tau_{SS})/\tau_{SS} \tag{46}$$

whose standard deviation (and mean) is

$$\sigma_\tau = \langle \tau_K \rangle = \tau_{SS} \tag{47}$$

and whose skewness is 2. We therefore expect the distribution of trapping (or hopping) times to be broad and of the same order as the steady-state time.

For isolated chains trapped inside of pores large enough to fully accommodate them (as in the case of the M=10 chain in Figure 7), we would expect the diffusion of the CM inside the pore to be Rouse-like and obey the scaling form

$$\tau_{relax} \approx \frac{r_{pore}^2}{2dD_{Rouse}} \sim M^{2\nu+1}, \quad (r_{pore} \gtrsim R_g) \tag{48}$$

where r_{pore} is the pore radius, R_g the polymer's radius of gyration, and where we have used the Rouse scaling form of the diffusion coefficient. The conformational entropy, S, scales as the natural logarithm of the number of available conformations Ω for the polymeric chain.

Therefore, the entropic potential barrier U (in units of k_BT) is simply related to the enumeration ratio of the number of available conformations for the M-monomer polymeric chain in the pores to that of the gel phase viz.

$$|\Delta U| \approx \ln\left(\frac{\tau_{SS}}{\tau_{relax}}\right) \approx \ln\left(\frac{\Omega_{pore}}{\Omega_{gel}}\right), \quad (r_{pore} \gtrsim R_g) \tag{49}$$

where the symbol ($\approx$) serves as a reminder of the crude application of a particle-like activated process to a polymer system with inherently strong finite-size effects (e.g., monomer spill-out into the gel phase).

When we introduced the SAW relation for Ω [see, Eq. (11)], it was remarked that the critical exponent, γ, is *universal*. Consequently, the *enhancement factor* $M^{\gamma-1}$ is known to be solely a function of the dimensionality of the space in the pure system. Therefore, if we make the *ansatz* that only the effective coordination number of the lattice is affected by the presence of obstacles in the gel phase, then, substituting Eq. (11) inside of Eq. (49), we have

$$|\Delta U| \approx \ln\left(\frac{z_{eff}^{pore}}{z_{eff}^{gel}}\right) \times M, \quad (r_{pore} \gtrsim R_g) \tag{50}$$

This expression relates the potential barrier to an *attrition factor* arising from the polymer-obstacle EV interactions. As such, this attrition factor is responsible for driving polymer chains into regions of lower density (the voids). Therefore, combining Eq. (48), Eq. (49), and Eq. (50), we have

$$D = \frac{R_{SS}^{\ 2}}{2d}\tau_{SS}^{-1} \tag{51}$$

where

$$\begin{aligned} \tau_{SS} &\approx e^{\ln\left(z_{eff}^{pore}/z_{eff}^{gel}\right)\times M + (2\nu+1)\times \ln M}, \quad (r_{pore}/\mathrm{R_g} \approx 1) \\ &\approx e^{\ln\left(z_{eff}^{pore}/z_{eff}^{gel}\right)\times M} \end{aligned} \tag{52}$$

and $R_{SS}>r_{pore}$ is the root-mean-square distance between pores.

For a perfectly periodic array of obstacles in the gel phase (a reptative gel in the case of Figure 7), we may express the *entropic trapping attrition factor* as

$$e^{\Delta U/M} \approx \frac{z_{eff}^{pore}}{z_{eff}^{gel}} = 1+\chi, \quad \text{(ET attrition factor)} \tag{53}$$

where we have incorporated Eq. (50), $\chi \geq 0$ is the (dimensionless) *entropic trapping strength (or ET attrition) parameter* for the system, and where $e^{\Delta U/M} \approx (1+\chi) \approx e^{\chi}$ such that $\tau_{SS} \approx e^{\chi M}$ for $\chi \ll 1$.

Thus, these expressions reveal that CM diffusion for our model ET system is exponentially slower with molecular size M than predicted by either the Rouse or reptation models.

Chapter 3

Entropic trapping and disorder effects of small random voids spaces on the dynamics of isolated migrating polymers

3.1 Simulation Method

For the simulation studies of this chapter, we employed Slater and Wu's particular implementation of the four-site bond-fluctuation algorithm (BFA) of Carmesin and Kremer (Carmesin and Kremer 1988), as described in the Introduction (section 1.4).

The initial polymer conformation is generated in a straight, vertical line of M monomers and M-1 segments separated by the minimum bond length (=2) and each simulation is preceded by a long warm-up period of many steady-state times τ_{SS} [see Eq. (32) and Figure 6], established from previous simulation data. Over the course of the warm-up time t, the vertical conformations completely relax [with characteristic time $\tau_{k=1}$, see Eq. (26)] such that the chain's CM position reaches equilibrium ($t \gg \tau_{SS}$) and for which normal (steady-state) diffusion can be exhibited. Simulation data for the static and dynamic properties of the chain are dumped into output files at regular time intervals so as to render large ensemble sizes. These long simulations are only stopped once all quantities are deemed to have converged sufficiently in the statistical sense with time and other practical considerations taken into account. Molecules ranging from M=5 up to M=200 monomers have been studied in an attempt to establish scaling behaviours, if indeed scaling can be exhibited for this range of molecular sizes in the given system.

The system size is 1260×1260, and contains $(1260/4)^2=315^2\approx10^5$ obstacles. In Figure 8, an M=25 chain is shown migrating in our model system for obstacle-site occupation probability c=0.9. We note the existence of several voids (9) among the 10^2 obstacles shown (~10 site deletions are expected), and a sub-portion of the chain (subchain) appears entropically trapped within a large pore created by the (random) deletion of 2 adjacent obstacle sites. We would expect pores made up of (at least) n contiguous deletion sites to have a probability of occurrence $p(n)=(1-c)^n$, with some possibly forming part of clusters in the system of obstacles.

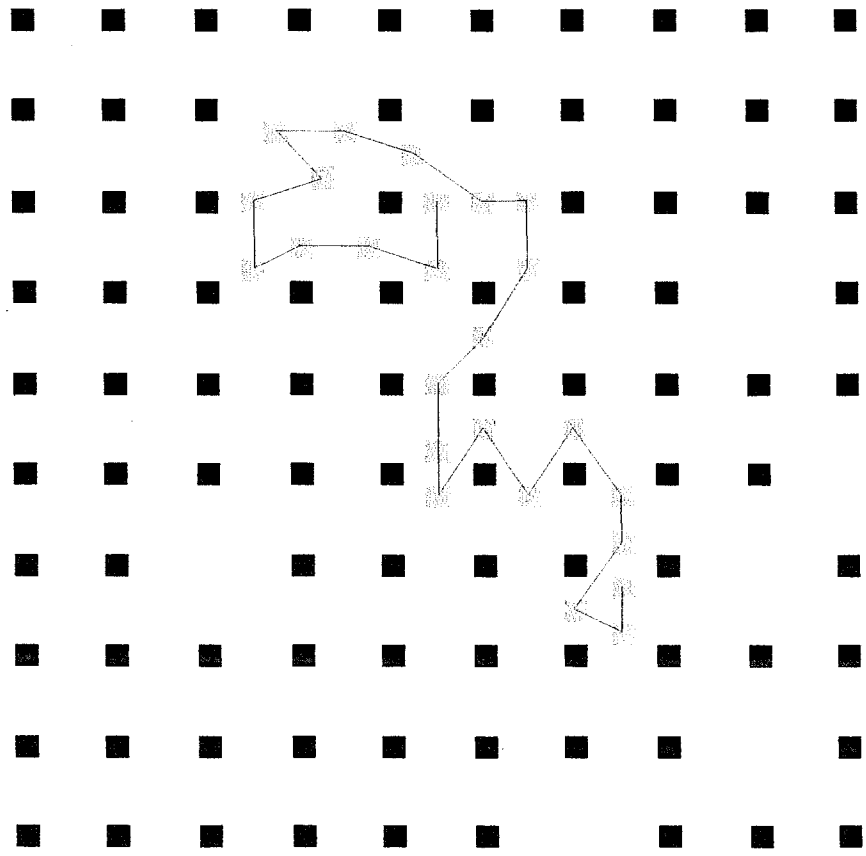

Figure 8. Actual simulation snapshot of an M=25 chain migrating in a quasi-periodic array of obstacles with sub-lattice concentration c=0.90. The trapped chain end is shown wrapped around an obstacle and the chain physically occupies a region characterized by 3 site deletions.

3.2 Static conformational dimensions

Because of the numerous analytical scaling predictions in the literature, and because of the many relevance of static conformational dimensions with regards to the practical problem concerning the transport of polymer chains in porous media (Baumgärtner and Muthukumar 1996), let us now investigate the effects of disorder on the conformational properties of polymer chains by extracting the mean square dimensions of polymer chains as a function of the obstacle concentration c.

But first, let us recall from our theory section in Chapter 2, that for a free chain (c=0), as well as for a chain in a tight periodic array (p=4) of fixed obstacles (c=1), the Flory exponent $\nu=¾$ holds because of the lack of the screening effect one would get in a melt.

In order to verify that our model system conforms with the scaling predictions of Eq. (34) for c=0 and Eq. (40) for c=1, we simulated many M-bead chains in both obstacle concentration limits and generated time-averaged statistics for both the mean square end-to-end distance h^2 and mean square radius of gyration R_g^2 and plotted them as a function of the number of monomer 'bonds' (M-1) on a log-log graph. The slope of the data was then compared with the predicted scaling laws.

In Figure 9, a fit with a forced slope of $2\nu=3/2$ is shown to conform to the data for long chains, exhibiting the expected Flory scaling $\nu=¾$ in the c=0 (i.e., the Rouse obstacle concentration limit).

In Figure 10, the mean square size scaling for h^2 and R_g^2 is not expected to conform with RW result $\nu=1/2$ but rather, with the SAW result $\nu=¾$ [see Eq. (40)] (i.e., EV is not screened for a chain in a fixed gel), as verified by our c=1 data for all but the shortest chains. We have forced the fit to yield the expected slope of $2\nu=3/2$ and the long chain data are shown to be consistent with the expected scaling predictions.

More interesting, however, is the question as to what happens to the Flory exponent for the case of intermediate concentrations $0<c<1$ which characterize disordered obstacle arrays and for which entropic trapping occurs (Slater and Wu 1995). For instance, for c=0.8-0.9, ET is particularly strong in the case of M=25 chains as we will see later (e.g., Figure 25).

We plot the mean square radius-of-gyration R_g^2 and end-to-end distance h^2 vs. (M-1) for concentration c=0.9 in Figure 11 along with fits exhibiting the same constant Flory ($\nu=¾$) scaling as for c=0 and c=1.

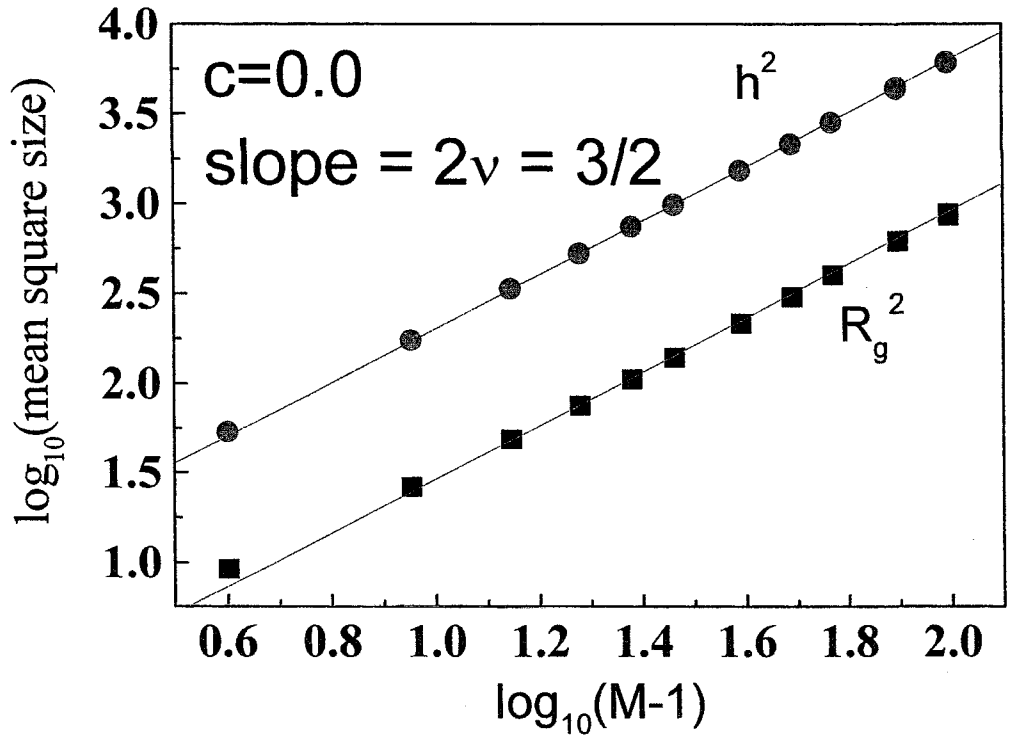

Figure 9. Log-log plot of mean square molecular size against the number of polymer segments (M-1) in the case of no obstacles (c=0). The Flory exponent, ν, of Eq. (4) for the molecular size scaling of the radius of gyration, R_g^2, and of the end-to-end distance, h^2, is verified to hold, as expected for long chains. The associated uncertainties in the data are too small to be discernable.

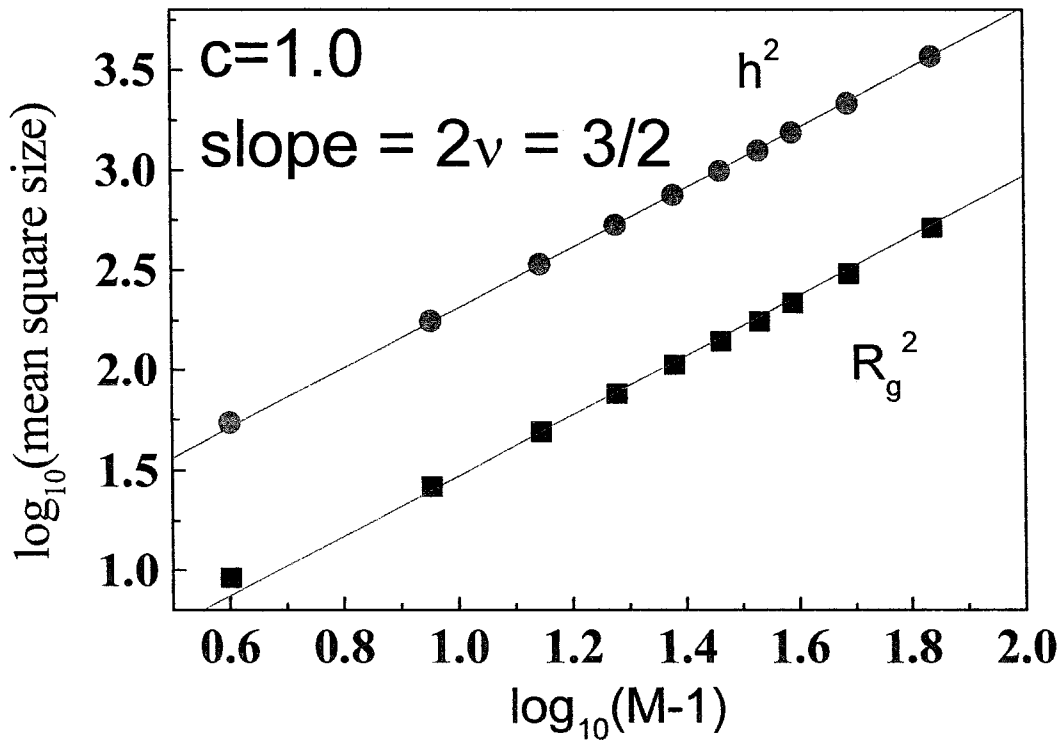

Figure 10. Log-log plot of mean square molecular size against the number of polymer segments (M-1) in the case of a perfectly periodic system of fixed obstacles with no voids (c=1). The Flory exponent, ν, of Eq. (4) for the molecular size scaling of the radius of gyration and of the end-to-end distance is verified to hold, as expected for long chains. The uncertainties associated with these data points are too small to discern (c.f., Figure 9) and have been omitted for clarity.

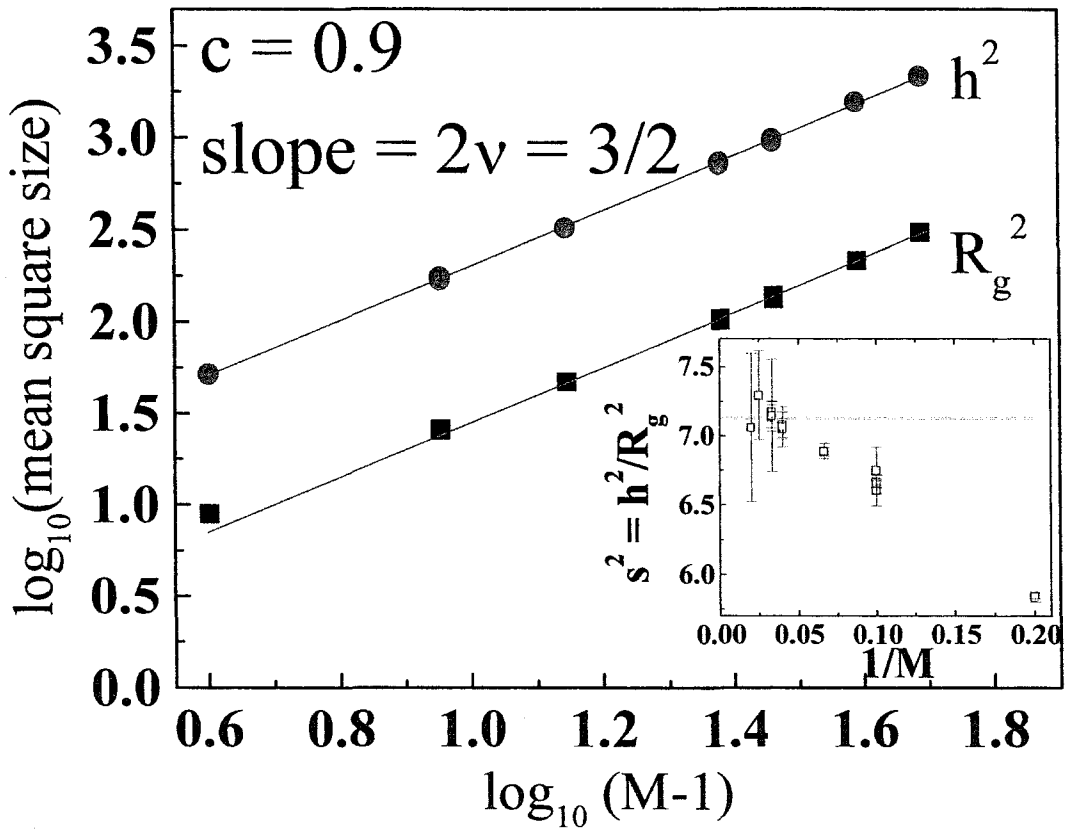

Figure 11. Log-log plot of mean square molecular size against the number of monomer segments (M-1) in the strong entropic trapping case c=0.9. The Flory exponent, ν, of Eq. (4) for the molecular size scaling of the radius of gyration and of the end-to-end distance is verified to hold for long chains. Again, the uncertainties in the data are too small to discern on the graph.

In the inset figure, the conformational compactness parameter S^2 defined in Eq. (14) is shown to be consistent with the expected c=0 result $S^2 \approx 7.13$ of Eq. (35), for the case of long chains, even though we are in the strong entropic trapping region.

The choice c=0.9 was motivated by the fact it lies within the strong-ET region. The inset shows the conformational compactness $S^2=h^2/R^2$ of Eq. (14) as a function of 1/M, again for c=0.9. Note that the intercept yields an $M\to\infty$ limit ratio of S^2 which remains fully consistent with the result $S^2=7.1296(56)$ found by Sokal et al. (Sokal 1995).

In Figure 12, the reduced radius of gyration $R_g^2(c)/R_g^2(0)$ is plotted as a function of concentration c for M=10 and M=25. We remark a minimum in the region $c\approx 0.6$-0.9 where strong ET is observed. This shallow minimum, the so-called polymer "collapse", is only of the order of 3% for the SAW chains studied while it is known to be much stronger in the case of RW polymers where the local concentration of (collapsed) monomers does not lead to any EV effects (Sommer 1996).

Also of interest in Figure 12 is the slight degree of overall swelling appearing for c=1.0 when compared to the c=0.0 results for small molecular sizes (M=10). This swelling effect is a consequence of the excluded volume effect (topological constraint) of the obstacles on the monomers. In the case c=1, the polymer chain's monomers no longer have access to sites previously–available in the case c=0 as these are now occupied by obstacles. The chain must therefore swell with respect to the c=0 case when maximizing its conformational entropy (i.e., number of chain conformations).

The inset of Figure 12 depicts the conformational compactness $S^2=h^2/R_g^2$ of Eq. (14) as a function of obstacle concentration c for M=10 monomer chains and bears witness to a very shallow minimum (−0.5%) for c=0.7 and a slightly elevated value (+1%) for c=1.0 as compared with the c=0 value. The latter is again due to the crowding effect at c=1.0 imposed on the chain by the concentration of obstacles. The latter effect tends to push-out the chain ends, which control much of the conformational entropy as well as govern much of the dynamics. This explains why reptation media more strongly swell the h^2 statistic than that of R_g^2 (see also Table 1). As the molecular size increases, the concentration dependence of S decreases, as can be verified from comparing the inset of Figure 11 with the tabulated values of S^2 for M=25 chains (~constant with concentration c) Table 1.

In order to help quantify these statistical properties, we list conformational statistics for an M=25 chain as a function of the obstacle sub-lattice concentration limit c in Table 1.

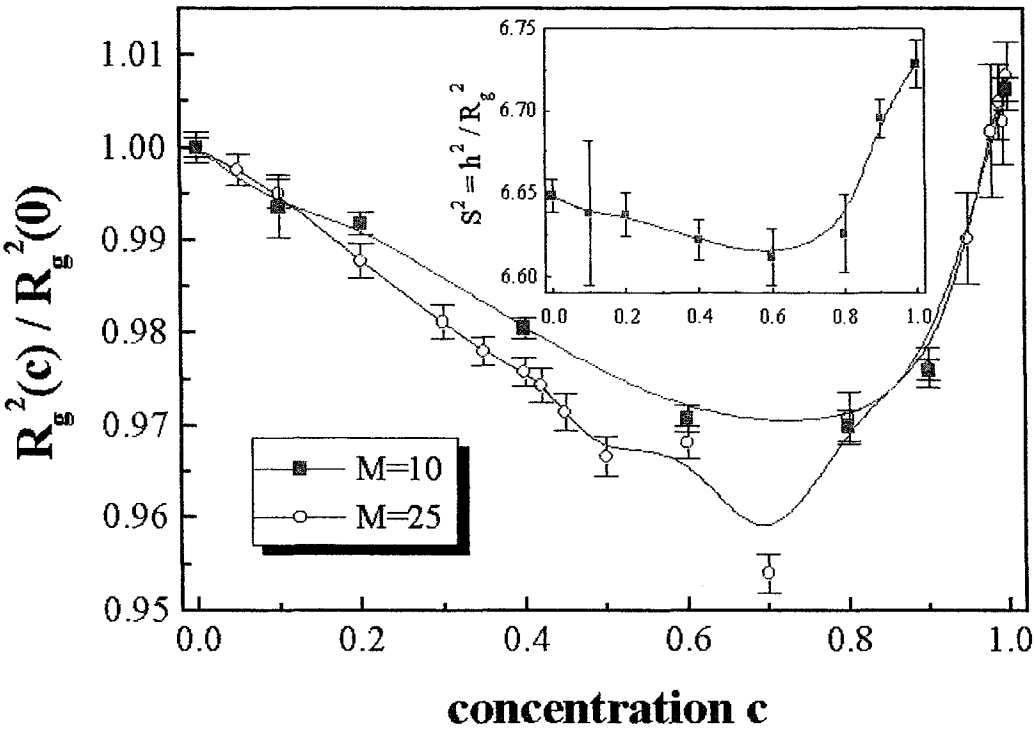

Figure 12. The reduced radius of gyration $R_g^2(c)/ R_g^2(0)$ as a function of obstacle concentration c for M=10 and M=25 chains. Inset: the span, given by ratio of the mean square end-to-end distance h^2 and the mean square radius of gyration $S^2=h^2/R_g^2$, is plotted as a function of obstacle concentration c for the case of an M=10 monomer chain.

In Table 1, we list several statistics describing the mean square end-to-end distance $\langle h^2 \rangle$ of Eq. (1), the mean square radius of gyration $\langle R_g^2 \rangle$ of Eq. (2), and the conformational compactness $S^2 = \langle h^2 \rangle / \langle R_g^2 \rangle$ of Eq. (14). Also shown are dispersion ratios $\Delta h^2 / \Delta R_g^2$ and the reduced dispersion values $\Delta h^2 / \langle h^2 \rangle$ and $\Delta R_g^2 / \langle R_g^2 \rangle$. Here, Δx signifies the standard deviation of x, noting that all properties x in the table are squared properties.

We further characterized the distribution of these observables via the skewness and kurtosis. In terms of moments μ_n, we have

$$\begin{aligned} \mu_n &= \left\langle (x - \langle x \rangle)^n \right\rangle \\ \text{std.dev.} &= \Delta x = \sigma = \sqrt{\mu_2} \\ \text{variance} &= (\Delta x)^2 = \mu_2 \\ \text{skewness} &= \mu_3 / \mu_2^{3/2} \\ \text{kurtosis} &= \mu_4 / \mu_2^2 \\ \text{kurtosis excess} &= \mu_4 / \mu_2^2 - 3 \end{aligned} \tag{54}$$

The skewness indicates the degree of asymmetry of a distribution and is generated by dividing the third central moment by the cube of the standard deviation. A negative (positive) value for skewness indicates that the distribution underlying the data has a long left- (right-) sided tail.

The coefficient of Kurtosis provides a measure of the degree of peakedness of a distribution and is generated by dividing the fourth central moment by the square of the variance of the data. For the kurtosis excess, one would expect a zero value in the case of the normal distribution, a positive value for distributions with a prominent peak and heavy tails, and a negative value for distributions with prominent flanks compared with a less pronounced peak when compared with a Gaussian shape.

In Table 1, both the mean square end-to-end distance $\langle h^2 \rangle$ and the mean square radius of gyration $\langle R_g^2 \rangle$ appear to be equally affected by disorder and contract slightly for intermediate concentrations c with a minimum around c=0.6. When ET is strongest (c=0.8-0.9), $\langle R_g^2 \rangle$ and $\langle h^2 \rangle$ decrease but are not at their respective minimum. All the statistical uncertainties in the last digits appear in round brackets. The time-averaged physical quantities have uncertainties derived using Eq. (65) together with the entire history of sampled observations (data output log) as well as the integrated conformational relaxation times, as per the discussion in Appendix B.

Table 1. The conformational properties and their statistical characterization [as per Eq. (54) on p. 46] for the case of M=25 monomer chains as a function of obstacle concentration.

M=25	*c =0.0*	*c=0.20*	*c =0.40*	*C=0.60*	*c=0.80*	*c=0.90*	*c=1.0*
$\langle h^2 \rangle$	746(3)	742(2)	726(3)	721(3)	726(5)	728(5)	754(6)
Median h^2	680.3	673.6	657.6	652.8	663.6	663.3	685.9
$\Delta\langle h^2 \rangle/\langle h^2 \rangle$	0.633	0.636	0.637	0.636	0.632	0.633	0.633
Skewness h^2	0.711	0.722	0.733	0.734	0.712	0.714	0.688
Kurtosis h^2	3.24	3.24	3.298	3.287	3.264	3.226	3.136
$\langle R_g^2 \rangle$	105.6(2)	104.3(2)	103.0(2)	102.2(3)	102.5(4)	103.1(4)	106.4(5)
Median R_g^2	99.9	98.6	97.4	96.4	97.24	98.19	100.87
$\Delta\langle R_g^2 \rangle/\langle R_g^2 \rangle$	0.361	0.362	0.363	0.363	0.363	0.361	0.355
Skewness R_g^2	0.773	0.779	0.798	0.808	0.757	0.790	0.739
Kurtosis R_g^2	3.51	3.54	3.60	3.61	3.51	3.57	3.38
$S^2=\langle h^2 \rangle/\langle R_g^2 \rangle$	7.07(4)	7.06(5)	7.05(4)	7.06(5)	7.08(8)	7.06(7)	7.08(9)
$\langle h^2/R_g^2 \rangle$	6.61	6.60	6.59	6.60	6.62	6.60	6.61
Median (h^2/R_g^2)	6.79	6.78	6.76	6.77	6.81	6.78	6.81
$\Delta h^2/\Delta R_g^2$	12.39	12.39	12.36	12.35	12.35	12.40	12.62
Skewness (h^2/R_g^2)	-0.167	-0.155	-0.157	-0.158	-0.180	-0.156	-0.174
Kurtosis (h^2/R_g^2)	2.32	2.33	2.32	2.33	2.33	2.33	2.29

In the table, the mean square end-to-end distance $\langle h^2 \rangle$ of Eq. (1), the mean square radius of gyration $\langle R_g^2 \rangle$ of Eq. (2), and the conformational compactness $S^2=\langle h^2 \rangle/\langle R_g^2 \rangle$ of Eq. (14) are shown as a function of the concentration of obstacles c. The quantity in round brackets represents the uncertainty in the final digit of the corresponding computed quantity. Also shown are dispersion ratios $\Delta h^2/\Delta R_g^2$ and the reduced dispersion values $\Delta h^2/\langle h^2 \rangle$ and $\Delta R_g^2/\langle R_g^2 \rangle$. In the table, $\Delta x=[\Sigma(x-\langle x \rangle)^2/(n_{eff}-1)]^{1/2}$ signifies the standard deviation of property x for an effective ensemble size n_{eff} of independent observations [see Eq. (66)] after combining the results of several independent simulation runs. The table also provides further characterization of the distributions for the quantities via the median, the skewness, and the kurtosis, as defined in Eq. (54) on p. 46.

The median values for h^2 and R_g^2 are smaller than the mean values $\langle h^2 \rangle$ and $\langle R_g^2 \rangle$, indicating the data are slightly skewed, as seen by skewness values >0. Moreover, the kurtosis values for h^2 and R_g^2 are greater than 3 (and thus the excess kurtosis>0). This signifies that the respective distributions for h^2 and R_g^2 are more strongly peaked than what would be expected were the distributions bell-shaped (normal distributions).

In the case of the conformation compactness S^2, it does not appear affected by the obstacle concentration, within the uncertainties of our data. The same can be said for the distribution of the relative values $\langle h^2/R_g^2 \rangle$ for the ensemble of chains where the latter value is somewhat smaller than that naively suggested by S^2 for the compactness. As such $\langle h^2/R_g^2 \rangle$ is perhaps a better measure of the asymmetry of the chain. The skewness of this chain asymmetry value h^2/R_g^2 is negative so the distribution is characterized by a long left tail of compact conformations with respect to the mean, yielding a media value for the h^2/R_g^2 distribution that is larger than the mean value. The kurtosis of h^2/R_g^2 is less than 3, indicating that the peak is less prominent than the normal distribution, indicative of a rather broad distribution about the mean.

Interestingly, as far as can be determined from the tabulated values, the concentration of obstacles does not appear to have a large effect on the distribution functions for the quantities measured (and in particular for $\langle R_g^2 \rangle$ and $\langle h^2 \rangle$). For instance, in the case c=0.9, despite the large number of obstacles in the lattice space, the mean square sizes appear only slightly decreased with respect to the zero obstacle lattice case c=0. There appears to be a small overall decrease in the mean square sizes $\langle R_g^2 \rangle$ (i.e., -3.1%) and $\langle h^2 \rangle$ (i.e., -3.4%) as we decrease c from c=1 to c=0.9. But the decrease are small, running counter to the notion of highly collapsed states existing in strong ET systems, as had been predicted by Sommer and Blumen in the case of RW chains (Sommer 1999). In fact, the most compact conformations for M=25 appear in the case c=0.6 where ET is actually much weaker (as shown later by its larger diffusion coefficient relative to the c=0.9 case) but where larger porous regions exist.

The most striking case is for c=1 where there is a perfectly periodic array of obstacles. Here, the chains are generally more extended, particularly in the case of the h^2 (+1 %) and to a lesser extent R_g^2 (+0.8%) when compared with the obstacle-free lattice case. The width of the distribution for R_g^2 also appears narrower than the widths for R_g^2 at all other concentrations c.

Therefore, in order to further characterize the influence of the environment on the conformational statistics of our linear polymers, we also investigated the behaviour of the distribution function

p(H,c), see Eq.(10), for the reduced end-to-end distance (amplitude) H in the case of M=25 and c=0.9 (where, as we will show, ET effects are strong). We recall, from Eq. (10), that for for c=0, we expect $p(H<1)\sim H^{4/9}$ and $p(H>1)\sim H^{2/3}\,\mathrm{Exp}[-\lambda H^4]$. The probability distribution function is derived from the history file of simulation outputs for the static properties output file which contains, among other things, the output for the moments of the end-to-end distance.

In Figure 13, we plot probability distribution function p(H,c) of Eq. (10) against the reduced end-to-end distance $H=h/\langle h^2\rangle^{1/2}$ for an M=25 chain. In the top left figure for c=0, the data are consistent with the expected scaling. Similarly, in the top right figure (c=0.90), the data are again consistent with predicted scaling form of p(H,c=0). In fact, both figures appear virtually identical within the limits of experimental error. We note that the graininess of the data is due to the discrete finite set of possible simulation conformations within the range $h\epsilon[2, (7488)^{1/2}]$ with $h_{min}=2$ being the minimum possible distance between monomers and $h_{max}=(13)^{1/2}\times(25-1)\approx 86.53$ for a I-shaped conformation with M-1 maximally extended bonds. The corresponding extreme values H_{min} and H_{max} vary somewhat with c but the approximate range $H\epsilon[0.07, 3.2]$ applies for all obstacle concentrations c.

By way of comparison, we coarse-bin the data and superpose both data sets (c=0 and c=0.90 for M=25 chains) in Figure 14. The overall degree of correspondence is very striking, confirming that the data appear almost identical in the cases c=0 and c=0.9.

In Figure 13 (bottom left), we plot ln[P(H<1,c=0.9)] against ln H and find the fit to be consistent with the scaling form expected for an M=25 chain in the c=0 case, despite chains experiencing strong entropic trapping. Specifically, the best fit=–1.537(64)+[4.19(54)/9] ln[H] is consistent with a slope 4/9 whereas the zeroth order term –1.537(64) is consistent with the value -3/2 expected for data in the c=0 limit.

In Figure 13 (bottom right), we plot ln[P(H>1,c=0.9)] against H^4 and note the correspondence with the H^4 dependence for large H one would expect in the c=0 limit. The best fit is given by

$-1.132(53)+(1/6)\ \ln(H^4) - 0.5153(53)\ H^4$, where the slope 1/6 was held fixed during the fit because the expected coefficient for the $\ln(H^4)$ term is 1/6 while that of the H^4 term is –1/2. The data are found to be consistent with the zero obstacle concentration form.

Even though c=0.9 corresponds to a case where ET is strong, we must conclude that disorder (and ET) has little effect, if any, on the predicted c=0 distribution function. However, in order to magnify

subtle differences, we now investigate the relative differential distribution function $\Delta p(h,c) \equiv [p(h,c) - p(h,0)]/p(h,0)$ against h, as shown in Figure 15 for M=25 and c=0.4, 0.8, 0.9 and 1.

If Figure 15, we see that dense conformations, $h < (\langle h^2 \rangle^{1/2} \approx 27)$, are slightly enriched ($\Delta p(h,c) \approx +3$-5%) for c=0.4 while swollen conformations are severely depleted.

For c=0.8, there is a slight overall degree of enrichment ($\Delta p(h,c) \approx +2\%$) for $15 < h < 30$ (possibly noise-related) and for $h < 5$ whereas the swollen conformations ($h > 34$) are highly depleted. For c=0.9, the depletion region begins earlier ($h > 30$) but now, we observe a net (and corresponding) enrichment ($\Delta p(c,h) \approx 5$-10%) for conformations $h < 27$.

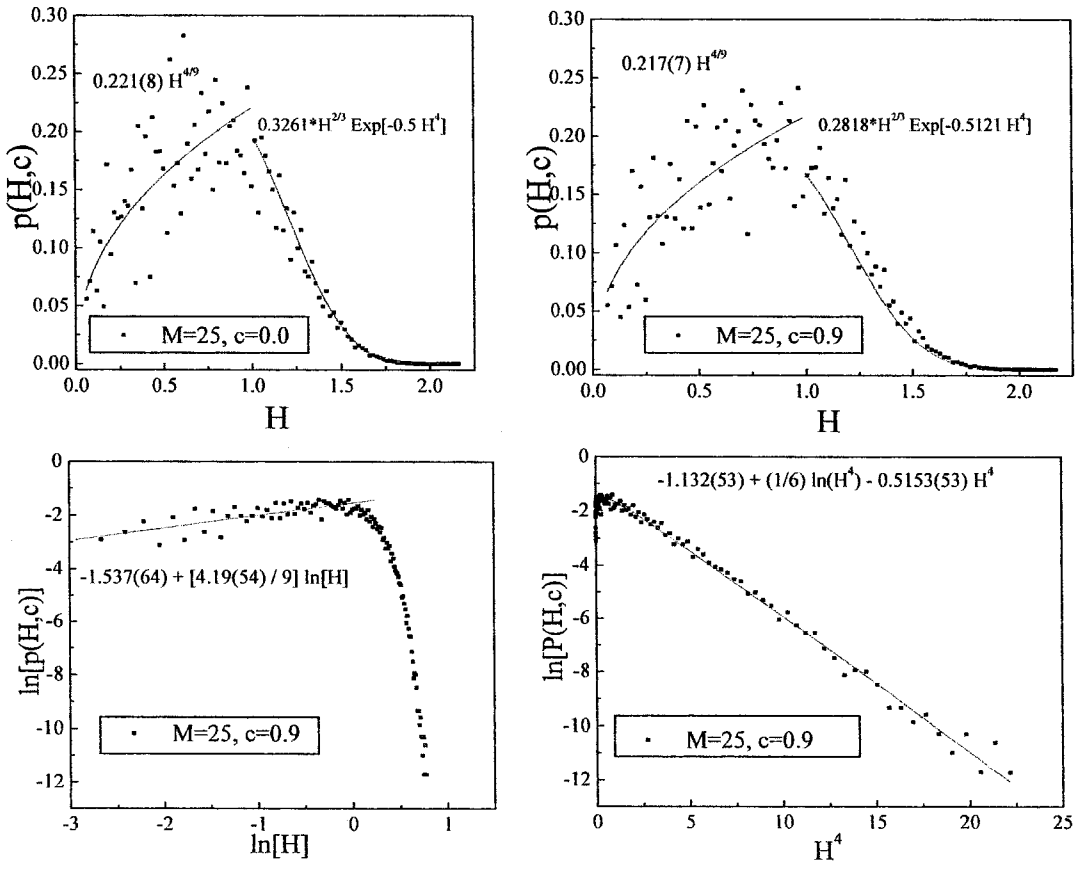

Figure 13. The probability distribution function p(H,c) of Eq. (10) is plotted versus the reduced end-to-end distance $H=h/\langle h^2\rangle^{1/2}$ for an M=25 chain where we have $H\epsilon[0.07, 3.2]$ as the maximum possible range of available conformations.

Top left: Here we plot ln[p(H,c=0)] vs. ln H and generate theory motivated fits consistent with $p(H<1, c=0)\sim H^{4/9}$ and $p(H>1, c=0)\sim H^{2/3}\exp[-\lambda H^4]$ with λ being a constant, as expected for c=0. Top right: This is the same plot, but now it is for an M=25 chain in the strong entropic trapping regime c=0.90. Bottom left: Here we modify the scales to highlight the small amplitude (H<1) scaling form of p(H,c=0.90). Bottom right: Again, we modify the scales but this time in order to highlight the scaling form of p(H,c=0.90) in the case of large amplitudes (H>1). We see that the scaling forms predicted for c=0.0 also remain valid in the strong trapping regime c=0.90.

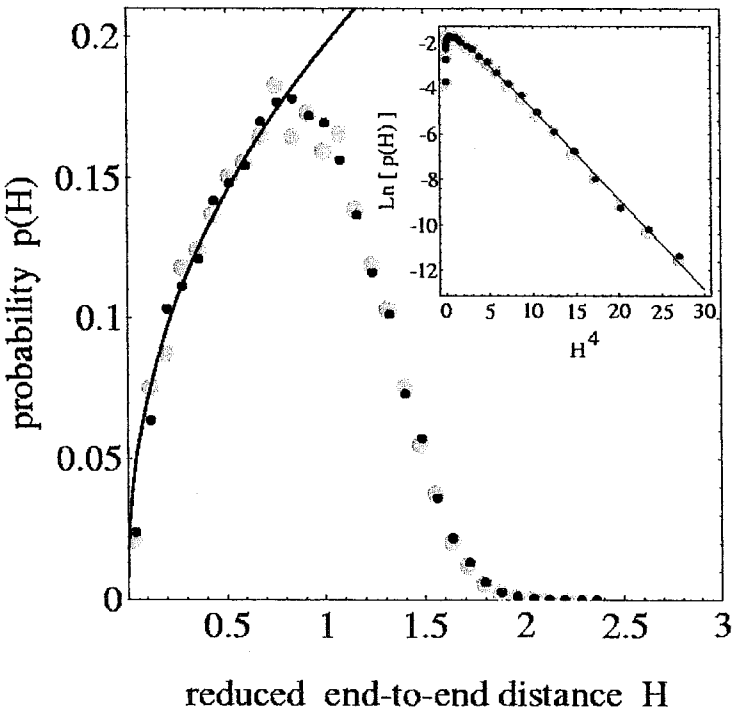

Figure 14. Superposed data for the coarsely-binned probability distribution function p(H,c) of Figure 13 where M=25 , c=0.0 (large filled circles) and M=25, c=0.90 (small filled black circles).

Main figure: The theory-motivated fit is $p(H)=(H/38.84)^{4/9}$ for all conformations H<0.9. Inset: The theory-motivated form of the fit yields the result $p(H)=(H/6.756)^{2/3}\ Exp[-0.4045\ H^4]$ for conformations H>1.2. The maximum possible range of available conformations is $H\epsilon[0.07, 3.2]$.

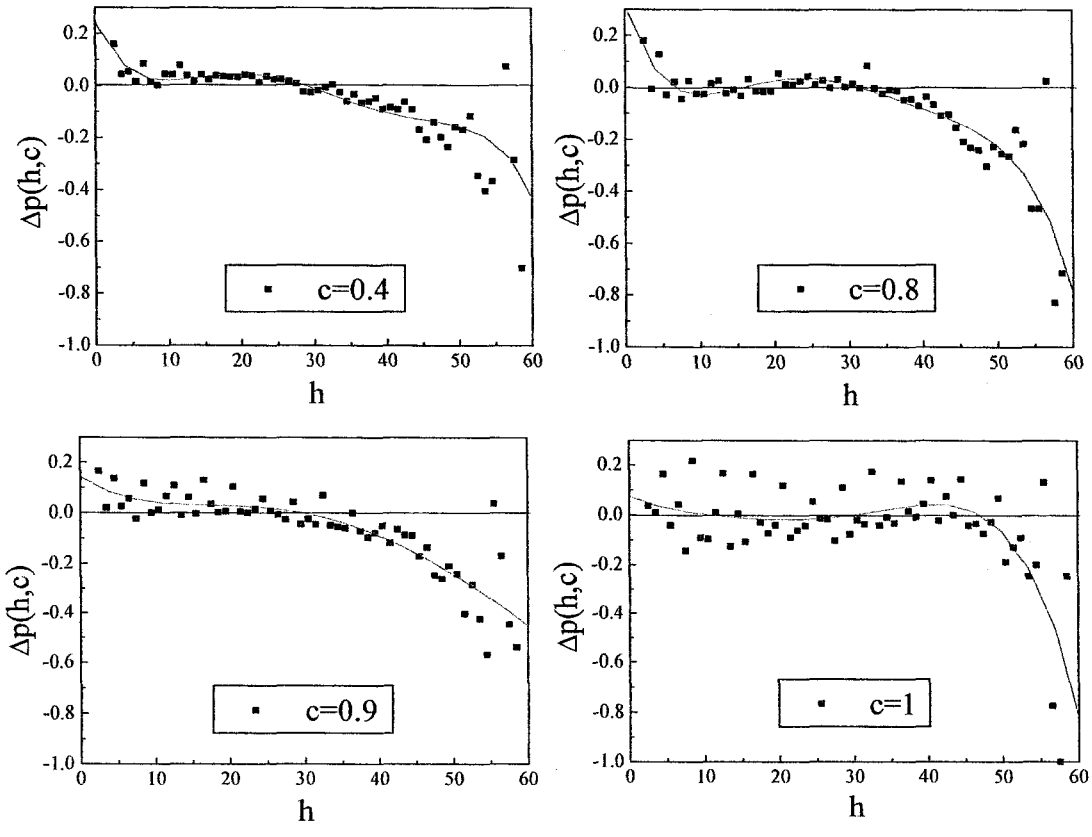

Figure 15. The relative differential distribution function $\Delta p(h,c) \equiv [p(h,c) - p(h,0)]/p(h,0)$ for a M=25 polymer chain is plotted vs. the end-to-end distance h for c=0.4, 0.8, 0.9, and c=1.0 respectively. In all cases, $\langle h^2 \rangle^{1/2} \approx 27$, as seen from Table 1.

These plots reveal subtle differences in p(h,c) as a function of concentration, with regions of depletion and enrichment becoming evident. Such information cannot be resolved in plots such as those of Figure 13 and Figure 14.

Finally, in the reptation limit (c=1.0), we observe no net overall trend in $\Delta p(h,c)$ of the end-to-end distance as compared to the free-chain. The appears to be a slight enrichment ($\Delta p(c,h) \approx 0$-10%) in the region $h \approx 41$ (or $H \approx 1.5$) but the contribution of these extended or swollen states to ensemble averages is small due to the low overall probability of these extended states (see Figure 14). The fluctuations observed for ($h<50$) stem mostly from a large intrinsic variability in the discrete occupation probability density p(c,h) due to the finite size of the chains with their smaller number of available conformations in our lattice system.

Statistical uncertainty becomes significant in the extreme tail region ($h \gtrsim 50$ or $H \gtrsim 2$). There, we observe large oscillations. Nonetheless, for all cases $c>0$, the presence of obstacles is always seen to deplete the density of these highly extended states.

Interestingly, there is a strong enrichment effect ($\Delta p(c,h) \lesssim 20\%$) for the smallest conformations h=2 for c=0.4, 0.8, and 0.9; this effect is due to entropic trapping. The competition between monomer crowding and conformational entropy will determine the degree of "polymer collapse" for the given system (unlike the case for RW polymers as shown, e.g., by Sommer and Blumen (Sommer and Blumen 1996).

In conclusion, we find that for intermediate concentrations of obstacles ($0<c<1$), the disorder so-created does not significantly affect the mean conformational properties of the polymer chains when compared with the obstacle-free case. This result is quite surprising. A slight enrichment in the compressed states causes both $\langle R_g^2 \rangle$ and $\langle h^2 \rangle$ to go through a shallow minimum at $c \approx 0.6$-0.8, but the effective M-scaling laws as well as the probability of a given polymer size appear essentially unaltered from that expected for a free chain (c=0).

3.3 Steady-State (normal) Diffusion

We will now look into the (effective) scaling properties of the steady-state (SS) diffusion coefficient D of Eq. (29). First we will establish that the model (BFA) conforms with the expected molecular-size (M) scaling forms in the extreme limits of zero obstacle sub-lattice concentration (c=0 or Rouse limit) and in the perfectly periodic obstacle concentration limit (c=1 or reptation limit, for which our chains are SAWs without the EV screening one has in the melt). Next, we will look at the effective scaling forms for intermediate concentrations of obstacles with random voids.

It may prove useful to first get an overall perspective of the matter at hand. To this end, we plot, in Figure 16, the variation of D throughout the obstacle concentration range (c=0 to c=1) for several molecular sizes M=10, 15, 20, 25, 30, 40, and 50. What is first apparent is that, for all species studied, we notice a monotonic decrease in the diffusion coefficient D(M,c) as c increases from c=0 to c=0.8-0.9. This decrease is followed immediately with an abrupt overall increase as we move from c=0.9 to c=1 (the reptation limit). At first, this behaviour may appear somewhat counter-intuitive as it implies that removing obstacles from a reptative lattice (c=1), which increases the amount of diffusion space for the chains, actually hinders the polymer's diffusivity through the fixed network of obstacles. The creation of a few isolated pores is thus a greater impediment to diffusion than the presence of a full set of obstacles at those sites. The reason for this behaviour, of course, is that the creation of these pores leads to conformational entropic trapping (ET) for the chains. Monomer segments become "trapped" at these pore sites, hindering CM diffusion because of the large entropic barriers that then populate the potential energy landscape. As such, this behaviour is a key signature of an ET system.

Entropic trapping has traditionally been studied in terms of the effective M-dependence of the diffusion coefficient $D(M,c)\sim M^{-\delta}$ of Eq. (30), despite the fact that D is expected to depend exponentially on M via $D\sim\exp(-\chi\times M)$, as per Eq. (51). In Figure 17, we reveal the molecular size dependency of D for concentrations c=0, 0.2, 0.4, 0.8, 0.9, and 1. The abscissas were scaled to nullify the expected reptational (c=1) molecular size dependence $D\sim M^{-3/2}$ for SAW chains devoid of EV screening. The data for c=1 is seen to asymptotically approach a horizontal slope for $M\gtrsim 80$ indicating that $\delta=3/2$, as expected [see Eq.(41)]. Interestingly, for all non-zero concentrations shown, we observe negative slopes indicating that $\delta>3/2$ (for those sizes studied here) with δ possibly decreasing slightly with increasing molecular size for c=0.2 and c=0.4. For the intermediate concentrations considered $0.2\leq c<1$, we note that the molecular size-dependency is in fact stronger than that for reptation, i.e. $\delta(c)>\delta(c=1)=3/2$ with a maximum found in the strong ET region (see Figure 17 inset). Note that the effective exponent values plotted in the inset are those of the best straight line fits (solid lines) over the range of sizes $5\leq M\leq 100$. We have not forced the exponents for c=0 and c=1 to conform to the expected values ($\delta=1$ and $\delta=3/2$, respectively) although our data are clearly consistent with these asymptotic values.

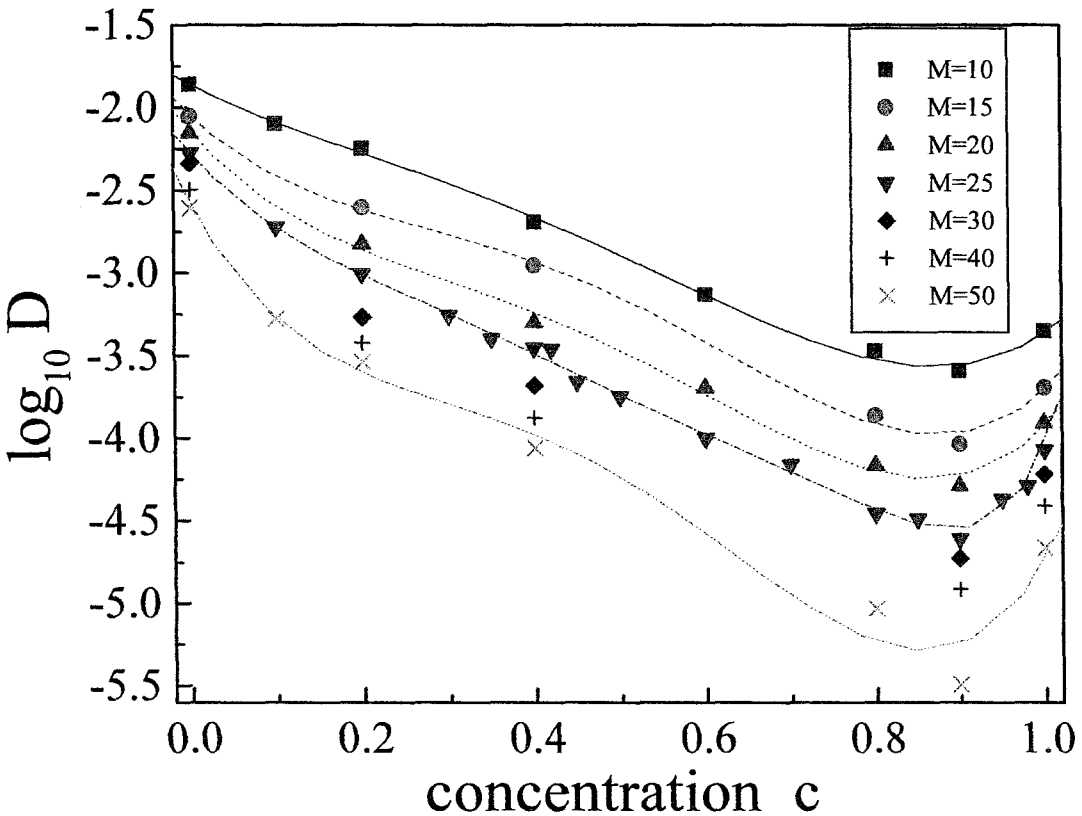

Figure 16. The steady-state diffusion coefficient is plotted as a function of concentration c for various molecular sizes M. The lines are merely guides for the eye.

We remark the monotonic decrease in D with concentration up to c=0.8-0.9 following which the values of D begin to increase up to the reptation limit c=1.

We also note, for c=0.2, that for large M, we appear to approach the same effective M-scaling as that of reptation, as indicated by the dashed line. Unfortunately, attempting to attain true $M\to\infty$ scaling (if indeed such a $D\sim M^{-\delta}$ scaling form exists) for intermediate concentrations, especially for the higher concentrations such as c=0.8 and c=0.9, is computationally prohibitive.

Figure 18 reveals the relative scaling of the diffusion coefficients D(c) to the reptational value D(c=1) via the log-log plot of D(c)/D(1) vs. M for c=0.2, 0.4, 0.6, 0.8, and c=0.9. We observe that some of the curves (c=0.6, 0.8, and c=0.9) are strongly concave-down indicating that the steady-state diffusion coefficients $D(0.6\leq c\leq 0.9)$ continue to decrease relative to the D(c=1) values as we increase M (for the sizes investigated).

The question as to what happens when chain spans over many entropic pores remains an open one. Yet, one might expect reptation to occur in the limit $M\to\infty$. However, as all systems are de facto finite, disorder effects may render reptation intrinsically unstable for most real systems.

It is also interesting to look at the distribution of steady-state hopping times. To this end, we plot (see first plot of Figure 19) the natural logarithm of the probability distribution function $p(s=10,\tau)$ for the time taken by a M=25 monomer chain to diffuse over a distance $s=R_g(M=25)\approx 10$ in a system with obstacle sublattice concentration c=0.80. Interestingly, we observe stretched exponential behaviour whose long-time behaviour is governed by the function $p(\tau)=\mathrm{Exp}[-(\tau/\tau_0)^{\alpha}]$ with $\tau_0=4.17(3)\times 10^5$ and $\alpha=0.568(6)$. The second figure has a slope that corresponds with the stretching exponent α. This slope ($\alpha=0.568\pm 0.006$) was then used to fix the value of the stretching exponent before performing the nonlinear fit for $p(\tau)$.

From the log-log plot, we see that a simple parsimonious stretched exponential function governs the distribution of diffusive hopping times, for times larger than the conformational relaxation time, over a distance equal to the radius of gyration. The data for the shorter times, which are not characterized by a single stretching exponent, are due to the fact that the distribution of times must return to zero at zero time for any finite hopping length. For example, in the absence of obstacles, the absolute minimum possible time for hopping a distance of 10 lattice spaces requires that all M monomer jump (one lattice spacing) in the same direction, ten times in succession. This extremely rare event would thus correspond to 10 MC time steps in this model.

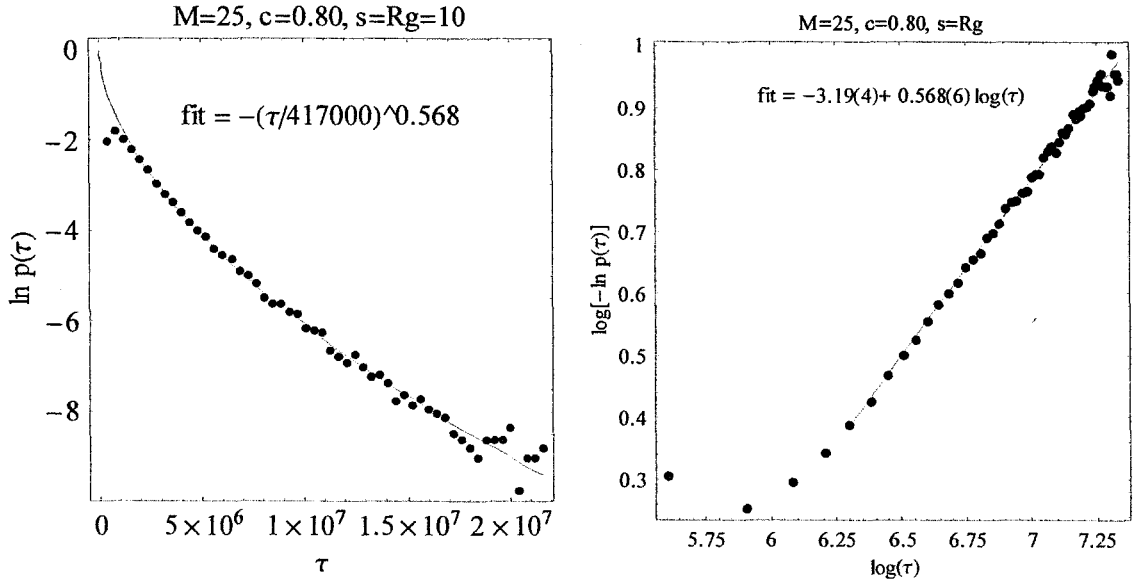

Figure 19. The probability distribution function for the time taken by an M=25 monomer chain to migrate over a root-mean-squared diffusion distance equivalent to its own radius of gyration $s=\langle R_{CM}^2\rangle^{1/2}\approx R_g(M=25)=10$ in a c=0.80 system. The second plot was used to determine the stretching exponent, which was then held fixed before performing the nonlinear fit in the first figure. The resulting solid line fit is $\ln[p(\tau)] = -(\tau/\tau_0)^{0.568(6)}$ with resulting parameter $\tau_0=4.17(3)\times10^5$ being of the same order as the conformational relaxation times of the M=25 chain $\tau_{k=1}$ and τ_h for c=0.8.

According to the theory of purely stretched exponential distribution functions, the stretching exponent α=0.568 corresponds to a relative hopping time distribution width of $\Delta_{\alpha=0.568}=\sigma_\tau/\langle\tau\rangle\approx 1.40$ [see Eq.(18)], representing a rather broad-tailed distribution.

In Figure 20, therefore, we plot the relative distribution width $\Delta_\alpha(\tau,s)=\sigma_\tau/\langle\tau\rangle$ for hopping times τ as a function of the relative root-mean-squared diffusion distance $s/R_g=\langle R_{CM}^2\rangle^{1/2}/R_g$ for the same M=25 chain in the same system and where the concentration of random voids is (1-c)=0.2. We note a characteristic maximum $\Delta_\alpha(\tau,s)\approx 1.65(10)$ occurring for distances $s\approx 4R_g$ which we will show (Figure 22) corresponds with R_{SS}. The distribution width of "hopping times" is seen to be very broad over distances quite long compared with the radius of gyration, as expected, because of the long transient diffusion regimes which are indicative of disorder over long length scales. The distribution widths appear to decrease progressively towards unity as the length scale is increased, consistent with the expected limit on the basis of Eqs.(46) and (47) as we exceed the steady state distance R_{SS} [see Eq.(31)].

In a later section, we will show that conformational relaxation is intimately-related to the anomalous subdiffusion (β<1) regimes. Next, however, we will look at the diffusion of the central monomers.

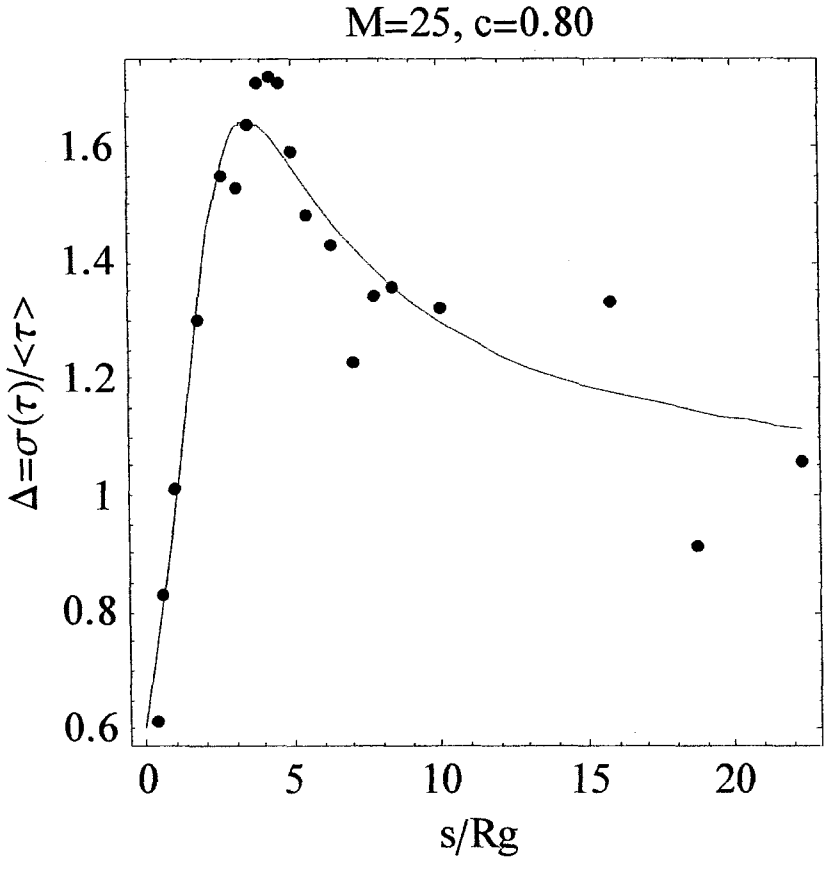

Figure 20. Ratio $\Delta_\alpha(\tau,s)=\sigma_\tau/\langle\tau\rangle$ for the distribution of diffusion (hopping) times τ as a function of root-mean-squared diffusion distance $s=\langle\Delta R_{CM}^2\rangle^{1/2}$, in units of the radius of gyration $R_g\approx10$, for an M=25 chain in a obstacle array with c=0.80.

The solid line is merely a guide for the eye. We note that the distribution has a characteristic maximum $\Delta_\alpha(\tau,s)\approx1.65(10)$ for $s\approx4R_g$ followed by a very broad tail that approaches unity (as would be typical for normal, steady-state diffusion) for large length scales $s\gg R_g$.

3.4 Subdiffusion

It is well-established that the diffusion of polymers over short time scales may be anomalous [see Eq. (27)] in disordered systems such that $\langle[\Delta R_{CM}(t)]^2\rangle=4D^*t^\beta$, with $\beta\neq1$ being the anomalous-diffusion exponent and D^* the anomalous-diffusion coefficient [see, e.g., (Baumgärtner and Moon 1989)]. In disordered systems such as ours, anomalous diffusion, when it exists, always takes the form of sub-diffusion (SD) where $\beta<1$ after which, for long-enough times, one recovers normal, steady-state (SS) behaviour ($\beta=1$) [see also Figure 6]. According to our definitions, Eq. (27) and Eq. (32), anomalous diffusion is observed only over time scales $t<\tau_{ss}$ and the anomalous exponent β is unity for c=0 and c=1. This is also reminiscent of the problem of the ant in the labyrinth (Baumgärtner and Muthukumar 1996), a simpler case of diffusion in a complex medium, and where it is found that $\beta=2/3$.

In Figure 21 (main figure) appears a log-log plot of the mean square displacement of the center of mass (CM) for an M=25 chain as a function of time t for concentrations c=0, 0.2, 0.4, 0.6, 0.8, 0.9, 1. Anomalous diffusion regimes precede the steady state for all intermediate concentrations $0<c<1$. The anomalous diffusion regimes become progressively longer, and particularly so as c approaches the strong entropic trapping regime (c=0.8-0.9), where the local residency time inside the porous regions can become extreme (as will be seen later in Figure 25). As such, SS diffusion is only attained very late and the diffusion coefficient for these concentrations thus becomes less than that for reptation, as we saw in Section 3.3 (see Figure 16).

Also note that the CM diffusion is seen to be normal for all times for concentrations c=0 and c=1, as expected, and the steady-state time $\tau_{ss}=(D^*/D)^{1/(1-\beta)}$, ($\beta\neq1$) [see Eq. (32)] becomes ill-defined, although nothing precludes assigning it a zero value by definition. Unfortunately, the definition of the steady state time and length scales render a systematic analysis of τ_{ss} very difficult because of the uncertainties in the determination of the anomalous and steady state diffusion coefficients (D^* and D, respectively), as well as in the determination of β, which get greatly amplified.

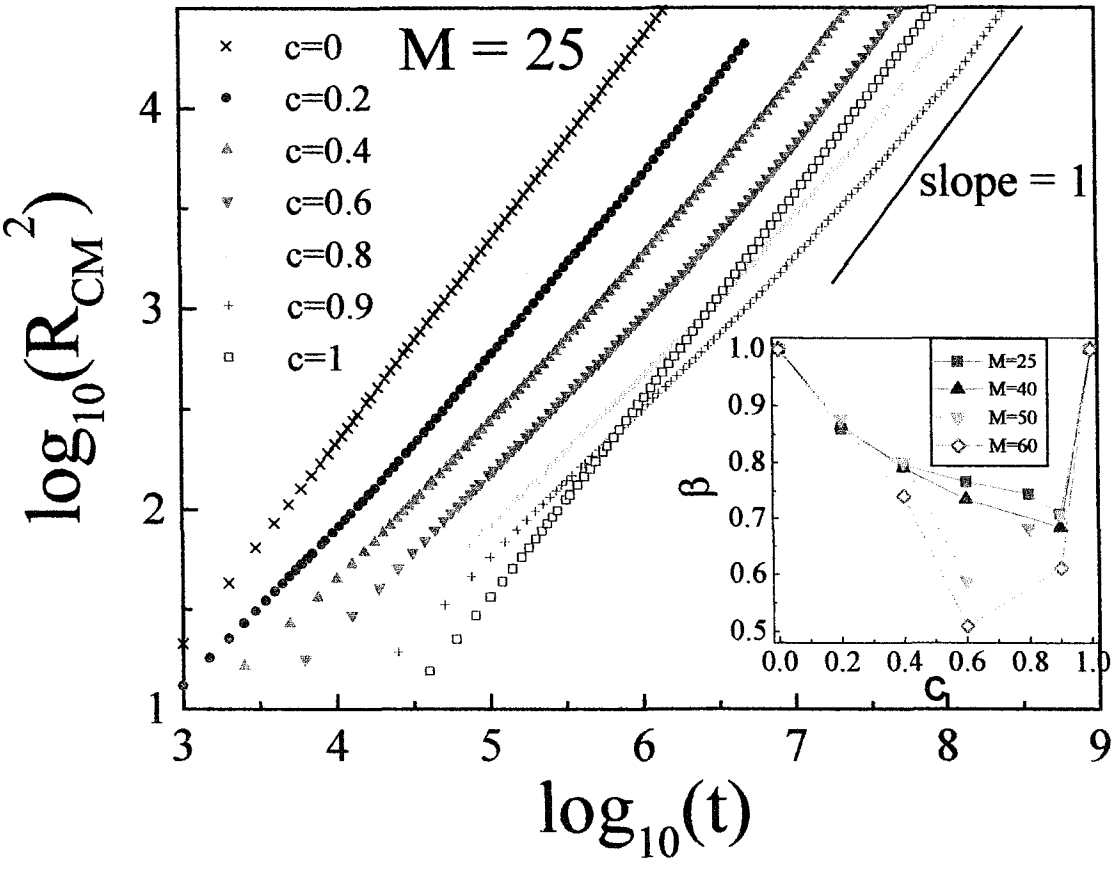

Figure 21. Main figure: Log-log plot of the mean square displacement of the center of mass for an M=25 chain as a function of time t for various obstacle concentrations (c=0, 0.2, 0.4, 0.6, 0.8, 0.9, 1). Inset: the anomalous diffusion exponent β is plotted as a function of concentration c for molecular sizes (M=10, 25, 40, 50, and 60).

In Figure 21 (inset), we plot the anomalous diffusion exponents β as a function of concentration c for molecular sizes M=10, 25, 40, 50, and 60. We remark that the anomalous diffusion exponents decrease monotonically from c=0 to about c=0.6-0.9 and then rise abruptly towards unity as c approaches c=1. This is much like the ubiquitous ET signatures seen when we looked at the SS diffusion coefficient of Figure 16 and that of the mean square sizes of the chains in Figure 12. The minimum values of β decrease with increasing molecular size and the concentration for which these minima occur also appears to decrease with increasing molecular size M. Therefore, anomalous diffusion in ET systems appears to be a strong function of molecular size.

In Figure 22, we have a log-log plot of the mean square displacement of the centre-of-mass for M=25 chains as a function of time t for concentrations c=0, 0.2, 0.4, 0.6, 0.9, 1. For the case c=0.9, we indicate the steady-state time τ_{SS}, as derived from Eq. (32). We see that normal diffusion for M=25 and c=0.9, as determined from the onset of unit slope for the data, is only attained for $t \gg (\tau_{SS} \approx 10^{7.4})$. Here, the steady normal diffusion is only attained for time $\approx$2 orders of magnitude longer that that for reptation ($\sim 10^{5.8}$, as shown later in Figure 33), a strong indication of the dominance of the ET phenomenon in controlling the dynamics in systems characterized with even few void defects in an otherwise perfectly-periodic obstacle lattice.

3.5 Short Time Dynamics: diffusion of the central monomers

A classic observable is the well-known dynamics of the central monomer in the Rouse (c=0) and reptation (c=1) limits. In particular, there are four (4) characteristic reptation time regimes that uniquely identify reptative monomer diffusion. Let us briefly recall the definition of the mean square displacement of the central monomer, $g_1(t)$, of Eq.(33), and the description of the scaling of g_1 with time in the case of reptation (section 2.4).

In the case c=1, for short length scales $g_1<d_T^2$ where d_T is the effective "tube diameter" (c.f., p=4), the motion is predicted to follow the Rouse-like scaling form $g_1(t)\sim t^{1/(1+1/2\nu))}\sim t^{3/5}$ for times $t<\tau_R(M_p)$= relaxation time of a "reptation blob", where M_p is the number of chain segments forming the blobs inside the effective reptation tube. For times $t>\tau_R(M_p)$, the chain's motion follows the "tube axis" and $g_1(t)\sim t^{\nu/2}\sim t^{3/8}$ up to the Rouse relaxation time. For $\tau_R<t<\tau_D$, the central monomer follows the diffusion of the CM in the random-walk tube and $g_1(t)\sim t^{\nu}\sim t^{3/4}$, followed by terminal CM diffusion $g_1(t)\sim t^1$ for $t>\tau_D$. Therefore, the monomers do not follow the CM motion until after conformational relaxation has occurred.

In Figure 23 (and Figure 24), the dynamics of the central monomer are revealed for the cases c=0, c=0.1, c=0.4, c=0.9 (c=0.8), as well as c=1. In Figure 23 (main figure), we have a log-log plot of the mean square displacement of $g_1(t)$ (for the "centre bead"=CB) in the case of an M=25 chain as a function of time. For reference, the Rouse relaxation time $\tau_R\approx 10^{4.20}$ as well as the reptation time $\tau_D\approx 10^{5.84}$ are indicated as "Rouse time" and "reptation time", respectively, as do the predicted temporal regimes (annotated slope values) for both the Rouse and reptation dynamics. Note that for c=1, we show only the last 3 regimes because the narrow reptation tube (i.e., our choice of small p=4) does not permit us to resolve the first. Strong finite-size effects cause our M=25 chains to deviate marginally from the predicted slopes. Note that the terminal, steady-state regime is clearly attained in all the cases shown, as revealed by the unit slopes. We note that, for M=25 (see Table 1), the mean square radius of gyration $\langle R_g^2\rangle\in[102,106]\approx 10^{2.02(1)}$ and mean square end-to-end distance $\langle h^2\rangle\in[721,754]\approx 10^{2.87(1)}$. In cases where c=0.8 (Figure 24) and c=0.9 (Figure 23), SS diffusion is attained for length scales $R_{SS}\approx 4R_g$ and time scales $\tau_{SS}\approx 10^{7.4}$.

Figure 23 (Inset), we have an expanded view of $g_1(t)$ in the vicinity of the reptation time. We note that, while the monomer diffusion in the Rouse case (c=0) and the reptation case (c=1) have attained the steady-state (i.e., $g_1(t)$ follows the motion of the CM), the monomer diffusion for the cases c=0.4

and c=0.9 remain well within the transient diffusion regime, indicative of fact that the distribution of the voids controls the onset of the steady-state.

In Figure 25, we have a density plot of the occupation probability for the central monomer for an M=25 chain inside a 60×60 lattice for an imperfect obstacle array with obstacle concentration c=0.9 and with periodic boundary conditions in effect. The four gray-shades represent regions for which the central monomer occupies 25% of it simulation time. As such, the gray-shades delimit 25% occupancy spaces, with entropic trapping being evident near void spaces. This is a striking pictorial example of the entropic trapping effect.

ET effectively removes the key reptative signatures expected for the central monomers despite the fact that the overwhelming number of obstacle sites is still present, constituting vast contiguous spaces of perfectly periodic obstacles where polymers simply must reptate. Clearly then, reptation, which must occur for the diffusing molecules when migrating from trap to trap although, given the time spent in the vicinity of voids Figure 25, the reptation proper makes a negligible contribution to the overall dynamical picture as far as diffusion is concerned. Reptation is thus not the dominant mode of diffusion in a system with even slight disorder (i.e., even for 1-c=10%). We conclude that reptation is intrinsically unstable with respect to slight, fixed disorder, certainly at least in the case of a polymer that cannot occupy several traps simultaneously. Figure 25 clearly demonstrates that time-averaged properties are dominated by the trapping regions where the chain spends most of its time ($\gtrsim$75%).

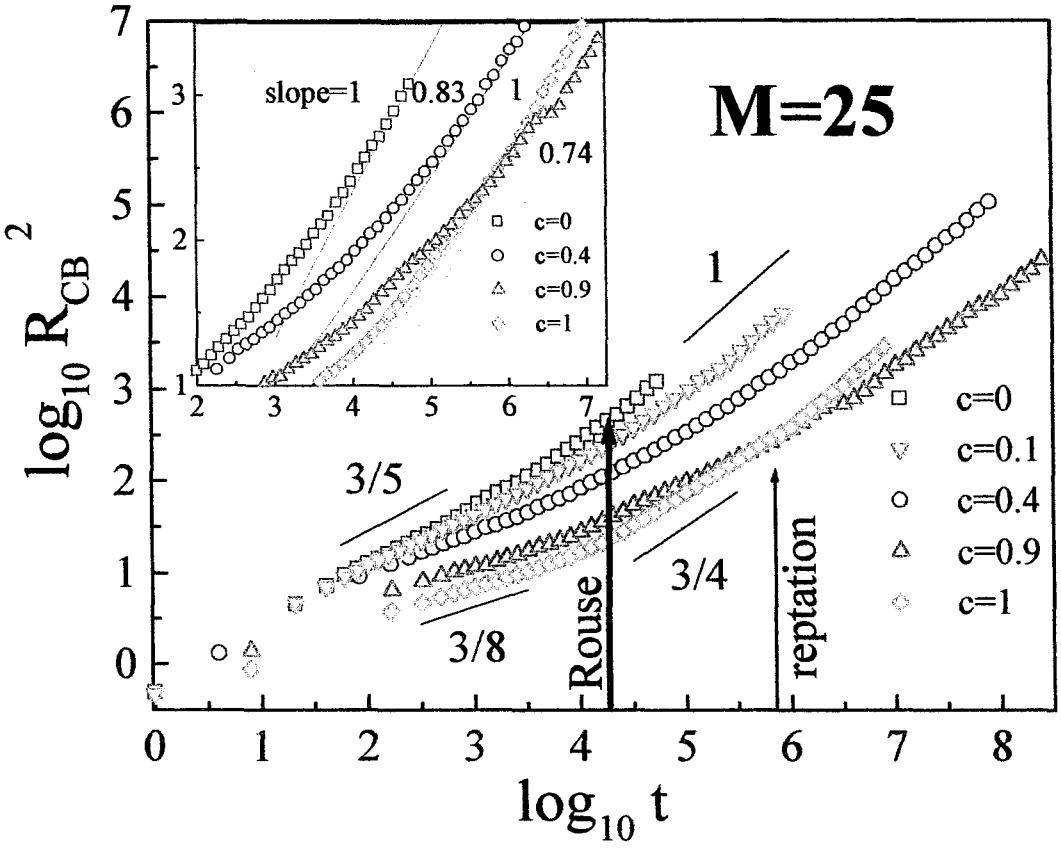

Figure 23. Main figure: Log-log plot of the mean square displacement of the central monomer ("centre bead"=CB) [$g_1(t)$ of Eq. (33)] for an M=25 monomer chain as a function of time at concentrations c=0 (Rouse limit), c=0.1, c=0.4, c=0.9, and c=1 (reptation limit).

The well-known Rouse relaxation time $\tau_R \approx 10^{4.20}$ as well as the reptation time $\tau_D \approx 10^{5.84}$ appear on the time axis for reference. Also shown are the expected regimes (as identified by the annotated slopes) in the case of Rouse and reptative dynamics. Inset: A slightly expanded view of $g_1(t)$, detailing the regime intermediate between the Rouse and the reptation times. We note that, when the monomer diffusion in the Rouse case (c=0) and the reptation case (c=1) first attain the steady-state, monomer diffusion for the cases c=0.4 and c=0.9 remain well within the transient regime $g_1(t) \sim t^w$ (with w<1).

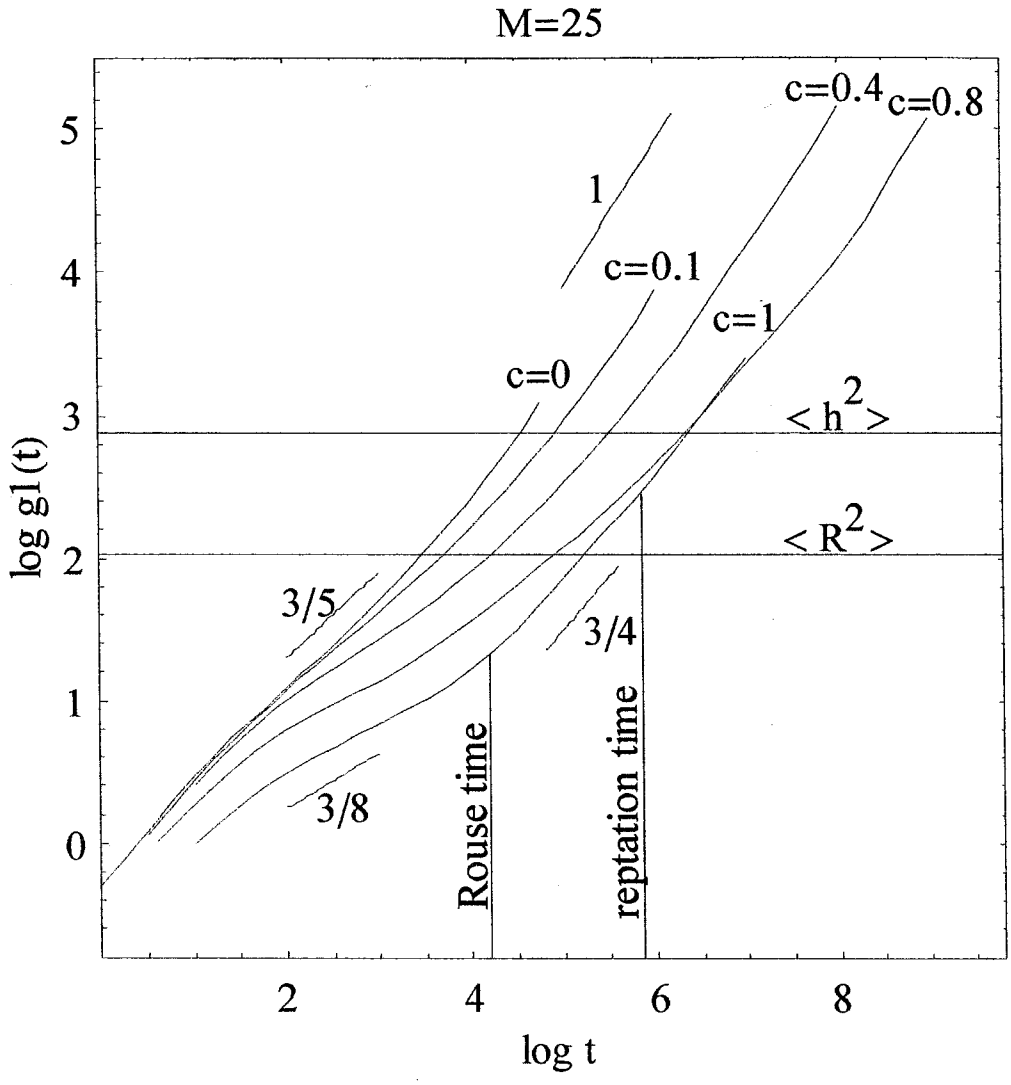

Figure 24. Log-log plot of the mean square displacement of the central monomer $g_1(t)$ of Eq. (33) for an M=25 bead chain as a function of time and concentrations c=0, c=0.1, c=0.4, c=0.8, and c=1.

The data have been smoothed in order to better compare the various power regimes, $g_1(t)\sim t^w$, predicted for Rouse and reptation dynamics. Nominal values for the Rouse time $\tau_R\approx 10^{4.20}$, reptation time $\tau_D\approx 10^{5.84}$, mean square radius of gyration $\langle R_g^2\rangle\approx 10^{2.02}$, and mean square end-to-end distance $\langle h^2\rangle\approx 10^{2.87}$ appear for reference. The long, transient, sub-diffusion regimes (w<1) for both c=0.4 and c=0.8 last well-beyond the reptation time. Terminal (steady-state) diffusion is attained for $\tau_{SS}\approx 10^{7.4}$ and $g_1(t)\gtrsim 10^{3.6}\approx(2.3h)^2\approx(4R_g)^2$ in the case of c=0.8.

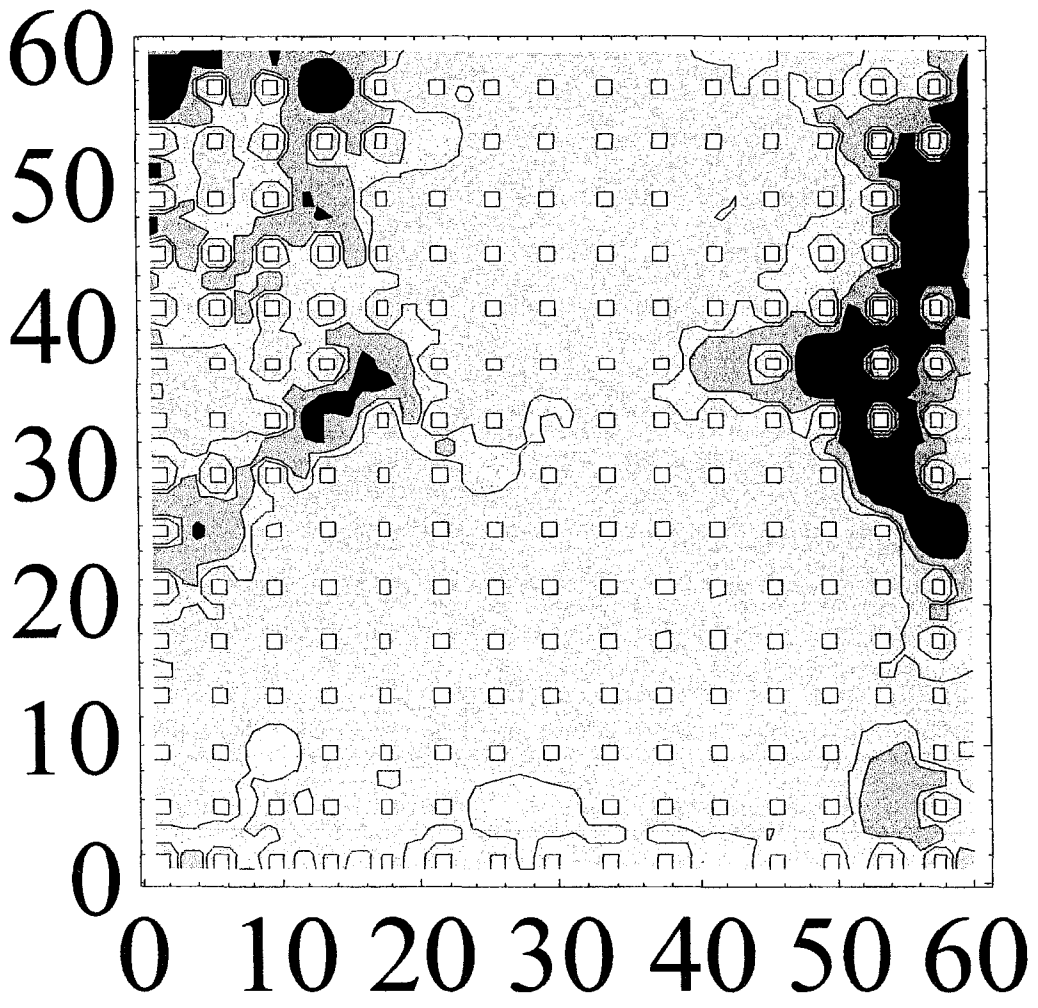

Figure 25. Density plot of the occupation probability for the central monomer for an M=25 chain inside a 60×60 lattice within an imperfect obstacle array with c=0.9 and with periodic boundary conditions.

The four shades of gray delimit 25% occupancy spaces, with entropic trapping being evident near void spaces.

3.6 Relaxation Times and Relaxation "Modes"

In Figure 26, we plot the decay curves for the autocorrelation function $C_k(t)$ for the first four "modes" k of a free M=25 chain (c=0); the inset shows the same information plotted for the reptation limit (c=1). In the case of c=0, we observe simple exponential decays and the predicted $\tau_k \sim (M/k)^{2\nu+1} \sim (M/k)^{5/2}$ scaling law of Eq. (38) is recovered as we have renormalized the time-axis via $k^{5/2}t$ which renders all the mode data collinear. However, there is slightly faster short time decay which is likely the result of mode-mode coupling caused by the self-excluded volume interactions, as described by Downey (Downey 1994). Downey has studied the relaxation modes of free (i.e., c=0) two-dimensional polymer chains using the BFA. He states that the relaxation is exponential for long times (α_k=1), and that the relaxation times scale as $\tau_k \sim (M/k)^{5/2}$, in full agreement with our results.

For c=1 (Figure 26, inset) however, the decay curves for the higher modes appear to be slightly concave for long times, and the $k^{5/2}$ scaling form for the modes, while not appearing inconsistent, is not so well-established as it is for c=0. Thus, the 5/2 exponent for the modes appears to be too large for the c=1 case, effectively stretching the data along the time axis.

In Figure 27, we show a log-log plot of the (integrated) relaxation time τ_k of Eq. (26) as a function of mode wavelength (M/k) for c=0 and for different sizes M. The slope of 5/2 corroborates the expected scaling $\tau_k(M, c=0) \sim (M/k)^{5/2}$ which is also in agreement with Downey (Downey 1994).

In the inset of Figure 27, we show the log-log plot of the scaled conformational relaxation time τ_k/M vs. mode wavelength (M/k) for c=1. Note that, for the sizes studied ($M \leq 100$), the scaling $\tau_k \sim M(M/k)^{5/2}$ conforms rather well with the data over the small to intermediate length scales ($4 \leq M/k \leq 40$), as corroborated by the M=25 data (inset of Figure 26) for which the various modes correspond very nearly for this effective scaling form. However, reptation theory, proper, predicts that $\tau_k(M) \sim M(M/k)^2$, with finite size effects scaling as $(k/M)^{1/2}$ to first-order (i.e., the so-called contour-length fluctuations) (Doi 1986). Therefore, using this predicted behaviour as a guide [as embodied by Eq. (42)], we are led to the theory-motivated fit

$$\tau_k(M) = M(M/k)^2[9.04(14) - 14.49(76)/(M/k)^{1/2} + 8.29(87)/(M/k)]^2 \qquad (55)$$

which has been taken up to second-order in view of the small length scales (note that the digits in round parentheses indicate the standard errors on the associated fitted constants).

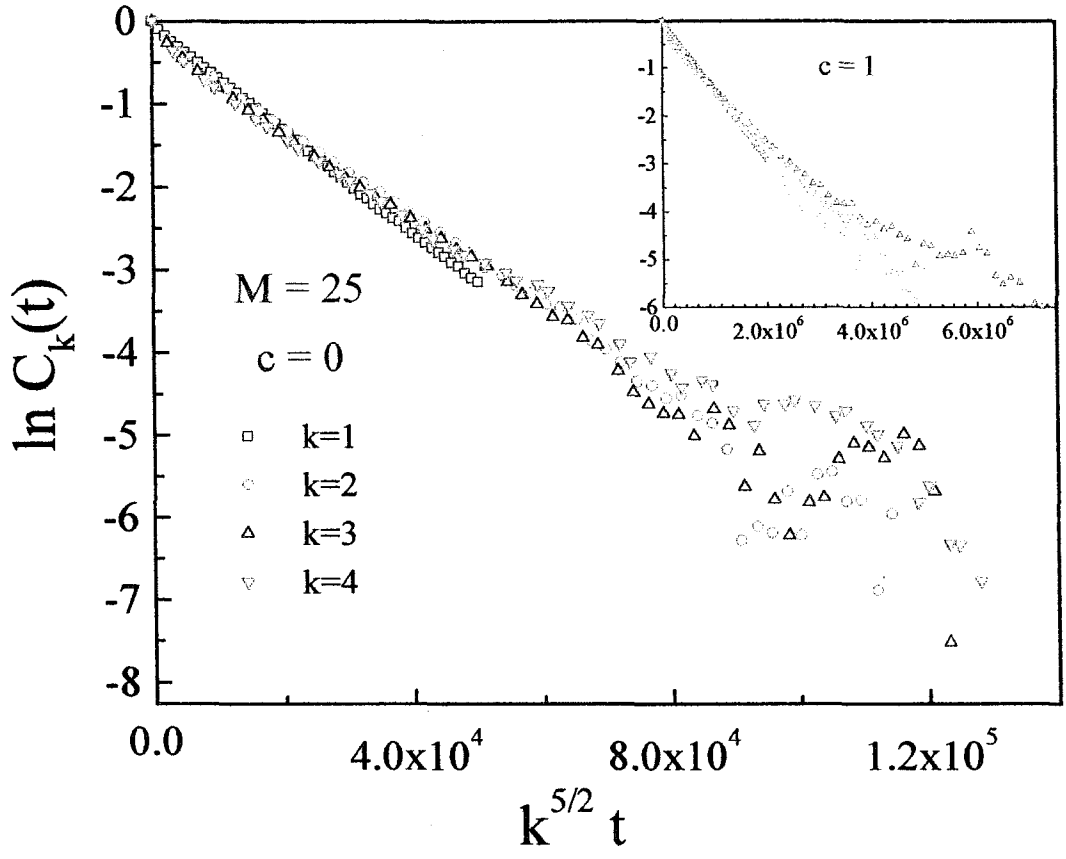

Figure 26. The natural logarithm of the autocorrelation function of the Fourier coordinates of Eq. (21) for an M=25 chain is plotted as a function of (mode-scaled) time $k^{5/2}t$ for the obstacle-free case (main figure) and for the perfectly periodic lattice of obstacles (inset). In the classical Rouse and reptation models, the relaxation for the "normal" modes (k =1-4) correspond to the relaxation of chain segments (subchains) of size M/k.

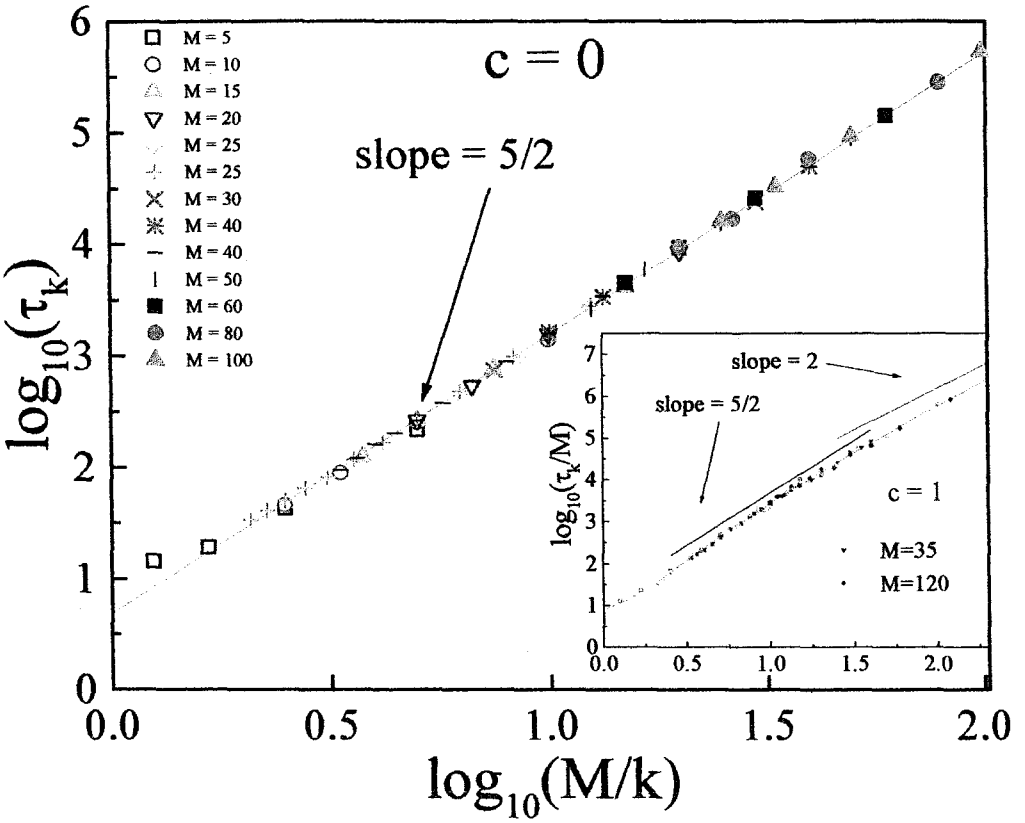

Figure 27. Log-log plot of the conformational relaxation time of Eq. (26) vs. mode wavelength (M/k) for the obstacle-free case c=0 (main figure) and the perfectly periodic lattice case c=1 (inset).

In the main figure, the slope of 5/2 is shown to correspond well with the data for M=5-100 and modes k=1-4. In the inset, the time has been scaled according to molecular-size (M=5-120) and thus a slope of 2 is expected [see Eq. (42)] for long mode wavelength, M/k, according to the reptation theory. The asymptotic behaviour of our data appears to be consistent with this expected form but confirmation is computationally prohibitive. Interestingly, we remark that an effective slope of 5/2 corresponds closely with the data for the intermediate mode wavelengths ($10^{0.6}\approx4$)$\lesssim$M/k$\lesssim$($10^{1.6}\approx40$) shown whereas the longer mode wavelengths appear to converge towards the expected slope of 2. The best overall fit (taking into account finite size effects) to the data is expressed in Eq. (55).

We remark that the agreement between the fit (solid line) and the data is excellent over the whole range of length scales studied. The lack of scatter in the data suggests that the proposed form effectively embodies the functional-dependence of $\tau_k(M)$ on M and k.

There are strong finite size effects present in the case of the conformational relaxation (i.e., we do not quite attain the asymptotic slope of 2 in the inset of Figure 27), although, our data for large M (i.e., M=100-120) appear to be consistent with the expected result.

In Figure 28, we have a log-log pot of the $\tau_k(M=25)$ of Eq. (26) against mode number k for the case of an M=25 chain for obstacle concentration c=0.9. We note the excellent correspondence of the data to a straight-line fit, indicative of an effective mode scaling $\tau_k(M=25)\sim(1/k)^{3.1}$.

In Figure 29, we plot the natural logarithm of the auto-correlation function $C_k(t)$ versus mode-scaled MC time for M=25 and c=0.9 for the modes k=1-6. Here we have used the scaling form proposed in Figure 28 for the mode numbers. All mode curves agree very well with the fitted exponent and appear characteristically concave (or "stretched" in time), unlike the contrasting case k=1 for c=1 (superposed in the same figure) where pure exponential decay is clearly manifested. In the inset, we have a log-log plot of the main figure [more precisely, $\log_{10}(-\ln C_k)$ vs. $\log_{10}(t)$]. Well-established constant slopes yielding the stretching exponents α_k, for modes k=1 through k=6 (as revealed by the slopes of the lines), are evident, justifying the use of the stretched exponential functional form of Eq. (23) for describing conformational relaxation in disordered polymer systems. Also evident is the fact that the essentially constant slopes (i.e., the exponents α_k) decrease with increasing mode number k.

In Figure 29, we also note that the C_k decay curves, while well-represented by simple stretched exponentials, appear to undergo another, somewhat distinct, relaxation process during a very early (transient) regime. For instance, for $\ln(C_{k=1})>-0.3$, as revealed by the inset of Figure 29 for $\alpha_{k=1}$, there appears to be a transition regime linking a discontinuity in the slope $\alpha_{k=1}$ at the time $t\approx10^5$ (c.f., $\tau_{k=1}\approx10^{5.8}$ in Figure 32 and Figure 33 for M=25 and c=0.9). However, for the time scales most of interest (i.e., for the overwhelming majority of the time over which the conformation relaxation process takes place), the data describing the decay of the auto-correlation functions confirm that the Kaulrauch-Williams-Watts (KWW), or stretched-exponential functional form $C_k\sim\exp[-(t/\tau_k)^{\alpha}]$ of Eq.(23) describes the conformational relaxation process exceedingly well.

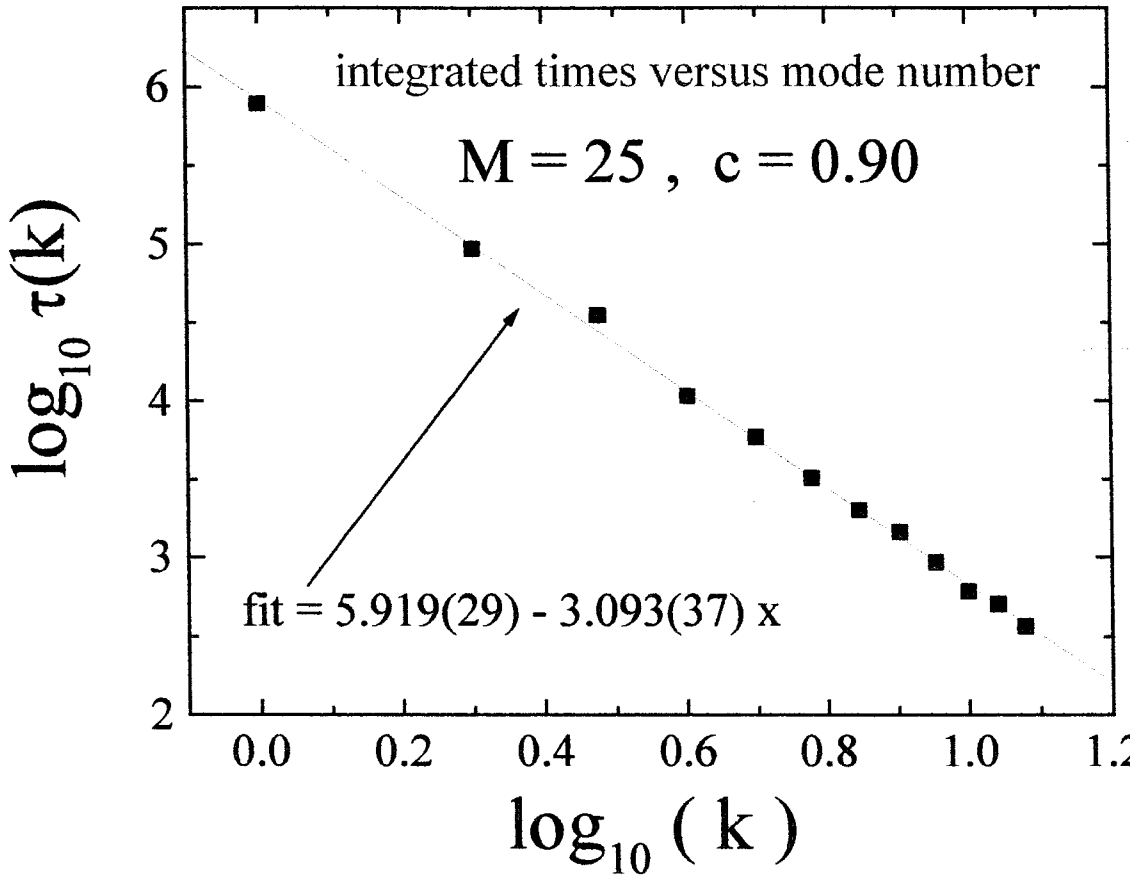

Figure 28. Log-log pot of the integrated conformational relaxation times τ_k of Eq. (26) against mode number k for the case of an M=25 monomer chain in a medium with obstacle concentration c=0.9. The mode scaling for the M=25 chain conforms well to the empirical form $\tau_k(M=25) \sim (1/k)^{3.1}$.

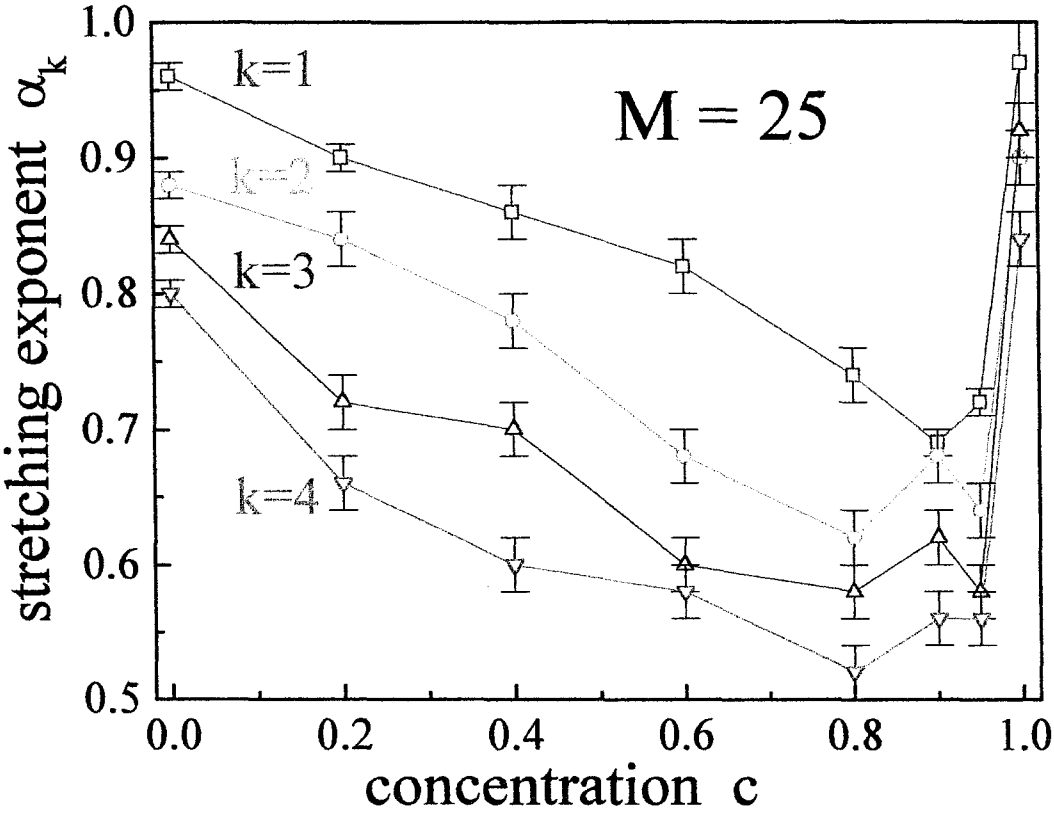

Figure 30. The stretching exponents α_k for modal conformation relaxation (for modes k=1, 2, 3 and 4) are plotted as a function of the obstacle concentration c in the case of an M=25 monomer chain.

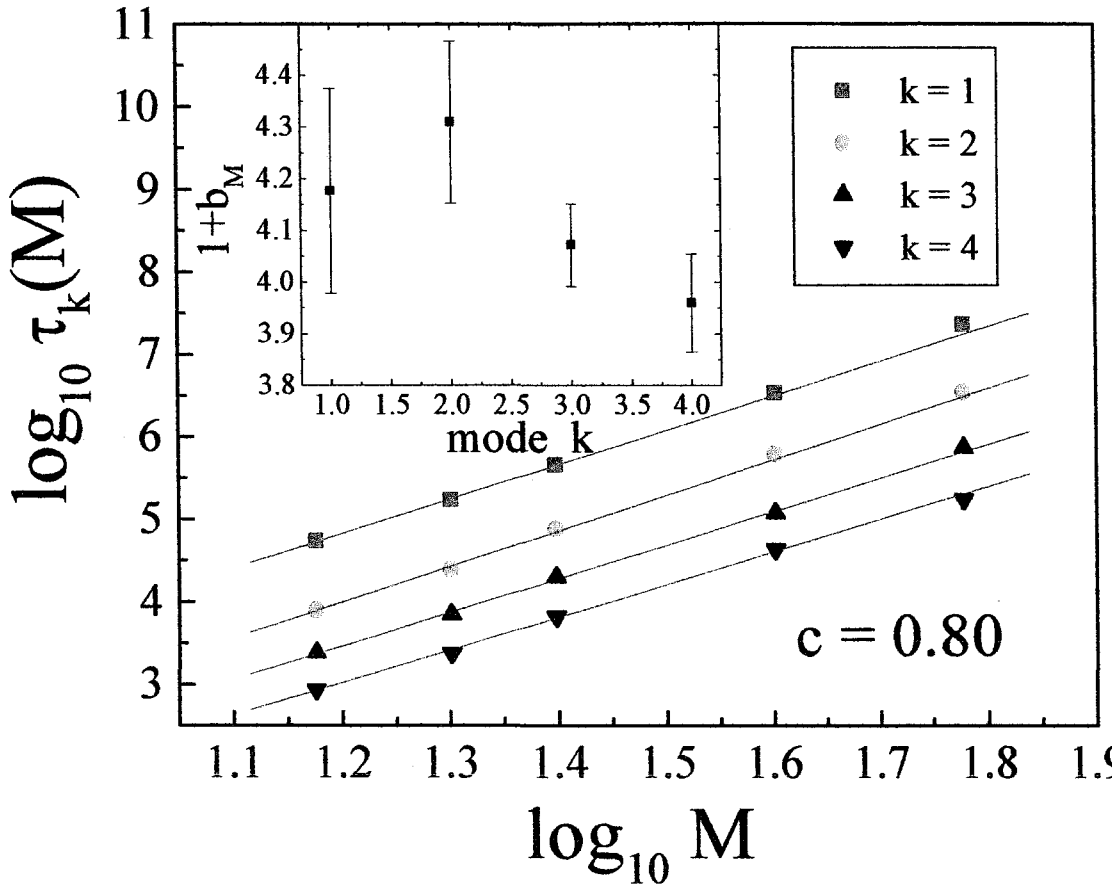

Figure 31. Log-log plot of $\tau_k(M)$ against M reveals the effective molecular-size dependence of the conformational relaxation times for the case c=0.8 for mode numbers k=1, 2, 3, and 4. We note that the exponent for the molecular-size dependence for the longest mode (k=1) is of the order of 4.18(20), as compared to b_M=1.5 for the Rouse limit c=0, and b_M=2 for the reptation limit c=1.

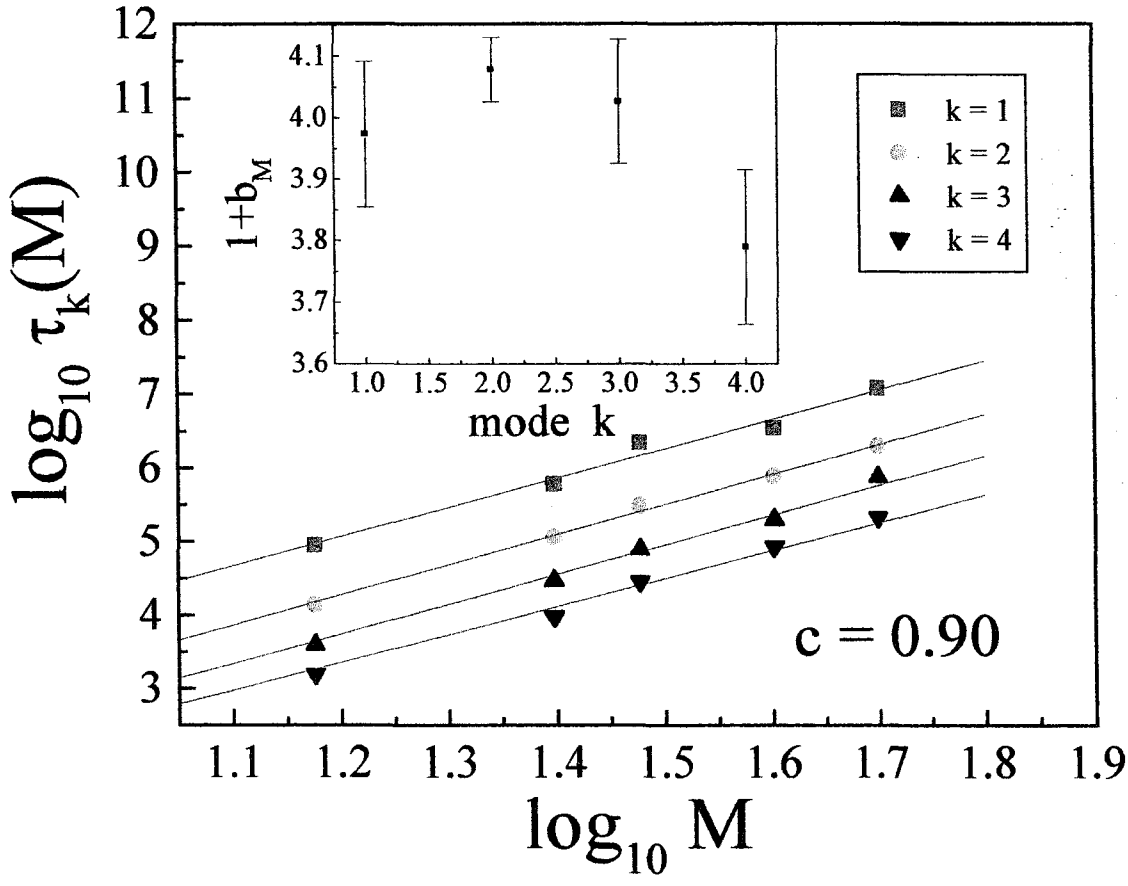

Figure 32. Log-log plot of $\tau_k(M)$ against M reveals the effective molecular-size dependence of the conformational relaxation times for the case c=0.9 for mode numbers k=1, 2, 3, and 4. We note that the exponent for the molecular-size dependence for the longest mode (k=1) is of the order of 3.97(12), as compared to b_M=1.5 for the Rouse limit c=0, and b_M=2 for the reptation limit c=1.

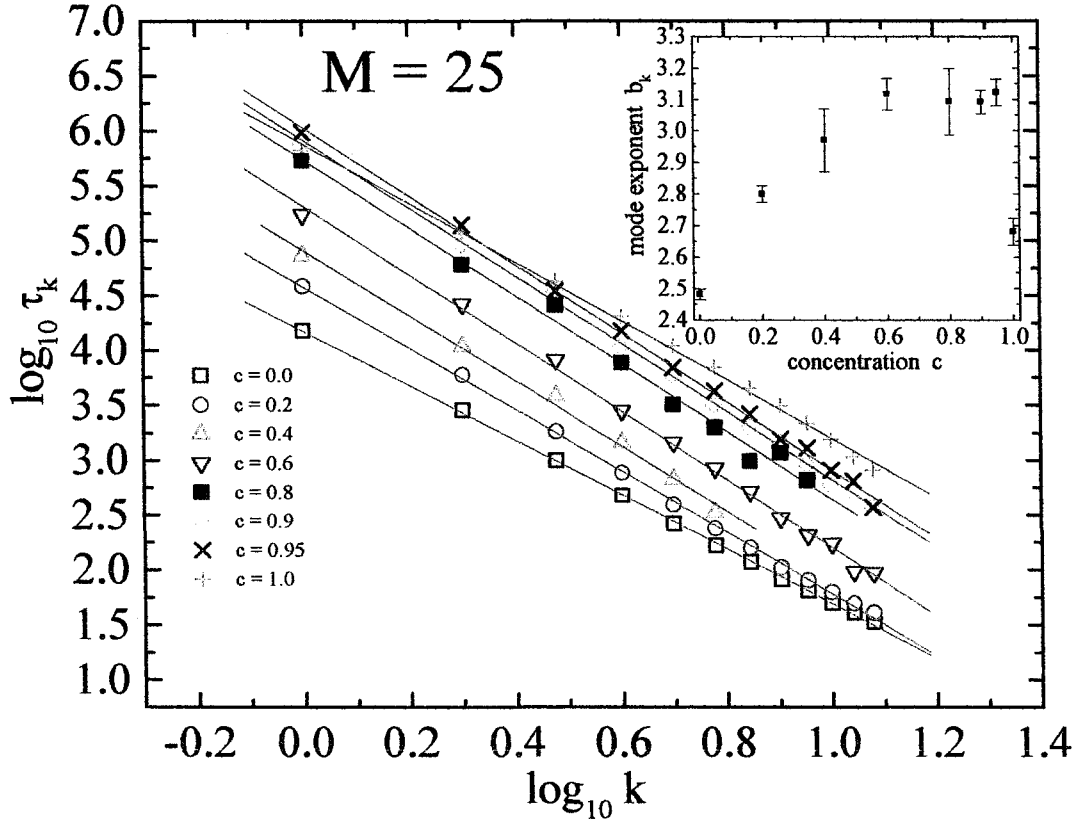

Figure 33. Main figure: Log-log plot of the integrated conformational relaxation times τ_k(M=25) against mode number k for various concentrations c=0–1. Inset: The mode exponent b_k is plotted as a function of concentration c.

In Figure 34, we have a log-log plot of the integrated conformational relaxation time for the end-to-end distance h as a function of molecular size M. We note that the effective values for the exponents are given by $b_{M,h}(c=0)=2.55(3)$, $b_{M,h}(c=0.2)=3.28(8)$, $b_{M,h}(c=0.4)=3.50(6)$, $b_{M,h}(c=0.9)=4.14(9)$, and $b_{M,h}(c=1)=3.36(4)$. While the c=0 result is in close agreement with the expected 5/2 scaling, all cases c>0 exhibit stronger molecular-size dependencies than what was found in the case of mode number k=1, a result that is somewhat surprising given the expected correspondence between h and $X_{k=1}$ of Eq. (21). However, this correspondence is only strictly established in the case of random walk chains.

In the inset of Figure 34, the exponents α_h and β are plotted against concentration c for the case M=25. We remark that the degree of stretching is most pronounced for $c\approx 0.7$-0.9 (i.e., in the presence of a small degree of disorder). We note the very close correspondence between these two exponents over the whole range of concentrations. The stretching exponents α_k decrease with increasing k (e.g. see Figure 30) as we involve the smaller length scales. We also note that the α_k increase extremely rapidly with concentration for c>0.9 towards the reptation value c=1, indicating the extreme instability of reptation with respect to slight disorder.

In Figure 35, we plot the "total molecular size scaling exponent" $(1+b_M)$ of Eq. (24) for $\tau(k=1) \sim M^{1+b_M} / k^{b_k} \sim \tau(h) \sim M^{1+b_M}$ as a function of concentration c for modes k=1-4 and $5 \le M \le 100$. The effective exponent $(1+b_M)$ is strongly concentration dependent and attains a global maximum $(1+b_M)\approx 4.2(3)$ in the vicinity $c\approx 0.8$ for modes k=1-4. In the inset, we plot $b_M(h)$, $b_M(k=1)$ and $b_k(M=25)$ against obstacle concentration c and remark that the mode exponent b_k attains a maximum value of about 3.1 ± 0.1 for M=25 at $c\approx 0.8$, consistent with what was observed in the case of M=25 with c=0.9, as seen in Figure 28 and Figure 29 where we found $b_k\approx 3.1$. We also see that $b_M(h)$ closely corresponds with $b_M(k=1)$, as expected. Note that the b_k are slightly molecular-size dependent. Interestingly, we observe $b_k \approx b_M$ for $c \ge 0.6$, similarly to what is expected in the reptation limit (c=1) as per Eq. (42). Unlike the case of reptation, however, for c=0.8, we yield the effective scaling relationship $\tau_k(c\approx 0.8) \sim M \times (M/k)^{3.1}$ for molecular sizes $M \lesssim 60$.

Next, we will show how the stretched-exponential behaviour for the relaxation is related to the anomalous diffusion regimes over which conformational relaxation takes place.

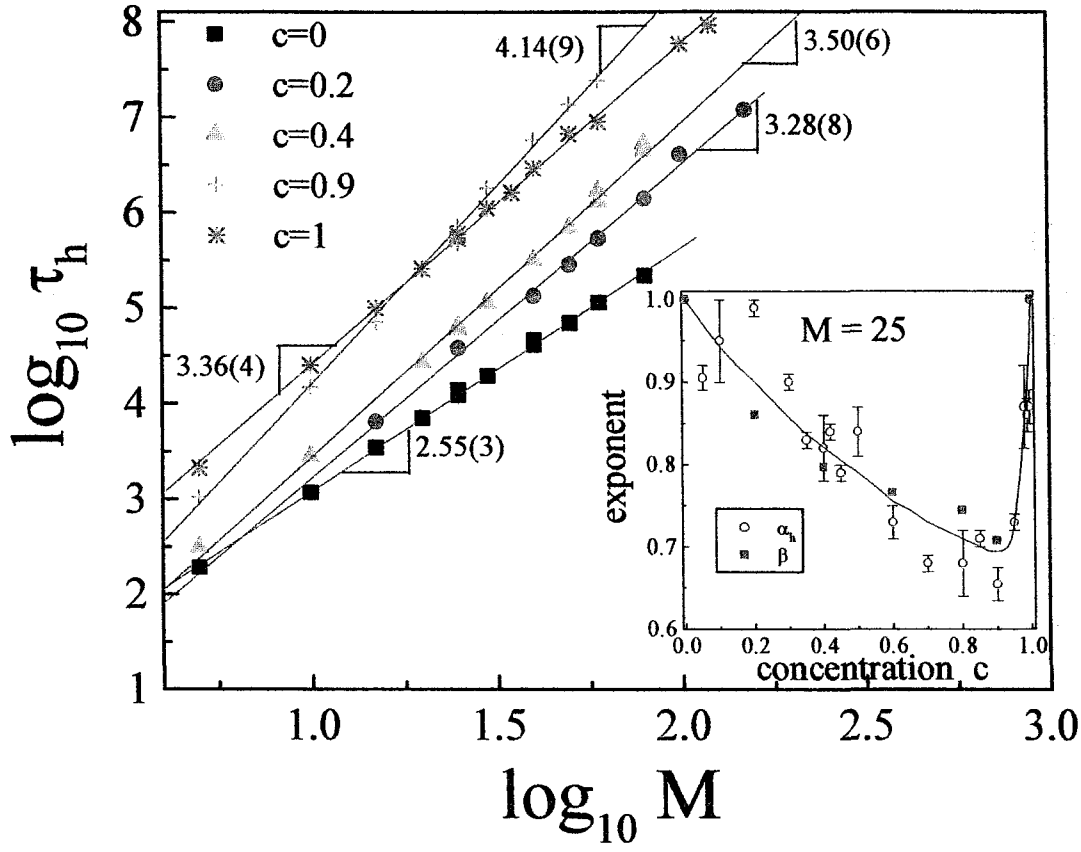

Figure 34. Log-log plot of the integrated conformational relaxation time for the end-to-end distance h as a function of molecular size M for the obstacle sublattice concentrations c=0, 0.2, 0.4, 0.9, and 1. Inset: The anomalous diffusion exponent β and the stretching exponent α_h are both plotted against concentration c in the case of an M=25 chain.

There is a marked correspondence, indicative of a coupling between conformation relaxation and anomalous diffusion.

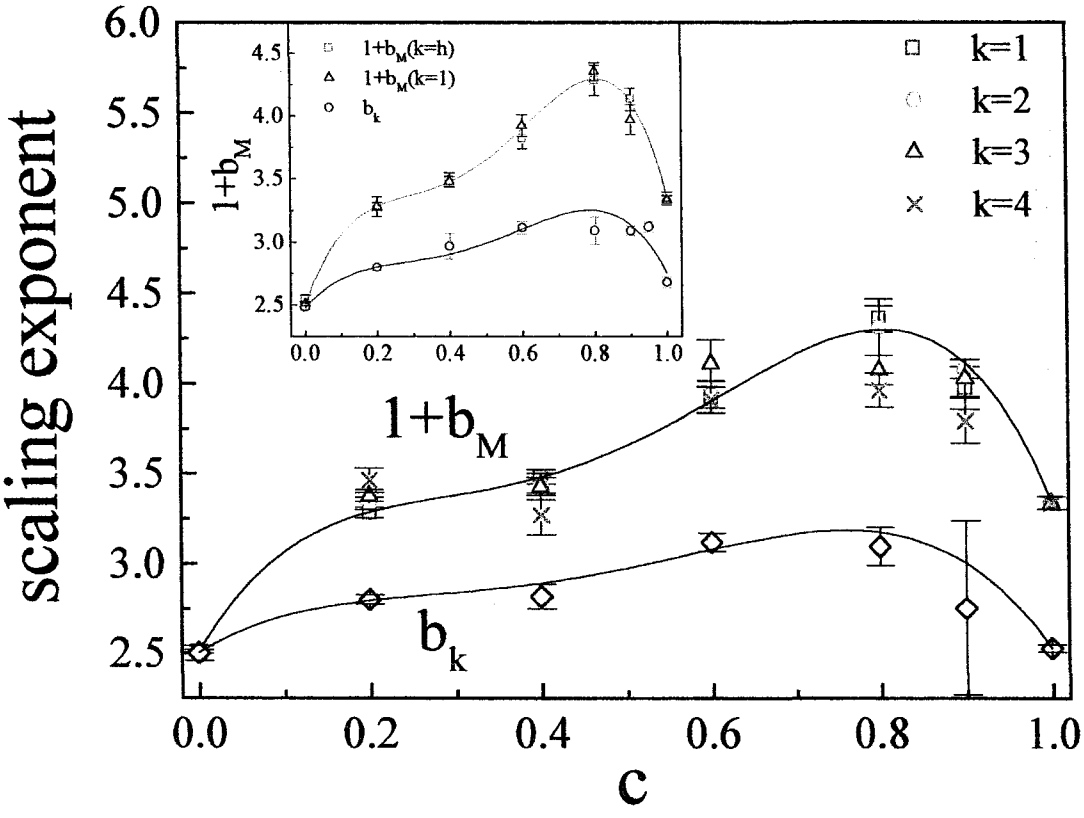

Figure 35. Main figure: The molecular-size scaling exponents b_M (for $5 \leq M \lesssim 100$) and mode scaling exponent b_k (for M=25) of Eq. (24) are plotted against the obstacle sublattice concentration c for the first four modes (k=1-4). Inset: the molecular-size scaling exponents b_M for both the conformational relaxation time of the Fourier mode τ(k=1) as well as that for the end-to-end distance h, are plotted simultaneously against concentration c together along with mode exponent b_k. The lines merely provide a guide for the eyes.

3.7 Relaxation length scales

In Figure 36, we plot ln $C_h(t)$ against $\langle (R_{CM})^2 \rangle$ for M=25 and c=0, 0.4, 0.9, and c=1. The predominance of straight lines implies that the stretching exponent α_h, which characterizes the conformational relaxation, corresponds directly with the anomalous diffusion (temporal) exponent β where $\alpha_h=\beta$ [see, also, inset of Figure 34]. Using Eq. (28), we see that the slope is given by ln $C_h(t)/[\langle (R_{CM})^2 \rangle = -[\lambda_h^2(c) \times t^{\beta-\alpha}]^{-1}$ which, because it is constant (i.e. no time-dependence to the slope), implies the existence of the characteristic relaxation length scales $\lambda_h(c) = 2dD^* \tau_h^{\alpha}$ which characterizes the conformational relaxation of the end-to-end distance in disordered media.

In Figure 37, we plot the conformational relaxation length scale $\lambda_{k=1}(t)$, directly, as per its definition in Eq. (28), to further establish the existence the characteristic (i.e., where $\beta=\alpha_{k=1}$) conformational relaxation length $\lambda_{k=1}(c)$ for M=25 chains in media with obstacle sublattice concentrations c=0, 0.2, 0.4, 0.9, and 1. In the inset of Figure 37, we have taken data from Figure 22 and have indicated the Rouse and reptation times for reference. We recall that the first Fourier "mode" of Eq. (21) corresponds closely with the end-to-end distance h. In the main figure, the plateau values yield the constants $\lambda_{k=1}(c)$ directly. The horizontal data indicate that $\lambda_{k=1}(c>0) \approx 14-15 \approx 1.4R_g-1.5R_g$ and $\lambda_{k=1}(c=0) \approx 18 \approx 1.8R_g$. Note that the mean square radius of gyration $\langle R_g^2 \rangle$ is indicated on the horizontal axis for reference. This raises the question as to whether R_g is truly an appropriate length-scale for characterizing the conformational relaxation of polymeric chains in disordered media. For instance, the diffusion of the CM in the obstacle-free case allows the chain to travel distances $\gtrsim R_g$ with little conformational change or rotation due to the absence of obstacles in the sublattice. And while R_g remains the only length scale of relevance in the case c=1 (as it was in the case c=0), this is not so clear for cases 0<c<1, as revealed by the observation $[\lambda_{k=1}(0<c)] < [\lambda_{k=1}(c=0)] < [\lambda_{k=1}(c=0)]$. Note, also, that $\lambda_{k=1}$ for c=0.4 appears conspicuous below that for the other intermediate concentrations c. One method of discerning the differences between λ_h, $\lambda_{k=1}$, and R_g may be to ascertain the molecular-size dependence of $\lambda^2 \sim M^{2\mu}$ for the various concentrations c and to compare this with the Flory exponent of Eq. (5) which, as we saw earlier, characterizes the molecular-size dependence $\langle R_g^2 \rangle \sim M^{2\nu}$ [see Eq. (4)] for all concentrations $0 \leq c \leq 1$.

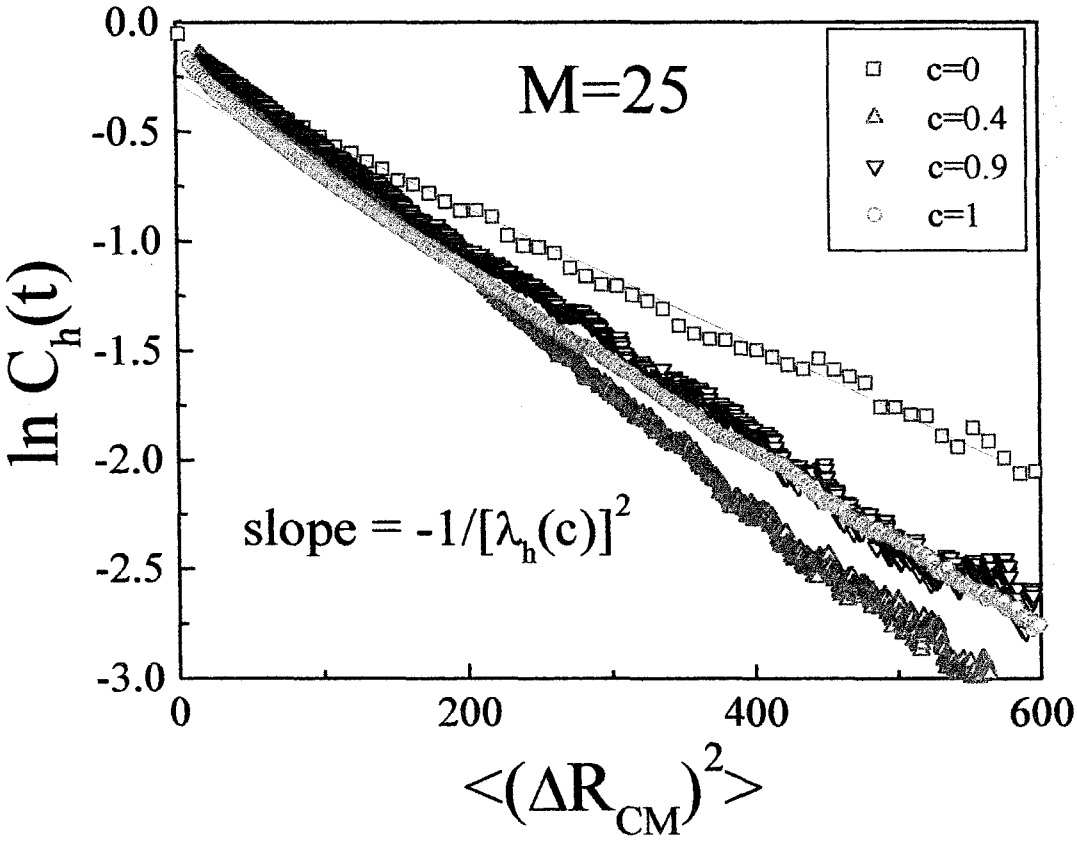

Figure 36. The natural logarithm of the autocorrelation function $C_h(t)$ is plotted as a function of the mean square displacement of the centre-of-mass $\langle(\Delta R_{CM}^2(t))^2\rangle$ for the case of an M=25 chain for concentrations c=0, 0.4, 0.9, 1.

The slope, as per Eq. (28), is given by $\ln C_h(t)/ [\langle(R_{CM})^2\rangle = -[\lambda_h^2(c) \times t^{\beta-\alpha}]^{-1}$ which, because it is constant (i.e. no time-dependence), implies the existence of relaxation length scales $\lambda_h(c)$ characteristic of stretched exponential conformational relaxation during anomalous diffusion.

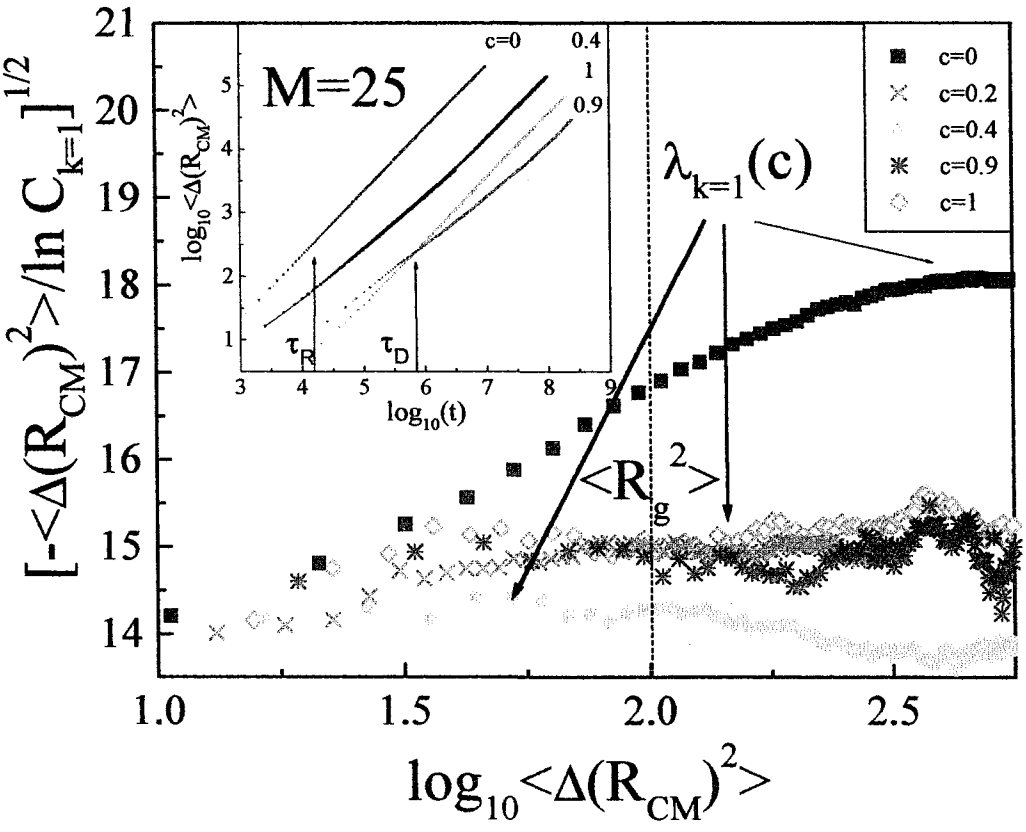

Figure 37. We establish the existence of a characteristic conformational relaxation length of Eq. (28) scale by plotting $\lambda_{k=1}(t)= [(R_{CM})^2\rangle/(-\ln C_{k=1})]^{1/2}=[2dD^*\tau_{k=1}^{\alpha}\times t^{\beta-\alpha}]^{1/2}$ for M=25 chains in media with obstacle sublattice concentrations c=0, 0.2, 0.4, 0.9, and 1. The plateau regions correspond to the characteristic length scales $\lambda_{k=1}(c)$ where the time-dependence vanishes because of the coupling relation $\beta=\alpha_{k=1}$.

In the main figure, the plateau value yields $\lambda_{k=1}(c)$ directly. The mean square radius of gyration is indicated on the horizontal axis for reference. For concentrations c>0, conformational relaxation is coupled to centre-of-mass diffusion for very early times as indicated by the horizontal plateaus for the data even for diffused distances much smaller than $R_{CM}^2=100\approx R_g^2$ [$R_g\approx10$ (see Table 1)]. The horizontal plateaus occur at $\lambda_{k=1}(c>0)\approx14\text{-}15\approx1.4\ R_g\text{-}1.5\ R_g$ and $\lambda_{k=1}(c=0)\approx18\approx1.8R_g$. The data in the inset is taken from Figure 22 and the Rouse and reptation times are indicated for reference.

In Figure 38, as well as in Figure 39, we have a log-log plot of the relaxation length scales λ^2 against M, for both h and $X_{k=1}$, respectively, for concentrations c=0, 0.4, 0.9, and c=1. The data exhibit effective molecular size scaling consistent with the existence of an effective scaling exponent 2μ. Therefore, in the inset of Figure 38, as well as that of Figure 39, we plot 2μ vs. c. The dashed line represents the Flory result $2\nu=3/2$ for d=2 dimensions. We find that μ cannot be distinguished from the Flory exponent ν, given the uncertainty of our data. Therefore, if the relaxation length scales λ are truly qualitatively distinct from R_g, then we may require much longer chains $M \gg 100$ in order to obviate any such qualitative difference. Therefore, the relaxation length scales λ do not appear to be qualitatively distinct from R_g, although the commonly notion that the relaxation length scale is given by $R_g^2 \approx 2dD\tau_{k=1}$ is certainly incorrect in the case of intermediate concentrations $0<c<1$ where long transient CM diffusion regimes couple with the conformational relaxation process, as we have shown.

In summary, we have characterized the static and dynamic properties of EV chains in media with varying degrees of disorder, finding that the static conformational properties are little affected by the surrounding system of fixed voids with varying degrees of disorder. This was surprising, given the strong ET effects, trapping chains within effective local entropic potential minima throughout the potential energy landscape of the lattice space. Having then turned our attention on to the diffusion coefficient, we found that the ET had a drastic effect on D which goes through a minimum for c=0.8-0.9 whose value was much lower that that for the reptation limit (c=1) despite the fact that fewer obstacles populated the environment. This is a well-known signature of ET that has been reported before by Slater and Wu (Slater 1995). We then looked at the anomalous, transient diffusion regimes, demonstrating how these long transients are affected by the varying degrees of disorder. We then characterized the relaxation times in terms of molecular size and mode number. Noticing that the onset of steady-state diffusion occurs for time scales much later than those characterizing conformational relaxation in the case of strong disorder, we were naturally led to investigate the possible relationship existing between conformational relaxation and the long anomalous sub-diffusion regimes. A coupling between the observed stretched-exponential time behaviour for the relaxation of the conformations and that for the anomalous diffusion process was then established and the time exponents were found to be equivalent. This in turn defined a new characteristic length scale, related to the anomalous diffusion exponent, which governs the conformational relaxation process in these disordered systems of fixed obstacles. We concluded the chapter by looking into the nature of this relaxation length scale, finding that the effective molecular-size scaling for this quantity could not be distinguished from that of the radius of gyration (and end-to-end distance).

Having characterized the effect of point defects on the static and dynamic properties of linear polymer chains in depth, we now turn our algorithm to the investigation of the diffusion of polymer liquids in finite, patterned mesoscopic void systems as a function of polymer concentration.

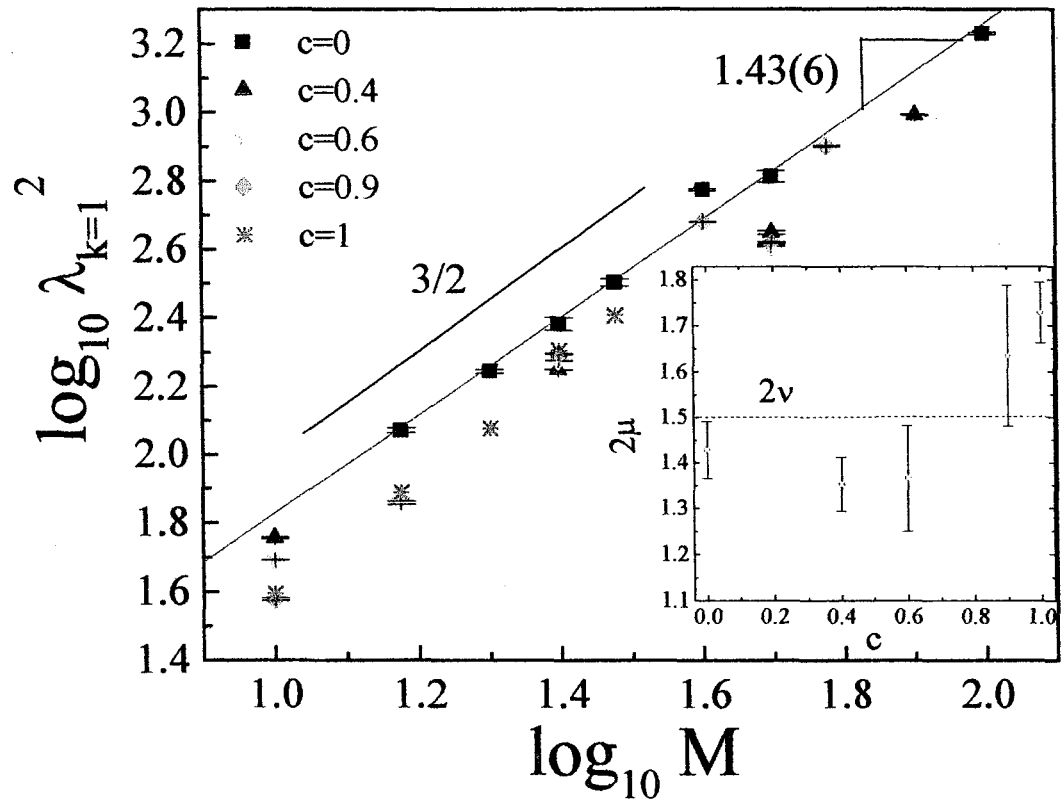

Figure 38. Log-log plot of the mean square relaxation length scale $\lambda_{k=1}^2 = 2dD^*\tau_{k=1}^{\alpha} \sim M^{2\mu}$ of Eq. (28) as a function of molecular size M for obstacle concentrations c=0, 0.4, 0.6, 0.9, and 1. The slope is given by $2\mu=1.43(6)\approx 2\nu=3/2$, as shown. Inset: The molecular size exponents of $\lambda_{k=1}^2$ are plotted as a function of obstacle concentration c. The data are consistent with the notion of the Flory exponent governing the molecular-size scaling for the conformational relaxation length scale $\lambda_{k=1}$.

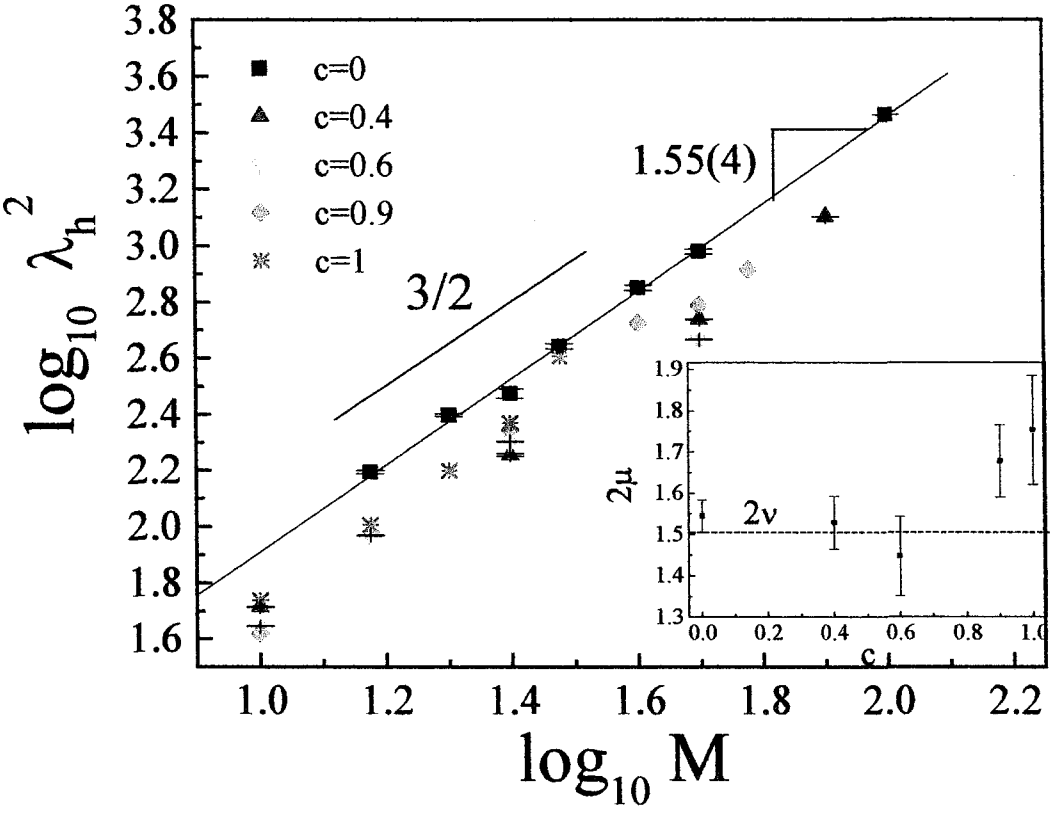

Figure 39. Main figure: Log-log plot of the mean square relaxation length scale $\lambda_h^2=2dD^*\tau_h^\alpha \sim M^{2\mu}$ of Eq. (28) as a function of molecular size M for obstacle concentrations c=0, 0.4, 0.6, 0.9, and 1. The slope is given by $2\mu=1.55(4)\approx 2\nu=3/2$, as shown. Inset: The molecular size exponents of λ_h^2 are plotted as a function of obstacle concentration c. The data are consistent with the notion of the Flory exponent governing the molecular-size scaling for the conformational relaxation length scale λ_h.

Chapter 4
Saturation and entropic trapping of monodisperse polymers in mesoscopic porous media

Here, we investigate the effect of polymer concentration on the diffusion and localization (entropic trapping) of linear polymer chains in a two-dimensional model system of small obstacles and large pores. The model used for this section is a modified version of the model of Slater and Wu adapted to accommodate systems of many chains and to create the mesoscopic void system (see Figure 7).

In the absence of specific interactions between the chains and the medium, the voids (entropic traps) control the chain partitioning between regions with different volume-constraining effects on the chain conformational entropy. Three distinct regimes are identified: the entropic trapping regime, a reptation regime where the larger pores are polymer-saturated and the un-trapped polymers reptate, and finally a crowding regime where intermolecular interactions dominate. In this model system, the entropic trapping, reptation, and crowding mechanisms compete and lead to a unique maximum in the diffusion coefficient for intermediate polymer concentrations.

4.1 Introduction

Recently, Liu, Li, and Asher (Liu, Li et al. 1999; Liu, Li et al. 1999) designed an elegant model experimental system where linear polymers were allowed to migrate in a hydrogel patterned with mesoscopic voids (or pores). Theirs is perhaps the first experimental system to be designed exclusively for the study of the ET mechanism. Non-trivial ET effects were reported at finite polymer concentrations.

In Liu, Li, and Asher's experimental study, a ~100 μm-thick polymer hydrogel was fabricated with an embedded face-centred cubic array of monodisperse (~50.5±3.0 nm spherical radius) water voids. A solution of linear sodium polystyrene sulfonate macromolecules (NaPSS), whose radii of gyration varied from ~0.6 nm to 30 nm, was then allowed to partition between the gel network matrix, the reservoir solution, and the embedded water voids. Entropic trapping (ET) is known to be strongest when the polymer radius-of-gyration R_g is comparable to the mean pore radius, a, inside a disordered medium (Baumgärtner and Muthukumar 1987; Muthukumar and Baumgärtner 1989; Muthukumar and Baumgärtner 1989; Baumgärtner and Muthukumar 1996). In accord with the phenomenon of ET,

those chains, whose radius of gyration most closely matched the size of the voids, were shown to be preferentially partitioned from the hydrogel into the aqueous holes.

Inspired by the experimental system of Asher et al., we adapted our 2D model system to investigate "patterned" or "imprinted" gels whose largest pores are, in fact, perfectly periodic as well as being comparable in size to the polymers ($a \cong R_g$). Specifically, we will investigate the effects of polymer concentration and trap saturation on the pore site occupation probability (a measure of the trapping or localization of the polymer chains) as well as on the diffusion properties of a monodisperse solution of polymer chains. Our model system is a crude, 2D representation of the elegant experimental system studied by Liu, Li, and Asher. Entropic trapping of polymer chains is a physical phenomenon, taking place in both two- and three-dimensional disordered media. Although the physics is quite similar, quantitative results will differ. For instance, excluded volume and crowding effects are much stronger in two-dimensions. In fact, the quantitative behaviour is strongly dependent upon the nature of the gel structure, the shape and spatial distribution and connectivity of the large pores or entropic traps, etc. We have thus designed our model to optimize its computational efficiency and to mimic as well as possible the general features of mesoscopic void systems in hydrogels.

4.2 Method

In Figure 40, we depict a simulation snapshot of a solution with N=3 polymer chains of size M=20 monomers diffusing in a 120x120 lattice model system with periodic boundary conditions. Figure 41 enlarges the section detailing the trapping of an individual M=20 chain. In our system, the obstacles form a periodic "gel" with periodicity p=4. The 9 large voids (entropic traps) were created by the removal of integral "blocks" of 2×2 obstacles with periodicity P=40 (for the smallest molecule of size M=10, some simulations were also carried out with a larger 400×400 systems with 10×10=100 large voids of the same size and periodicity). The initial polymer conformation is generated as a straight "I-shaped" chain of M monomers and M−1 links of length 2. Each simulation is preceded by a long warm-up period consisting of many steady-state times.

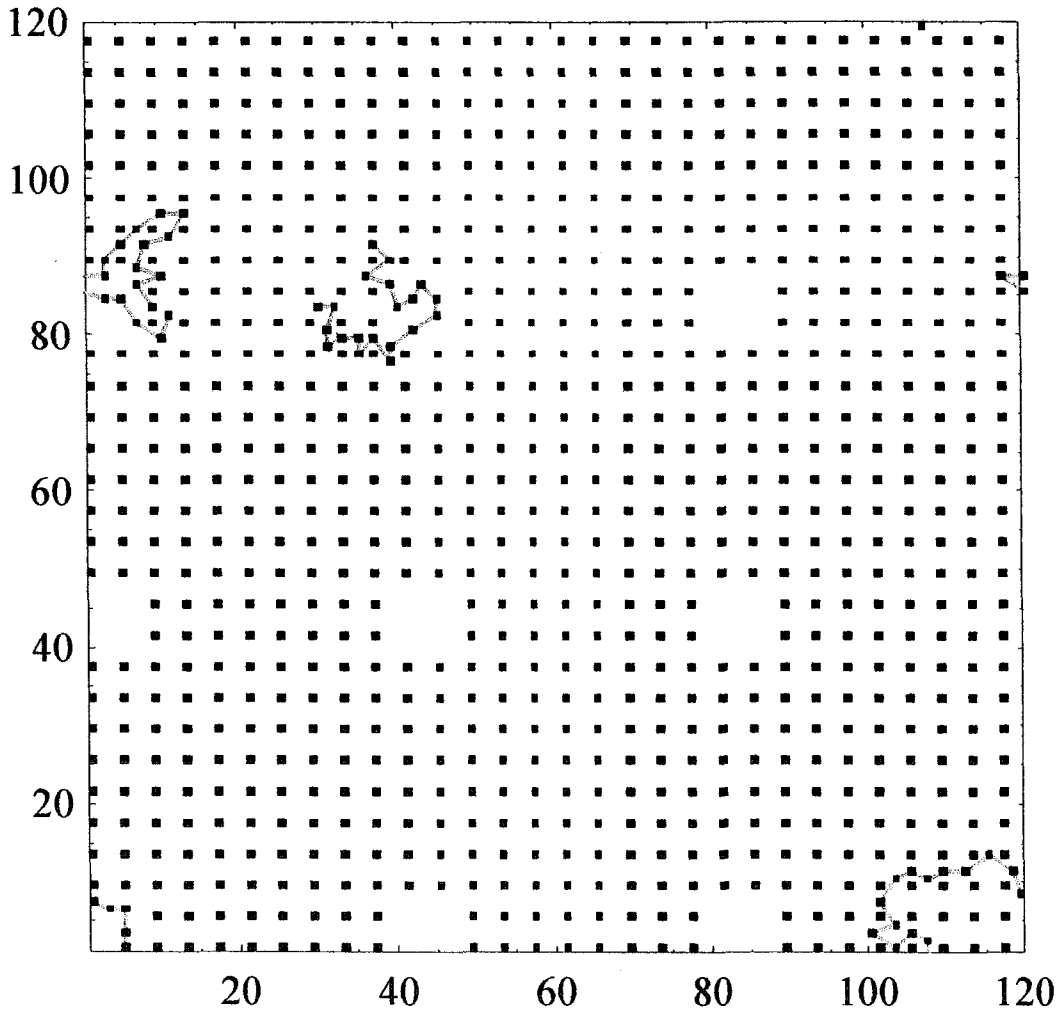

Figure 40. Simulation snapshot of a monodisperse solution of N=3 chains of molecular size M=20 among a system of macroscopic voids. A snapshot of three M=20 polymer chains diffusing in our model system. Monomers and obstacles are shown as squares, and the monomers are linked with "bonds". The obstacles form a periodic "gel" with a periodicity p=4. We create the nine large voids by removing integral "blocks" of 2×2 obstacles; the 9 entropic traps have periodicity P=40 in this 120×120 lattice system. Periodic boundary conditions are used.

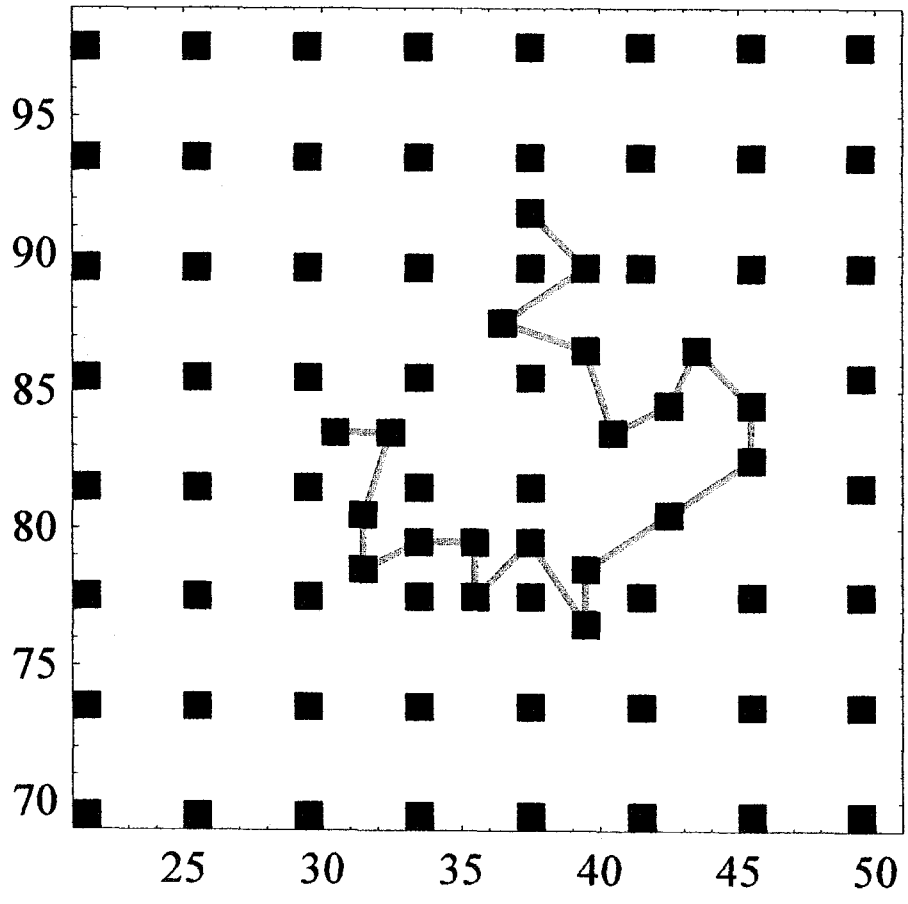

Figure 41. Enlargement of a section of Figure 40 showing a void containing an entropically trapped polymer of size M=20.

Let us characterize the simulated medium (consult Figure 40). Within a perfectly-periodic gel of obstacles (i.e., all obstacle present and no voids), only 6,300 (or 7/16 of the 120^2 = 14,400) lattice sites can be occupied by monomers and only 1/16th of all sites (=900) can be occupied by obstacles. Upon the introduction of the 9 voids, we remove 9 (voids) × 4 (obstacles/void) = 36 (obstacles) and free-up 9 (sites/removed obstacle) for a total of 324 (newly-available due to voids) for the monomers. Therefore, we have 6,624 lattice sites accessible to the monomers with only 864 sites being occupied by obstacles. The accessible (c.f., fluid phase) space for the monomers thus accounts for $6624/120^2$=46% of the total space. While the obstacles (c.f., gel phase) physically account for only $864/120^2$=0.06 (6%) of the total space, they actually sterically deplete the accessibility of $9\times864/120^2$=0.54 (54%) of the space because of the BFA's double occupancy restrictions. Each trapping void area comprises of approximately 93 sites, but this value depends slightly on how the void perimeter is defined. The corresponding effective pore radius is $a=\sqrt{(93/\pi)}\approx5.4$ and thus the voids account for about 9 (voids)×93 (sites/void) / 6624 (available sites) = $93/736\approx12.6\%$ of the available (fluid phase) sites.

It would prove convenient, however, to consider an analysis based on a discrete radial occupation probability density function $\sigma(r)$ for the CM over a unit cell for our system, in discrete increments of $\Delta r=1$. In Figure 42, we depict the pore-centred unit cell and superpose a circle depicting the effective pore radius $a=\sqrt{(93/\pi)}\approx5.4$. The centre of the pore has coordinates (20.5, 20.5) which we renormalize to position r=0. As such, the further cells with respect to the pore centre has radius $r_{max}=[2\times(40-20.5)^2]^{1/2}=27.5772\approx28$. Therefore, to completely cover the space, the probability density function $\sigma(r)$ must account for the occupation probability density over the sites whose radius r falls within $(1\pm\Delta r/2)$, $(2\pm\Delta r/2)$, …, and $(28\pm\Delta r/2)$ on our unit cell.

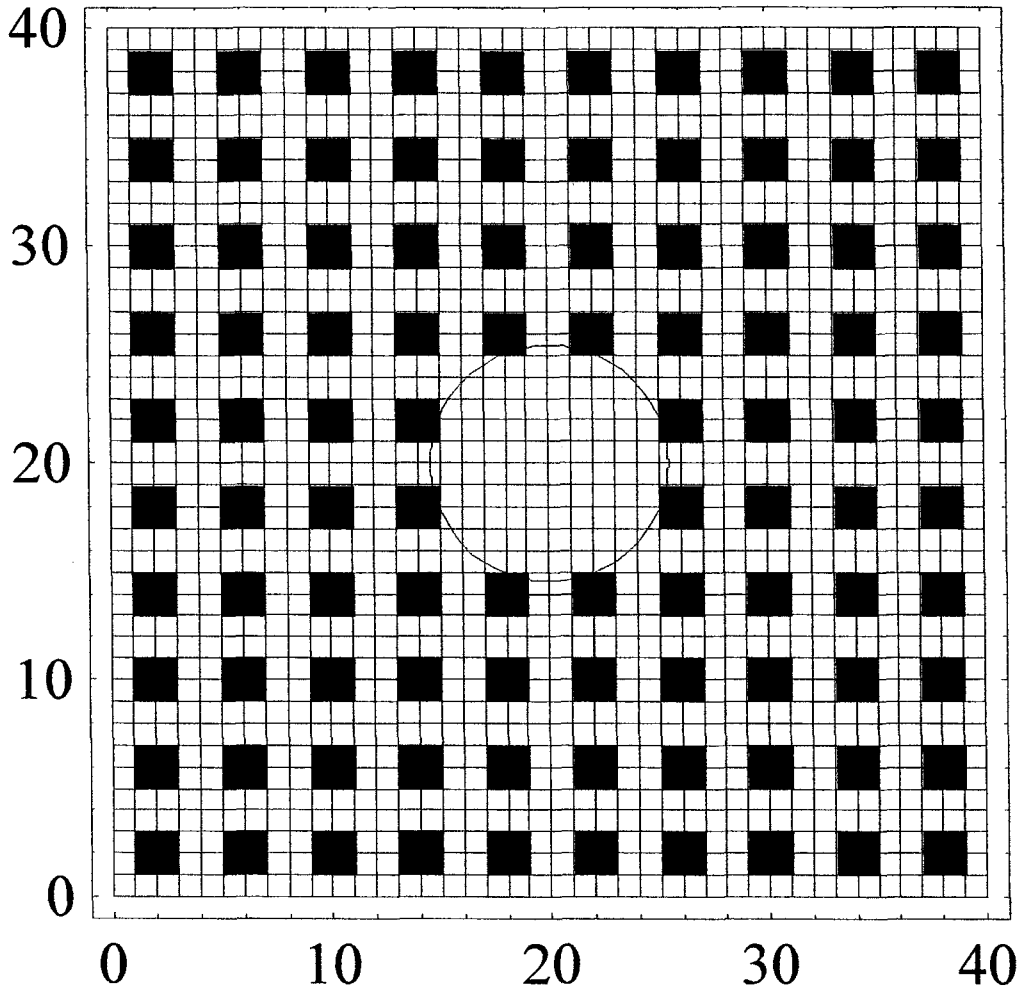

Figure 42. Depiction of the effective 40×40 "primitive cell" for the entropic trapping system, centred about a pore site. In this picture, a point-like monomer would move on the vertices of the square mesh. The (black) obstacles occupy integral blocks of 4 sites with periodicity p=4. The large void is created by the removal of an integral block of 2×2 obstacles at periodicity P=40. Centred on the pore site is a contour depicting the pore's effective radius $a=(93/\pi)^{1/2}$.

As the CM of the polymer will necessarily reside on a continuum of coordinates, unlike the coordinates of monomers, the CM positions have been coarse-binned based on the CM's nearest integer coordinates within the unit cell. These unit cell bins are then integrated over the unit cell space to yield the discrete probability density function $\sigma(r_i)$, which we choose to define implicitly through the total cumulative occupation probability density function

$$P(r) = \sum_{r_i=1}^{r} \sigma(r_i) * 2\pi r \Delta r \tag{56}$$

where we have taken $\Delta r=1$ and $r_i=1, 2, \ldots, 28$ for our analysis throughout. The choice $P_{pore}=P(a)$ provides a convenient definition for the trapping probability, although, it is to be understood that we linearly interpolate in $\sigma(r_i)$ when computing P(r) for non-integer values of r.

We note that a small complication arises when dealing with radii r>20 for which we lose the apparent spherical symmetry about the pore's centre (i.e., the radial shells become discontinuous areas). Because of the lack of general interest in the $\sigma(r_i)$ concept in this region, and for reasons of expedience and simplicity, we will choose to preserve the convenient form expressed in Eq. (56) and avoid the inconvenient renormalization of $\sigma(r_i)$ required for this region due to the effective area of integration no longer being $2\pi r\Delta r$. As such, we still have P(28)=1 but $\sigma(r_i)$ is greatly underestimated for the region r>20 while only being slightly over-estimated for r<20. This poses no serious difficulties, however, our radial probability concept being mostly qualitative in nature, the effective radius being somewhat subjective, and given that we are interested primarily in the qualitative behaviour in $\sigma(r_i)$ and P(r) for the regions r≤20.

In absence of entropic effects, and in thermodynamic equilibrium, the ratio of the number of monomers present in the two phases (gel to traps) should thus be $K\approx(6624-9\times93)/(9\times93)= 643/93\approx6.91$. This would be the case, for instance, for a one-monomer (M=1) probe molecule performing a random walk in the system, although we are interested in the polymer's CM, which is point-like.

In Figure 43, we now superpose effective contour lines drawn about the central pore of the "primitive cell" assuming a constant occupation probability density over available lattice sites. The 3 contour lines delimit 4 concentric regions of equal area. As such, they depict 25% occupancy regions for a zero-potential surface, much as in the case of a point-like particle.

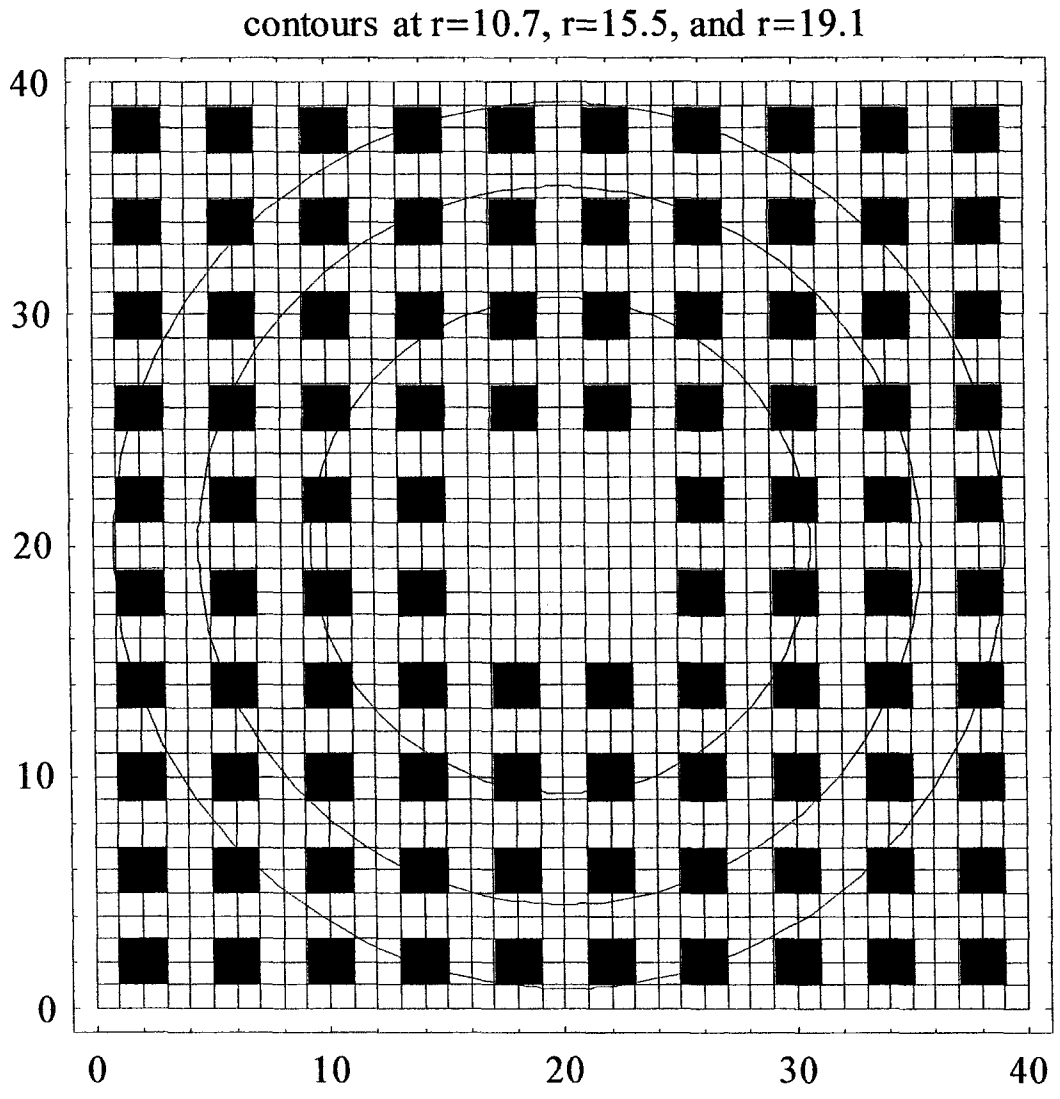

Figure 43. The effective contour lines drawn about the central pore of the "primitive cell" delimit lattice site regions of 25% occupancy in the case a uniform occupation probability density for the available lattice sites (white regions) in the absence of potential gradients. In this pictorial representation, a point-like monomer would move on the vertices of the square mesh.

In Figure 44, therefore, we plot the discrete radial occupation probability density function $\sigma(r_i)$ of Eq. (56) for the discrete radii $r_i=\{1, 2,\ldots, 28\}$ in the case of uniform occupation probability density for available lattice sites (c.f., a point-like particle migrating on a zero potential surface in the gel-phase). The vertical line denotes our choice for the effective pore radius $a=(93/\pi)^{1/2}$. The coarseness of the function is due to the discrete nature of the lattice space. We note that the probability density is essentially constant (as would be expected the continuum limit), with some fluctuations about $\sigma(r)\approx 0.006$ due to the resolution of our bins ($\Delta r=1$). For $r>20$, we are beyond the edges of the primitive cell and have consequently ignored the renormalization factors for the sake of convenience.

In Figure 45, we plot the cumulative radial occupation probability P(r) of Eq. (56) for a constant or zero-potential (U=0) surface in our system of mesoscopic voids. We see that using an effective pore radius $a=(93/\pi)^{1/2}$ reduces the expected (rectangular) pore-site occupation probability from $p\approx 12.6\%$ to the value $p\approx 8\%$ for the case of a point-like particle in a zero-potential medium.

We studied polymer molecular sizes M=10 and M=20. Their radii-of-gyration are $R_{g,c=0}(M=10)=5.102(6)$ and $R_{g,c=0}(M=20)=8.69(1)$ without obstacles (free chains), and $R_{gl}(M=10)=5.147(6)$ and $R_{gl}(M=20)=8.71(3)$ when all obstacles are present (i.e., no large voids), as per Figure 9 and Figure 10, respectively. Therefore, the M=10 molecules can fully fit inside the traps (of effective radius $a\approx 5.4$) while those with M=20 monomers cannot. For reference (Figure 16), the corresponding single-chain (N=1) diffusion coefficients in the trap-free system of p=4 periodic obstacles are $D(M=10)=4.55(5)\times 10^{-5}$ and $D(M=20)=1.25(12)\times 10^{-5}$.

This study will focus on both the trapping probability for the CM as well as the diffusion coefficient D(M) of the migrating species as a function of the number N of chains (or the polymer concentration).

For the centre-of-mass (CM), an effective occupation probability density P(x,y) of Eq. (43) can be calculated for each site (x,y), as well as a local entropic trapping potential energy U(x,y), measured in units of k_BT, as given by Eq. (43). In other words, the motion of the CM of the chain, in principle, can be replaced by the motion of a point-like particle (a single monomer for example) in the potential energy landscape U(x,y). A theoretical description applicable to this situation is provided in section (2.5.2).

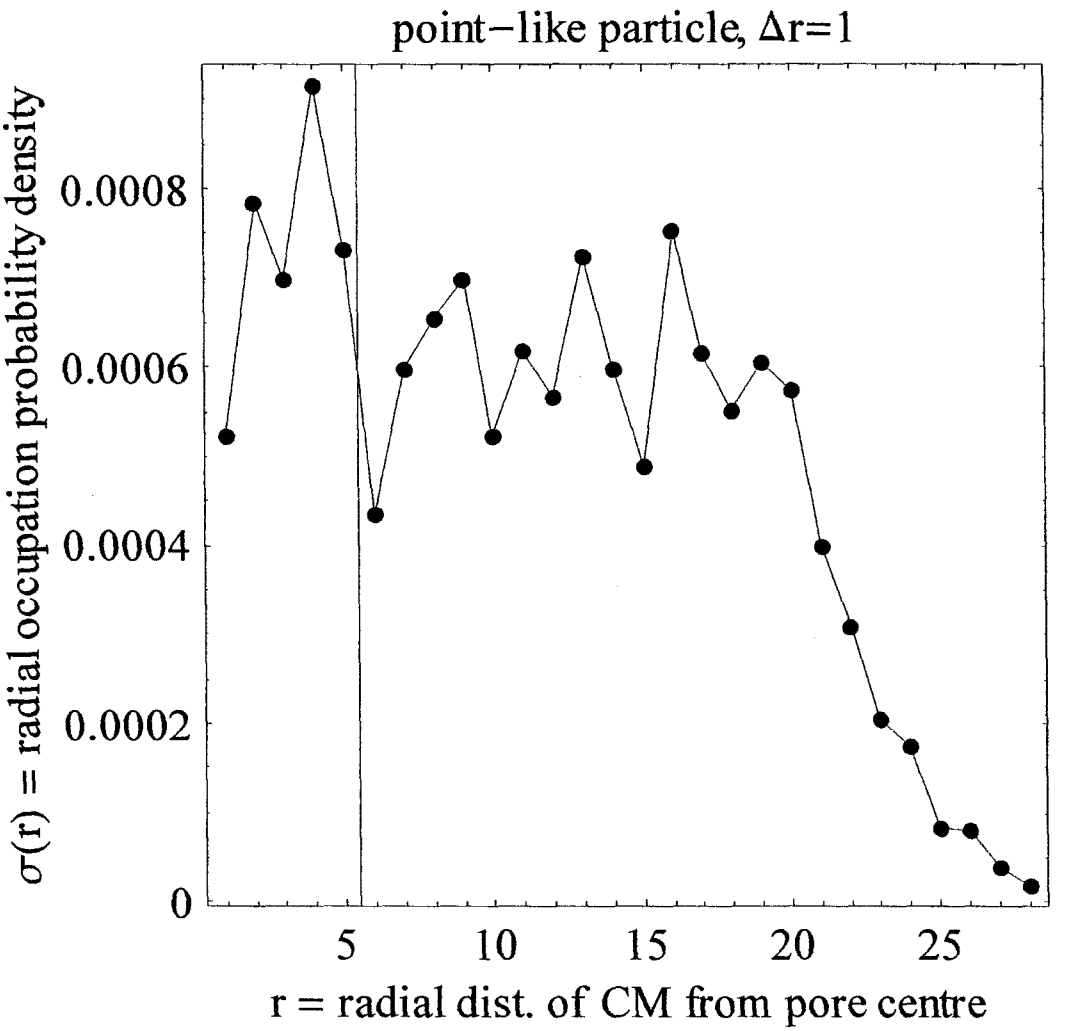

Figure 44. The discrete radial occupation probability density function $\sigma(r_i)$ of Eq. (56) is shown for the case of uniform occupation probability density for the available lattice sites (where U=0). The vertical line denotes the effective pore radius $a=(93/\pi)^{1/2}$ for which the integrated sum of $\sigma(r_i)$ from 0 to a yields the pore-site occupation probability $P_{pore}=P(a)$.

The probability density is essentially constant (as would be expected in the continuum limit), with some fluctuations about $\sigma(r_i)\approx 0.006$ due to the resolution of our binning ($\Delta r=1$) being comparable to the lattice spacing. For r>20, the density drops-off because we are beyond the edges of the primitive cell and have chosen to ignore the renormalization required for this region for convenience.

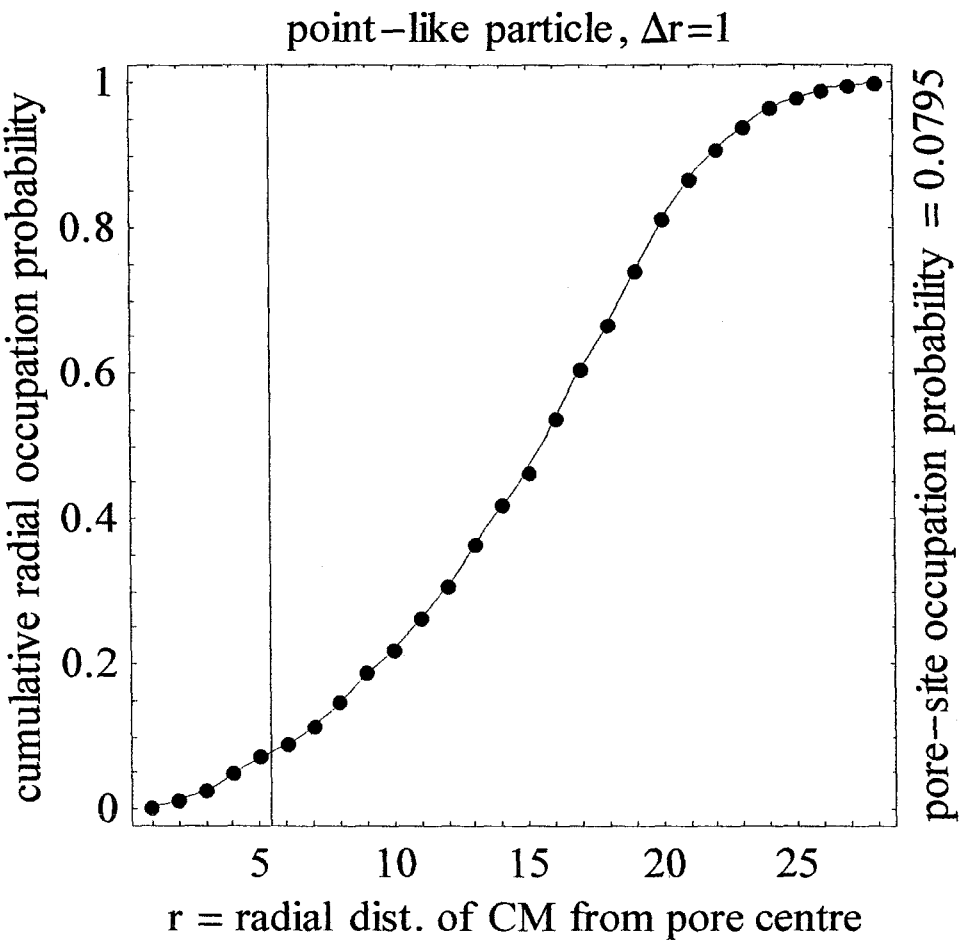

Figure 45. Cumulative radial occupation probability P(r) of Eq. (56) for a constant or zero-potential (U=0) surface in our system of mesoscopic voids. This coresponds closely with the expected behaviour of a point-like particle migrating in our system, in the absence of potentials. The point for which the effective pore radius $a=(93/\pi)^{1/2}$ (vertical line) crosses the cumulative probability (summing over increments of $\Delta r=1$ the function depicted in Figure 44), defines our choice for the pore-site occupation probability. For a point-like particle, the probability of pore occupation is $p\approx 8\%$ for our system.

As the number N of chains increases, the entropic traps begin to saturate and the void spaces can no longer accommodate any extra monomers. Beyond a critical population number N_{sat}, we thus expect D(M) to increase as more and more chains will be free to reptate between the filled traps that will then act as passive obstacles of surface area $\cong\pi a^2$. As N is increased further, polymer "crowding" will eventually slow down the dynamics of the polymer chains diffusing in the gel phase. Therefore, a plot of D(M) vs. N should show a characteristic maximum at $N_{MAX}>N_{sat}$ followed by a monotonic decrease in the crowding regime. The position N_{MAX} of the maximum should of course decrease for larger polymer sizes (M) because longer chains have larger radii-of-gyration which more effectively fill entropic traps *and* contribute to crowding effects more readily.

4.3 Results

We begin our study by first investigating the evolution of the diffusion coefficient D when a finite number of M=10 or 20 monomer chains evolve in our special ET system (Figure 40). The diffusion data (Figure 46) is plotted vs. the effective polymer concentration $\rho=N/N_{traps}$, where N_{traps} is the total number of entropic traps (large voids) in the system. We recall that the N_{traps} trapping voids (of effective radius $a \cong 5.4$) are just large enough to accommodate polymers of size M=10 (radius of gyration $R_g\cong5.1$). Therefore, for M=20 (radius of gyration $R_g\cong8.7$), monomer "spill-out" must occur for the trapped polymers [this phenomenon has been studied by Chern and Coalson (Chern 1999)]. In both cases, the diffusion coefficient D abruptly increases upon increasing ρ beyond the critical value $\rho=\rho_{sat}=1$, that is, when the number of polymers exceeds the number of traps. Clearly, trap saturation then takes place and this shields the next polymer chains from most of the attractive influence of the entropic traps. However, we note that the mobility of the M=20 chains then increases faster than that of the shorter M=10 chains. This is due to the fact that more than one M=10 chain can be slowed down (adsorbed) by a single entropic trap while, in the case of trapped M=20 chains, this effect is less likely. In other words, the monomers of a M=10 chain do not completely saturate a trap whereas monomer saturation of traps is more complete for trapped chains as M increases (i.e., as the R_g increases with respect to the pore size). Undoubtedly, one can have $\rho_{sat}>1$ for shorter polymer chains [which was indeed the case in the experiments reported in (Liu, 1999)] and even $\rho_{sat}<1$ for large chains that can occupy more than one pore at a time (this last situation is a very different problem as we are then moving towards the reptation regime in the presence of disorder).

Figure 46 also shows the diffusion coefficient D for M=10 chains in a system without big pores; in this case, the overlap concentration (i.e. the concentration at which the polymer chains start touching one another) of the two-dimensional solution of polymer chains corresponds roughly to $\rho^* \cong 20$ or about N=175 chains (these numbers would be $\rho^* \cong 7$ and N=60 chains for the larger M=20 polymers). We do observe some crowding effects at $\rho \gtrsim \rho^*$, as evidenced by the fact that D decreases slightly at concentrations larger than about ρ^*. In the system with pores, a very similar trend is clear for concentrations $\rho > \rho^*$, thus leading to the characteristic peak at a concentration $\rho_{sat} < \rho_{MAX} < \rho^*$. The effect is much stronger for the M=20 chains because the critical concentrations ρ_{sat} ($\cong 1$) and ρ^* ($\cong 7$) are much closer to one another.

Therefore, in the bottom of Figure 46, we have scaled D on the vertical axis by the factor $M^{3/2}$ to factor-out the reptation molecular-size-dependence; on the horizontal axis, the number N was also multiplied by $M^{3/2}$ to better account for the area $\sim NR_g^2$ occupied by the chains. We observe that, in the high concentration limit, entropic traps become monomer-saturated, and we appear to recover universal behaviour, consistent with the notion of many reptating chains.

It is also interesting to note that the two upper curves cross at $\rho \cong \rho_{MAX}$. This means that the diffusion coefficient is actually slightly larger in the system with entropic traps beyond the position of the maximum; this is simply due to the fact that the total free volume available to the dense solution of polymer chains is larger in such macroporous systems. It is thus vital to work at very low polymer concentrations $\rho \ll \rho_{sat}$, far from pore saturation, when studying ET effects in random systems. Indeed, these results indicate that the effective molecular size-scaling exponent δ of the steady-state diffusion coefficient (i.e., $D \sim 1/M^{\delta}$) would otherwise be a strong function of the polymer concentration ρ (and would consequently be meaningless). This raises serious question regarding the proper interpretation of experimental results in ET systems as the finite-concentration effects can actually *mask* very strong ET effects.

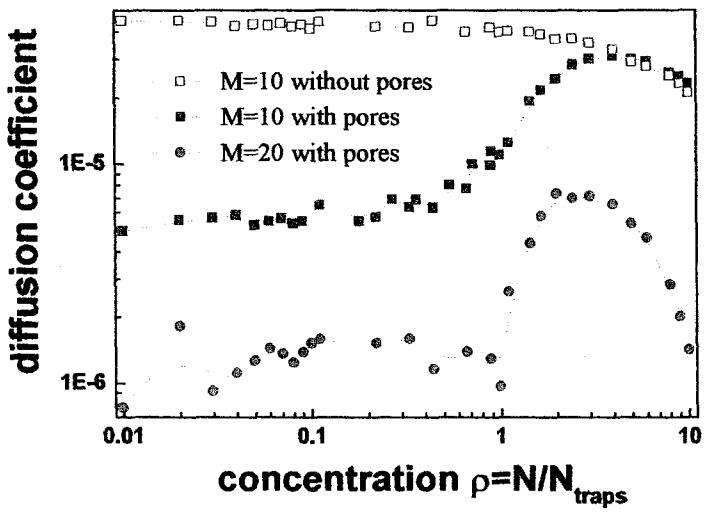

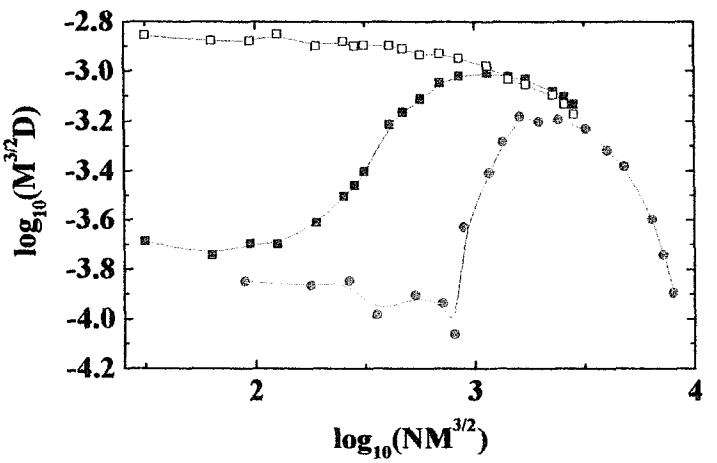

Figure 46. Top figure: Log-log plot of the diffusion coefficient D as a function of the effective polymer number concentration ρ (defined as the number N of polymer chains divided by the number N_{traps} of entropic traps) for M=10 and M=20 chains. Bottom figure: on the vertical axis D has been scaled by $M^{3/2}$ to remove the reptation molecular size scaling; on the horizontal axis, N was also multiplied by $M^{3/2}$ to reflect the area occupied by the chains. In the high concentration limit, ET gets squeezed-out, and we recover universal behaviour, consistent with reptation.

In Figure 47, we plot the radial occupation probability density $\sigma(r)$ where r is the distance between the polymer centre-of-mass and the centre of the nearest void. In each case, a single polymer chain (N=1 or $\rho \ll \rho_{sat}$) was used. From these probability distributions, isolated M=10 chains appear more strongly localized, consistent with the notion of strong entropic trapping for molecules which can be entirely trapped inside the large voids ($R_g<a$). The M=20 chains cannot be fully accommodated by the pores and monomers are thus forced to spill out (see also Figure 7), as evidenced by the long tail of the distribution for distances $r>a\cong5.4$. Moreover, although these longer chains typically remain in the vicinity of the traps for low population N, their centre-of-mass may not always reside inside the pore space.

Figure 48 depicts a contour plot as well as a three-dimensional view of the corresponding entropic potential well of Eq. (43) for a N=3, M=10 system. For this small polymer concentration $\rho<\rho_{sat}$, the overall occupation probability P(x,y) is densest in the large pores, as expected for ET systems. In fact, we observe here that the polymer chains spend more than 75% of the time in the pores while the latter cover less than 13% of the total accessible surface area; a similar result was seen previously in Figure 25 for a slightly different system. This corresponds to a partition coefficient of $K\cong0.75/0.25=3$. The potential well is quite deep (the lowest energy is several times k_BT while the average depth is about $2k_BT$), which explains the strong polymer localization, unlike the case for a zero-potential surface (Figure 43). However, as we will show (indirectly) next, the effective depth of the entropic well is a strong function of chain concentration ρ when $\rho>\rho_{sat}$.

Figure 49 depicts the total probability P_{pore} of pore-site occupation for the CM of a polymer chain as a function of the polymer effective number concentration ρ. We see that the M=10 chains are much more strongly localized in traps (the plateau at low concentrations is higher). As ρ increases beyond $\rho_{sat}=1$, however, the pore occupation probability decreases towards the expected asymptotic value of ~8% (the effective area of the pores) for both species. It is to be remembered that our expectation value was based on a point-like particle that could occupy all the square sites within the pore. The difference for the polymer situation is partly related to the subjective use of an effective (and subjective) pore radius a in the case of an extended object like a polymer.

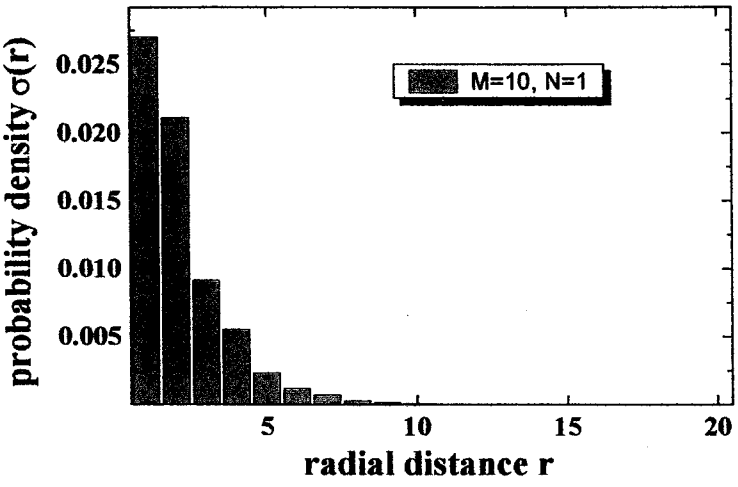

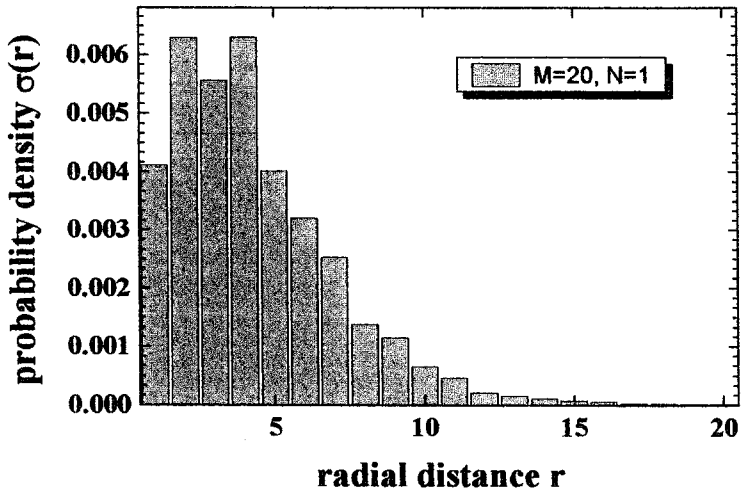

Figure 47. The radial occupation probability density σ(r) of Eq. (56) is plotted as a function of the distance r between the centre-of-mass and the position of the centre of nearest pore for the case of a single M=10 chain (top figure) and a single M=20 chain (bottom figure). These σ(r) are to be contrasted with the case of a zero-potential surface, devoid of ET (see Figure 44) where the density is much smaller for small r and consequently higher for the region 10<r<28.

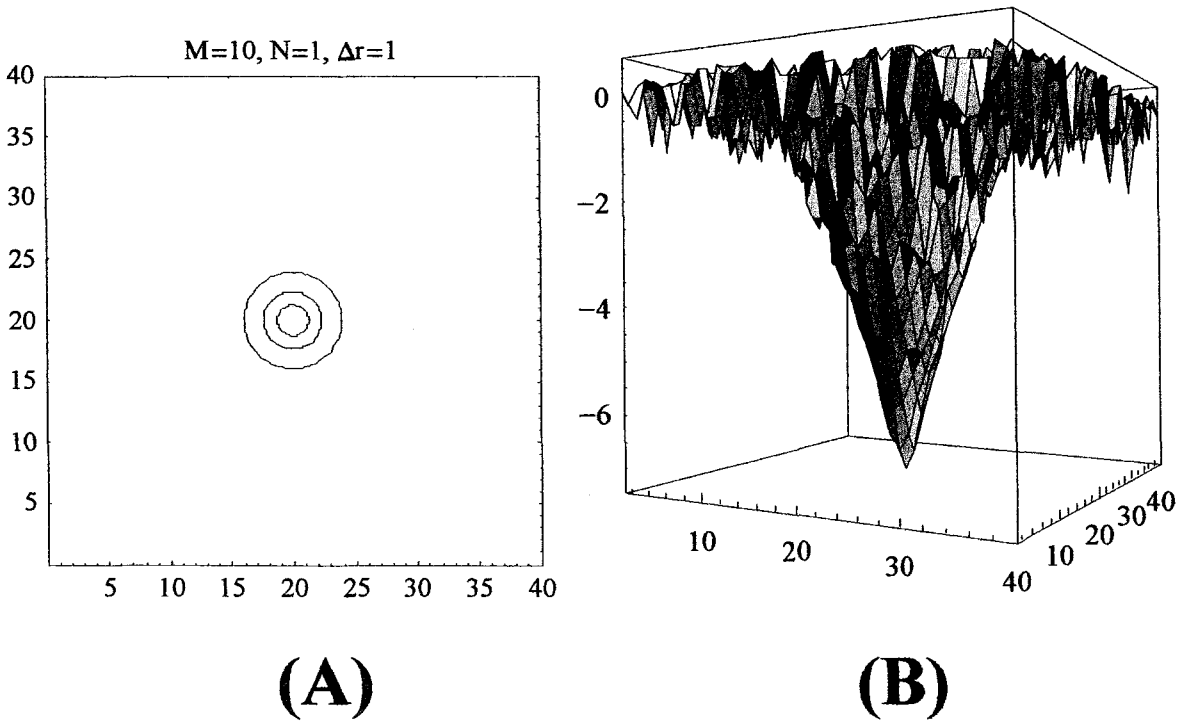

Figure 48. The single-site occupation probability P(x,y) of Eq. (43) is plotted for the case of a single M=10 monomer chain on an effective "primitive cell" (see Figure 42) of the lattice with the pore centred at (20.5, 20.5).

In (A), we generate a contour plot of ΔP(r)=0.25 with each of the four regions delineated corresponding with 25% of the total occupation probability (including the space occupied outside the final contour). This is to be contrasted with the result for a zero-potential surface in Figure 42. In (B), we generate the corresponding entropic trapping potential energy U(x,y) of Eq. (43), in units of k_BT.

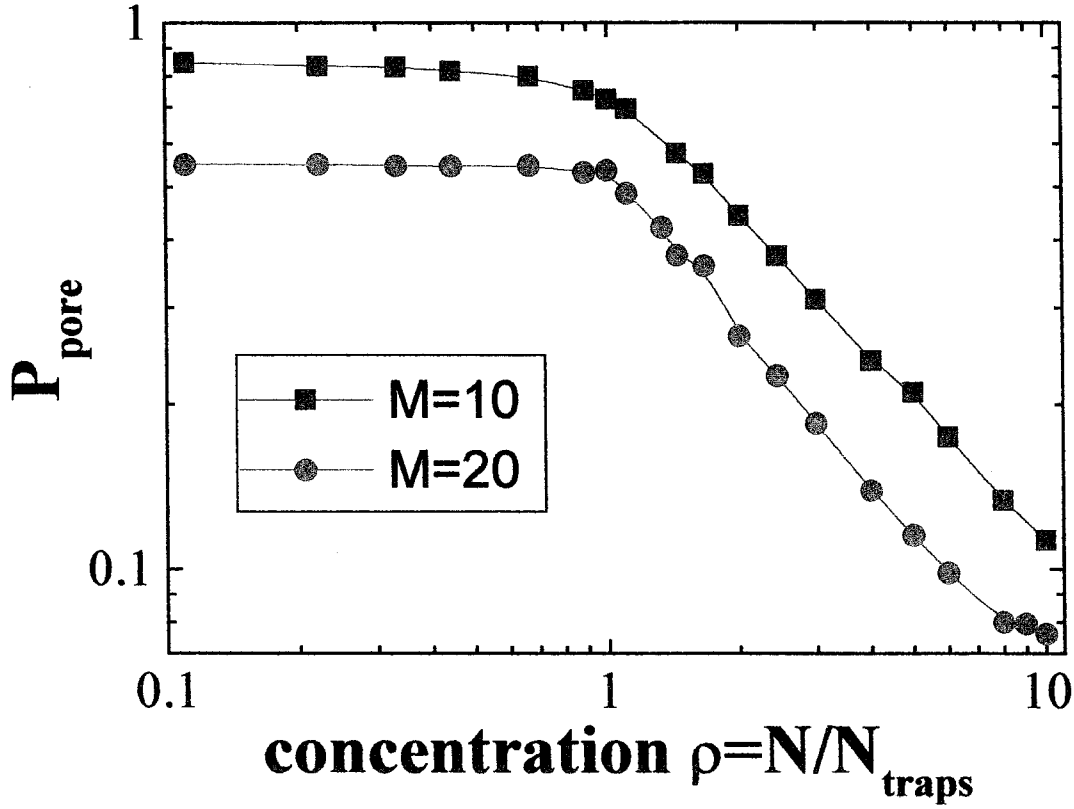

Figure 49. Log-log plot of the CM trapping probability as a function of the effective concentration $\rho=N/N_{traps}$ of polymer chains in the system for the two chain species of size M=10 and M=20.

However, particularly in the case of trapped M=20 chains, monomer spill-out from the traps may further reduce the probability of pore-site occupation because of the steric exclusion zone, caused mostly by the trapped chain's end monomers, about the saturated traps. Indeed, in Figure (50), the existence precisely such a steric exclusion zone about the fully saturated pore is indicated as a 'halo' of lower gray-scale intensity about the dark pore position, for a dense solution [i.e., $(\rho=6)>(\rho_{sat}=1)$] of M=10 chains.

4.4 Discussion

We have presented a simple computational model of the effect of finite concentrations on the entropic trapping of monodisperse polymer chains in disordered media. Two critical concentrations were introduced: the saturation concentration ρ_{sat} at which all of the major entropic traps are filled by polymer chains, and the overlap concentration ρ^* beyond which diffusion is slowed down because of crowding. As predicted, a large increase of the diffusion coefficient $D(\rho)$ is observed for $\rho>\rho_{sat}$ because the entropic potential wells have minimal effect on the part $\rho-\rho_{sat}$ of the population of molecules. This increase, however, competes with the effect of crowding. Since one always has $\rho^*>\rho_{sat}$, this competition leads to a marked maximum in the $D(\rho)$ vs. ρ curve at an intermediate concentration ρ_{MAX}. As far as we know, this phenomenon has never been observed or predicted before. Interestingly, the position of this maximum is a direct measure of the concentration of large voids in a porous material; this thus suggests a new method to probe the porosity of such systems.

We have qualitatively reproduced the salient features reported by Liu et al. (Liu, Li et al. 1999; Liu, Li et al. 1999) with the exception of the increase in localization of long polymer chains at low polymer concentration [see panel (A) of Figure 48]. We note that our polymers are comparable to their longest polymer chains in that they fill or nearly fill the large voids. Liu et al. suggest (point 2 in their Discussion section) that this unexpected increased localization might be due to the entropic trapping of these chains in the gel part of their system. Obviously, our polymer chains could not get entropically trapped in the gel itself because we created our gel obstacles is such a way as to yield a fully periodic gel. On the other hand, large pores obviously exist in the polyacrylamide gel that separates the entropic traps in the experimental system. Our failure to observe this subtle effect can thus be seen as supporting the hypothesis proposed by Liu et al.

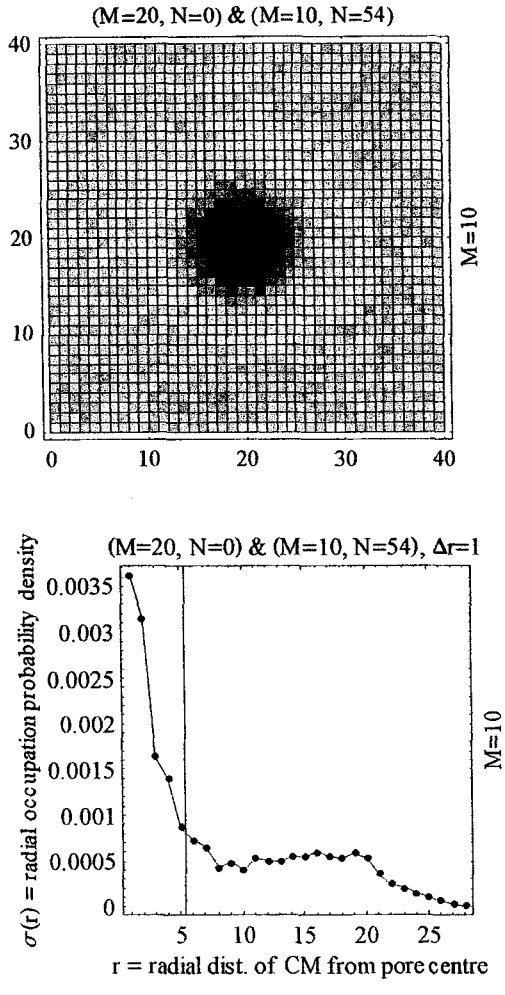

Figure 50. The lattice site occupation probabilities of the centre of mass for the case of N=54 chains of size M=10 are characterized.

In the top figure, a density plot depicts the lattice site occupation probability of the centre of mass for the case of N=54 chains of size M=10. We note the existence of a steric exclusion zone about the fully saturated pore, as indicated by a halo of lower gray-scale intensity around the black pore.

In the bottom figure, the corresponding radial occupation density $\sigma(r)$ indicates strong localization just within the pore's effective radius a (a is indicated with a vertical line). The steric exclusion zone just beyond the pore space is revealed as a sudden drop in the radial occupation density function as r increases to a distance $r>(a\approx 5.4)$. This is followed by a gradual increase in $\sigma(r)$ as $r\rightarrow 20$.

We also examined the effect of the polymer's molecular size M on this partitioning. In one case (M=10), more than one chain can be trapped or affected by a single entropic pore (see Figure 7). The increase of the diffusion coefficient beginning at $\rho=\rho_{sat}$ is then slow, and depending on the distance between the traps, the resulting peak can be rather broad (see Figure 46). In the second case (M=20), a single chain can fill a pore (with some monomer spill out) and we must have $\rho_{sat}\approx 1$. Since the two critical concentrations (ρ_{sat} and ρ^*) more closely correspond, the resulting peak is much narrower. We did not study the extreme cases where we need lots of chains to fill a single pore (which would lead to $\rho_{sat}>>1$) or where a single chain can fill many pores ($\rho_{sat}<<1$). In the former situation we have a problem quite similar to the case M=10 studied here, while in the latter, we may no longer be able to speak in terms of chain entropic trapping as the situation may then correspond to that of reptation in a fixed, disordered environment.

Our results clearly indicate that any effective molecular size scaling[11] of the steady-state diffusion coefficient, D, would be strongly dependent upon the polymer concentration. Due accounting of finite concentration effects are required in the proper interpretation of experimental data because the results may vary greatly depending on system parameters (e.g., the number of pores, the average pore size, and the molecular size of the probe polymers). The interplay between trapping, pore saturation, and crowding on the bulk transport of the monodisperse polymer solutions, as we have shown, can lead to the masking of strong entropic trapping effects. Thus, commonly held notions about entropic trapping systems leading to slower dynamics must be tempered with finite size effects in mind, especially for non-negligible polymer concentrations.

In the next chapter, we investigate the bulk transport of a bimodal polymer sample in the same entropic trapping system. Selective saturation of certain species could have a strong bearing on the interpretation of diffusion data in the presence of even moderate polydispersity. On the other hand, such biases would be exploitable, e.g., for selective filtering applications.

[11] We recall that we predict an exponential-dependence for D in this system, as per Eq. (51).

Chapter 5

Saturation effects and entropic trapping of a polydisperse solution of polymer chains in a periodic array of obstacles with embedded voids

This chapter is an extension of the work presented in Chapter 4. There we studied the effects of the effective number concentration $\rho=N/N_{traps}$ parameter on the entropic trapping and the bulk diffusion of monodisperse solutions. Also, we there had N representing the number of polymer chains and $N_{traps}=9$ representing the number of mesoscopic pores. The cumulative pore site occupation probability $P_{pore}=P(a\approx5.4)$, together with the bulk diffusion coefficient D, were studied as a function of ρ. We found that the diffusion coefficient (D) is a strong function of the polymer number concentration. It was shown that the interplay between ET, pore-site saturation, and crowding on bulk diffusion can lead to the masking of strong ET effects

In this chapter, we investigate the trapping of a bimodal mixture of flexible polymer chains (the simplest form of polydispersity) inside our mesoscopic void system.

5.1 Introduction

The model system was characterized previously in Chapter 4. Briefly, the space accessible to monomers (fluid phase) accounts for 46% of the total space while that of the obstacles (gel phase) physically accounts for 6% but sterically depletes 54% of the space. The effective radius of the traps is $a\approx5.4$ with the traps accounting for $\approx12.6\%$ of accessible sites for the monomers (fluid phase) but for which $P_{pore}=P(a\approx5.4)\approx0.08$ when using the radial pore-size approximation (see Figure 45). The pore saturation thresholds are $\rho_{20}^{*}=1$ for the M=20 chains and $\rho_{10}^{*}\gtrsim1$ for the M=10 chains (see Chapter 4, Figure 46).

As the number concentration ρ increases beyond ρ_{sat}, the entropic landscape is being depleted of deep traps and more chains become free to reptate in the gel phase. This drives-up the bulk diffusion coefficient D(M). However, as we further increase ρ, polymer "crowding" leads to an eventual slow down and finally a decrease D(M). This was revealed as a characteristic maximum followed by a monotonic decrease in the crowding regime for the monodisperse solutions (see Figure 46).

In Figure 51, we depict a simulation snapshot of a dilute bimodal solution of $N_{10}=2$ and $N_{20}=1$ polymer chains where $N\equiv N_{10}+N_{20}=3$ and $\rho=N/N_{traps}=1/3$. The system depicted is a 65×65 cross-

section of our 120x120 lattice model system with periodic boundary conditions. The resulting periodic "gel" of fixed obstacles has periodicity p=4 and the 2×2 voids have periodicity P=40, resulting in a total of N_{traps}=9 large (periodic) entropic traps, of which 4 appear in the figure.

In the dilute concentration regime ($N<N_{traps}$), we find that the smaller molecular sizes have a higher affinity for the entropic traps (ETs). For intermediate concentrations, above the pore saturation threshold ($\rho\approx1$), we find that the larger chains have a slightly higher affinity to trapping. Finally, in the crowding concentration regime, steric effects overwhelm the entropic potentials and both chains have nearly the same (reduced) affinity for the voids.

In real systems of experimental relevance, we note that, even for samples labeled "monodisperse", the actual system almost invariably consists of a polydisperse sample, characterized by a molecular-size distribution of finite-width. If we are to understand the various effects of polydispersity and concentration effects in finite systems of experimental relevance, it proves useful to begin by characterizing the behaviour of the bimodal system (the simplest form of polydispersity). As such, this chapter represents a preliminary investigation of this important issue.

5.2 Results

We begin our analysis by first describing the CM's cumulative radial occupation probability P(r) of Eq. (56) and the entropic trapping potentials U(x,y) of Eq. (43).

In Figure 52, we plot the cumulative radial occupation probability P(r) of the centre-of-mass CM for molecular sizes M=10 (A) and M=20 (B) for the special case of N_{20}=9=N_{traps} chains of size M=20 and N_{10}=27=3N_{traps} chains of size M=20. In (A), we find that the probability of CM trapping is $P_{pore}(M=20)\approx0.18$ whereas that for the M=10 chains is $P_{pore}(M=10)\approx0.26$, both being much higher than the corresponding potential-free case for a point particles $P_{pore}(U=0)\approx0.08$.

As we will see, when $\rho>3$, M=20 chains become preferentially trapped over M=10. The potential energy surface U(x,y) experienced by the migrating species varies according to the molecular size of the chains. Hence, the resulting potential for the CM of M=10, as plotted in (C), differs from that experienced by the CM of the M=20 chains in (D), when plotted on a pore-centred primitive cell. Even though the M=10 chains are more highly localized when trapped (the width of U is larger for M=20), CM trapping is favoured for M=20 chains [i.e., $P_{pore}(M=20)>P_{pore}(M=10)$]. The maximum well depths seen here are of the order ~2 k_BT whereas the average well depth is ~1 k_BT.

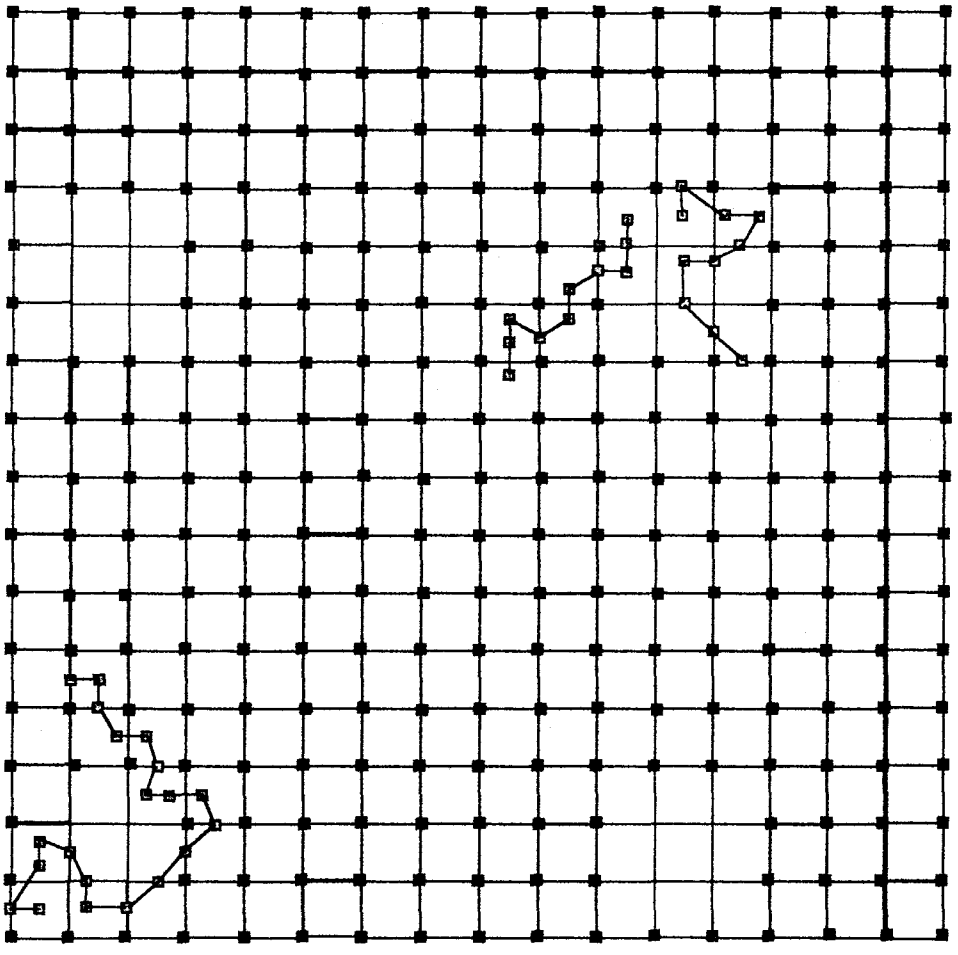

Figure 51. Pictorial representation of a 65×65 cross-section of our mesoscopic void system. The black square plaquettes (shown smaller than actual size for clarity) represent fixed obstacles in the otherwise perfectly-periodic (p=4 lattice spacings) obstacle array whereas the periodic (P=40) white spaces represent mesoscopic voids created by the removal integral 2×2 sections of obstacles. Also appearing are one (N_{20}=1) chain of size M=20 and two (N_{10}=2) chains of size M=10.

The chains are entropically trapped by the (white) mesoscopic voids (entropic traps), with effective radius a≈5.4. The denser obstacle sections appear in gray in order to highlight the voids. We note that, in the case of the M=20 chain, the mean-square radius of gyration is R_g(M=20)≈8.7 and monomer spill-out occurs. In the case of the M=10 chains, R_g(M=10)≈5.1 and the voids are of sufficient size to fully accommodate the chain's monomers. As depicted, the voids can also trap monomers from more than one chain.

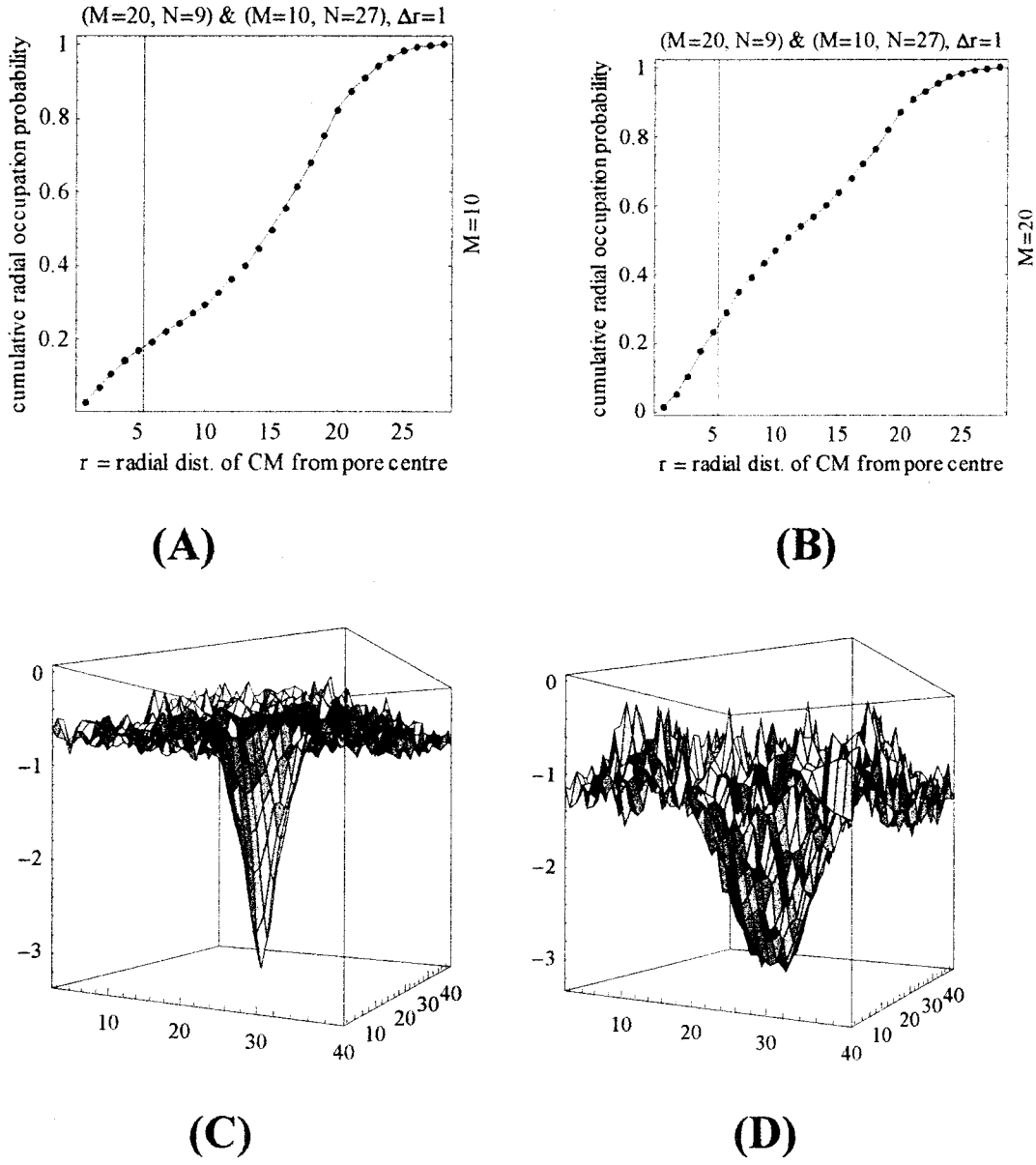

Figure 52. The centre-of-mass' (CM) cumulative radial occupation probability, P(r), of Eq. (56) as well as effective surface potential U(x,y) of Eq. (43), in k_BT units, is plotted for species M=10 (items A and C) and M=20 (items B and D), respectively, for linear polymer chains on a primitive cell centred about a void space (entropic trap).

In (A) and (B), the vertical line designates the effective void radius a≈5.44. The value P(r=a) defines the pore-site occupation probability, P_{pore}, of the chain's centre-of-mass CM (c.f. Figure 45). In (C) and (D), we plot U(x,y) for the CM of M=10 and M=20 chains, respectively.

In Figure 53, we plot the CM pore-site occupation probabilities $P_{pore}(M=20)\equiv P_{20}$ for several groups of bimodal solutions as a function of the effective number concentration, $\rho=N/N_{traps}$. Each solution group has N_{20} fixed but where N_{10} varies thus driving-up ρ. We remark that the cases for which $\rho<1$ are essentially immaterial as both species has free traps they can occupy, leading to virtually identical results.

The first solution depicted corresponds with the case of a single M=20 chain ($N_{20}=1$). Because the single chain must be trapped for $\rho\leq 1$, and because the M=10 chains are least effective at saturating the pores, the CM trapping probability $P_{20}[N_{20}=1=(1/9)N_{pore}]$ of the CM is the upper limit for all solution groups and is the last to be affected by crowding.

Conversely, in the case of the monodisperse M=20 solution, because the M=20 are more effective at saturating the pores, and at populating the gel phase as well, the monodisperse case represents the lower limit value for $P_{20}(\rho)$ for $\rho\gtrsim 1$.

All other solutions fall between these two limits, with gradual convergence to some small limit value of P_{20} ($\rho\rightarrow\infty$) for large ρ, because crowding effects begin to destroy ET.

In Figure 54, we plot the effective slopes of the solution group data, as taken in the vicinity of the solid curve of the M=20 monodisperse solution ($N_{10}=0$) for $\rho>1$ data. In the region $\rho\approx 1$, the competition for pores is fierce, and the preferential trapping of the M=10 chains (as seen in Chapter 4) causes the sharp dip in slope at $\rho=1$ as M=20 chains lose-out. However, the data reveal an asymptotic increase in the slope toward zero as ρ increases from $\rho=1$ to $\rho=5$, indicative of the polymer crowding effect driving down the pore-site occupation probability towards a constant value.

In Figure 55, we plot the CM pore site occupation ratio P_{10}/P_{20} as a function of number density ρ for all cases studied. We expect some basic intrinsic scatter because $\rho_{20}^{*}=1$ while that for M=10 is $\rho_{10}^{*}\gtrsim 1$, on account of M=10 being slightly smaller (and less efficient for saturating pores) and M=20 being slightly larger than the pore size (and thus essentially 100% efficient at filling the pores).

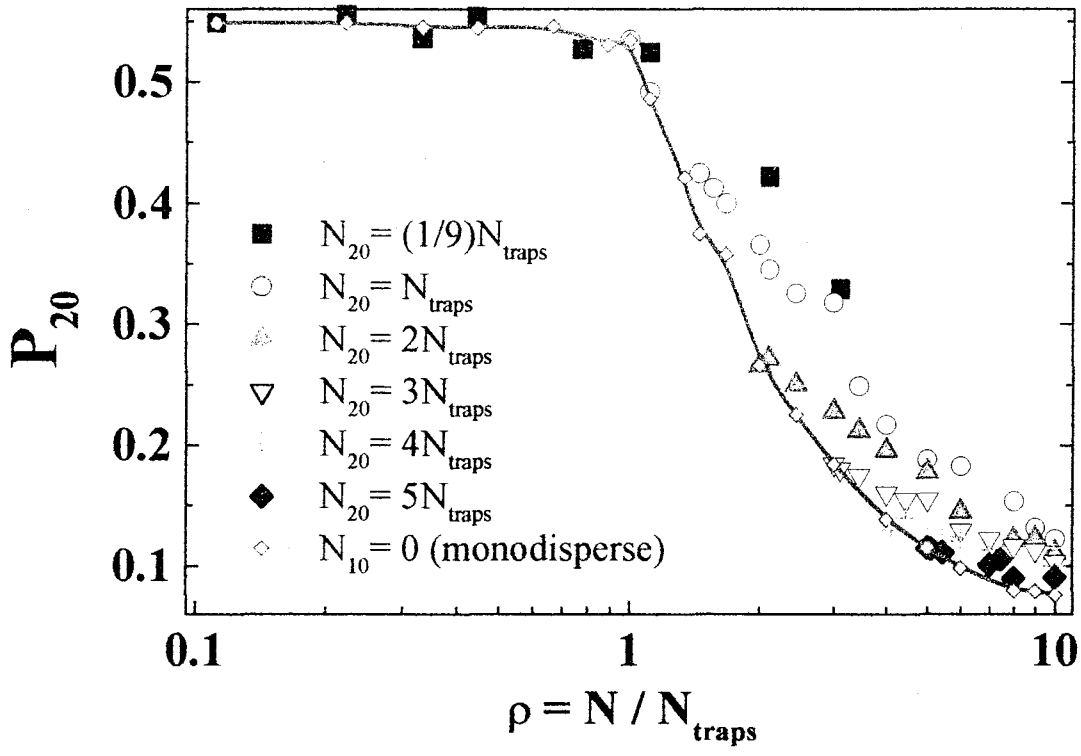

Figure 53. The CM pore-site occupation probabilities $P_{20}=P_{pore}(M=20)$ are plotted for several groups of bimodal solution realizations as a function of the effective concentration, $\rho=N/N_{traps}$, defined as the total number, N, of polymer chains divided by the number, $N_{traps}=9$, of entropic traps in the system. Each data group is defined by a fixed number N_{20} of M=20 chains but with varying numbers N_{10} of M=10 chains. In our model system $N_{traps}=9$. The solid line is the result for monodisperse M=20 solutions ($N_{10}=0$).

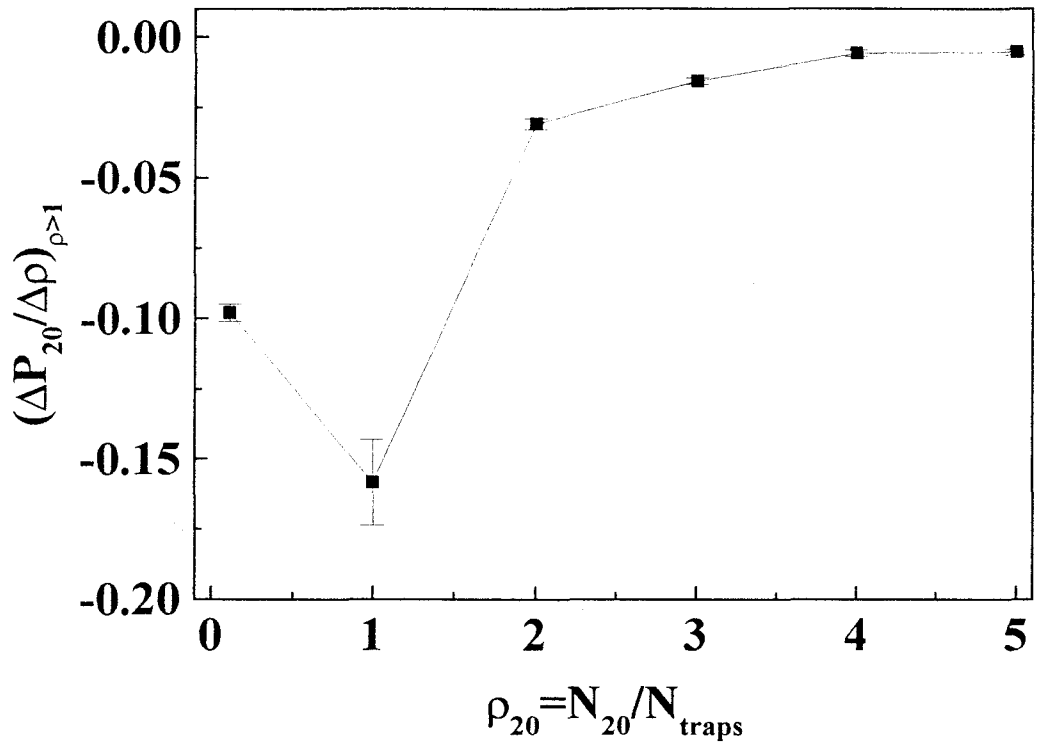

Figure 54. The slope of the pore occupation probability ($\Delta P_{20}/\Delta\rho$) is plotted as a function of the number density ρ_{20} of M=20 chains for data nearest to the pore saturation threshold $\rho=(N=N_{10}+N_{20})/N_{traps} \approx$ constant>1 in Figure 53.

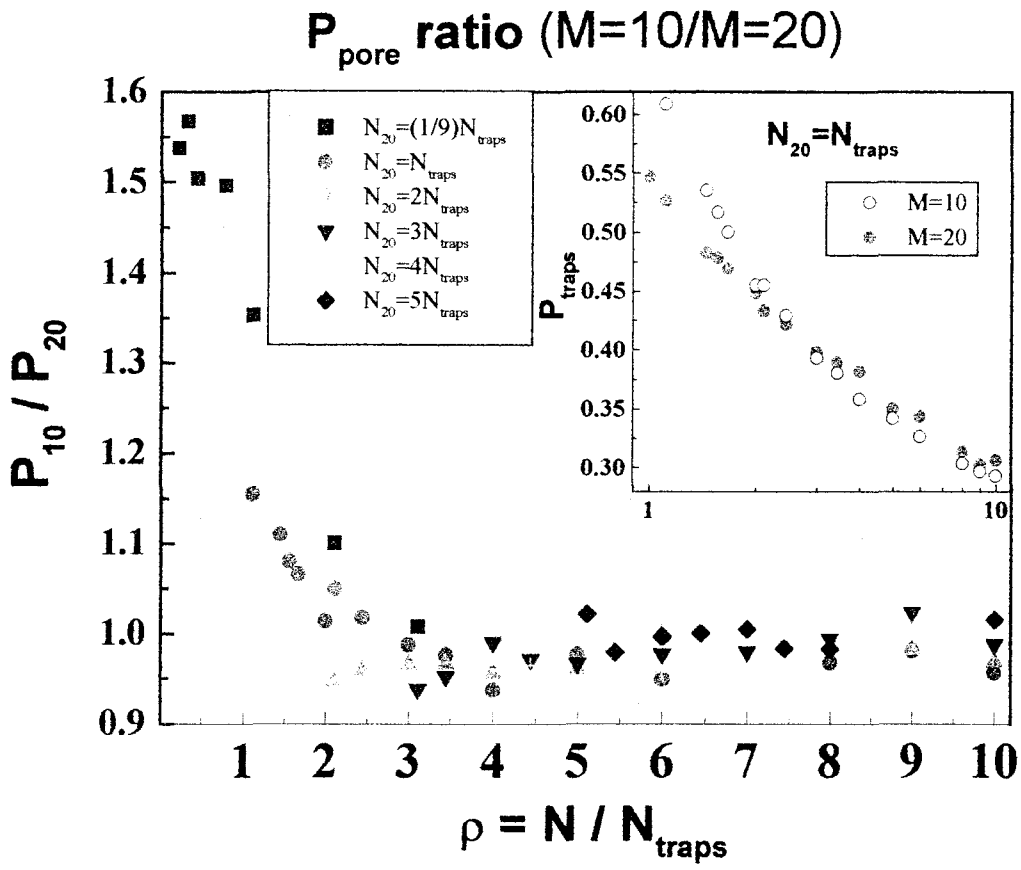

Figure 55. Main figure: The ratio of the pore site occupation probabilities P_{10}= P_{pore}(M=10) to P_{20}=P_{pore}(M=20) is plotted as a function of the effective number concentration ρ=N/N_{traps} of polymer chains in the system. We observe preferential trapping of M=20 over M=10 chains, universally, as the number density increases beyond about 3 (i.e., ρ>3). Inset: The pore site occupation probabilities P_{10} and P_{20} are plotted against ρ=N/N_{traps} for the case N_{20}=N_{traps}=9. The pore-site occupation probability P_{20} for the inset solution (N_{20}=N_{traps}=9) is taken from Figure 53.

In Chapter 4, we found that $P_{10}(\rho)>P_{20}(\rho)$ in the case of monodisperse solutions. Because this should also apply in the case where the isolated pores are not yet saturated, we expect that the ratio $P_{10}/P_{20}>1$ for $\rho<1$, as found in the main figure of Figure 55. Also, as the number density increases towards the heavy crowding regime ($\rho\rightarrow 10$), we expect to attain the crowding limit $P_{10}(\rho)/P_{20}(\rho)=1$ as the traps become monomer-saturated, and as the coverage in the system becomes more uniform. Again, our data are consistent with this notion. It follows, therefore, that, in the intermediate regions $0<\rho<10$, the ratio $P_{10}(\rho)/P_{20}(\rho)$ must decrease towards unity. This we observe with the decrease being very rapid. In fact, we observe that P_{10}/P_{20} effectively undershoots the asymptotic limit $P_{10}/P_{20}=1$ for $\rho\gtrsim 2.5$ or for $N\gtrsim 23$. This indicates that preferential trapping for the M=10 chain has ceased and, instead, the M=20 chains then preferentially trap. This trapping inversion effect was an unexpected result. Clearly for $N\gtrsim 23$, the traps must fully saturate, even for the M=10 chains. Therefore, the addition of extra chains then populates the gel phase where there is translational entropy (unlike within the traps). Preferential trapping for M=20 chains would then allow more M=10 chains to populate the gel phase, on a ratio greater than one to one.

We would expect that M=10 chains are more likely to doubly-occupy traps on account of the inefficiency of single M=10 chains in filling the pore space. This is unlike the case for M=20 chains where monomer spill-out occurs, lowering the chances of voids doubly-trapping M=20 chains. Therefore, preferential trapping for one M=20 chain may effectively result in liberating one or more M=10 chains. This would constitute a loss in translational entropy for the M=20 chain, which would then also gain some conformational entropy. In the case of the one or two M=10 chains, there is a net gain in translational entropy at the loss of come conformational entropy.

In the inset of Figure 55, we see the change in the centre-of-mass trapping probability in the case where there are $N_{20}=N_{traps}$ of the M=20 chains. Upon introducing M=10 chains, the trapping probability of the M=10 chains is higher, as expected from the results found in Chapter 4. However, upon increasing the number of M=10 chain to the point where ρ increases to $\rho\approx 3$ (i.e., $N_{10}=18$), there is a crossing in the CM trapping probabilities, favouring M=20 trapping as the number density increases. As ρ increases towards 10, however, we again see that the two probabilities begin to converge, as expected for strong crowding.

In Figure 56, we have a very complicated graph of the diffusion coefficients D_M as a function of the effective number concentration ρ for M=10 and M=20 chains. The solid lines are the results for monodisperse M=20 and M=10 solutions reported in Chapter 4.

For all $\rho<1$, the diffusion coefficients for both species, D_M, do not show significant differences with varying ρ because the traps must first saturate before the dynamics can be greatly affected. Some variation is seen for $\rho<1$ but this is mostly due to noise in the data.

For $1\lesssim\rho<2.5$, the data are consistent with the notion of preferential trapping for the M=10 polymers. Therefore, $D_{10}(N_{20}=0)$ for the monodisperse solution represents the lowest diffusion coefficient for M=10 chains in the range whereas $D_{20}(N_{10}=0)$ for the monodisperse M=20 chain solution represents the highest diffusion coefficients for the M=20 chains in the range.

As we further increase $\rho>2.5$, the pores are fully saturated. The data are then consistent with preferential trapping for the M=20 chains, and the result for the monodisperse solution M=20 diffusion coefficient becomes the lowest value for the M=20 diffusion data whereas the monodisperse M=10 solution data then represents the maximum M=10 diffusion coefficient values. The solutions for M=20 having the least number of M=20 chains are then characterized by higher values for the bulk diffusion coefficient $D_{M=20}(\rho)$ whereas solutions for M=10 having the most number of M=20 chains are characterized by lower values for the bulk diffusion coefficient $D_{M=10}(\rho)$, due to preferential M=20 trapping.

In the strong crowding limit ($\rho\gg2.5$), the solution sets having the least number of M=20 chains are characterized by higher values for the bulk diffusion coefficient D(M=20) because the preferential trapping of M=20 chains dissipates and the diffusion coefficient for each species merely become a function of the available free space in the lattice.

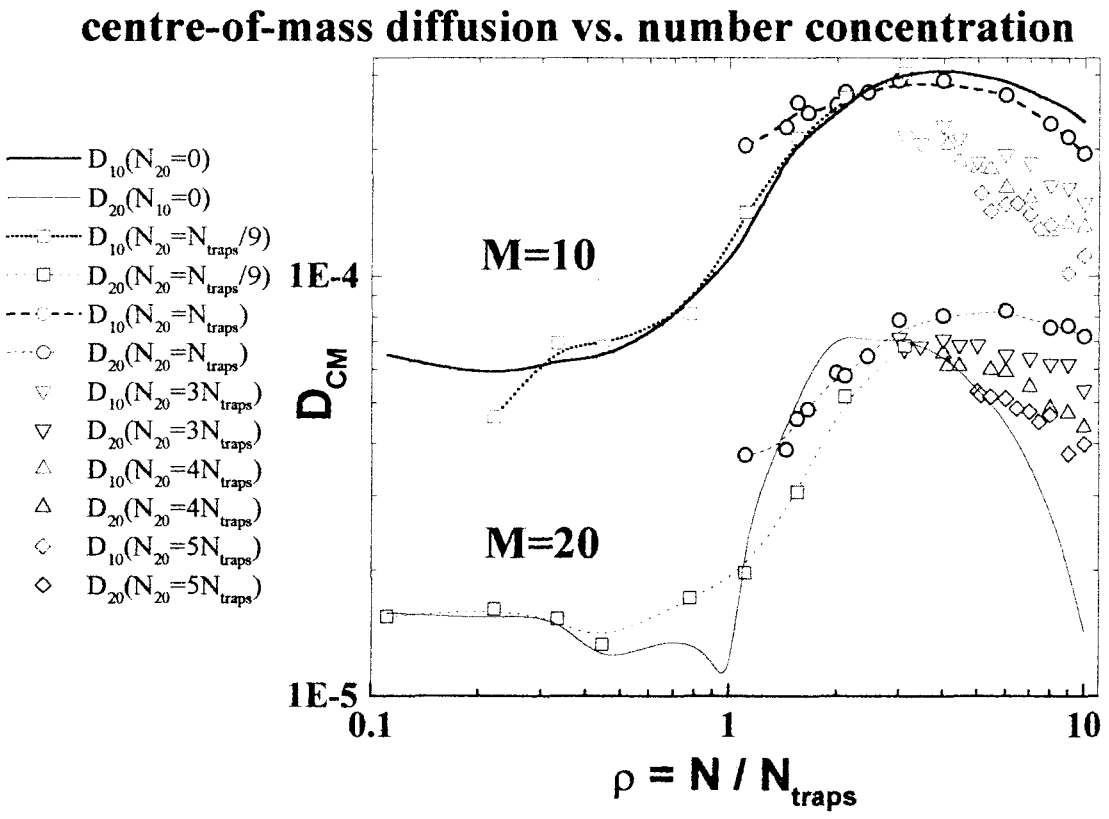

Figure 56. Plot of the diffusion coefficients D_{CM} as a function of the effective polymer concentration ρ for M=10 and M=20 chains. The solid line represents D_{CM} for monodisperse solutions.

5.3 Discussion

We have briefly investigated the thermodynamic equilibrium between polymer concentration, entropic trapping, and translational entropy of polydisperse polymer solutions in finite porous systems. This study complements that of Chapter 4 on monodisperse solutions, which served as our terms of reference and helped guide us in our qualitative description of polydisperse systems.

In the case of dense polymer solutions, the partitioning of real polymer solutions (which are typically polydisperse) in porous media is fairly complex. Yet, despite a host of recent studies dealing with the subject of entropic trapping systems (e.g., Liu, Li et al. 1999; Liu, Li et al. 1999; Chen and Escobedo 2001), none so far have ever clearly established qualitative agreement with the scaling laws predicted on the basis of entropic trapping. This is so despite the fact that the subject of entropic trapping (ET) is now almost 20 years old. And while the concept has indeed proven a useful one for explaining deviations from the often-expected results of the classical-reptation theory seen in Doi and Edwards (Doi and Edwards 1986) as well as for extending the reptation theory in order to include the effects of entropic traps (Cule and Hwa 1998), the state of the subject is still largely unsatisfactory. For instance, there have been no dynamical studies to date that have addressed issues such as the competition existing between the various forms of entropy in the system (conformational and translational in our case). Yet, such an understanding may in fact be vital for understanding the results of experimental data generated using polydisperse solutions in porous media.

We have observed some interesting dynamics that cause a reversal in preferential trapping of species as a function of number concentration ρ. We suggest that this dynamic may be related to a balance struck between translational and conformation entropy and that this may also be related to the double trapping of M=10 chains. However, further study would be required to qualify this statement and to properly characterize this interesting dynamic.

Our results do suggest that the molecular size scaling of the steady-state diffusion coefficient, D, is strongly dependent upon the polymer concentration of each of the differing molecular species. Concentration effects must be taken into account, and one must also understand the nature of this apparent competition between the conformational and translational entropies for dense polymer solutions. Such an understanding could help in the interpretation of experimental data, where the results often vary greatly. The results, in fact, may depend on the following system parameters: the number of pores, the average pore size, the molecular size of the probe polymers, the topology and

translational entropy, etc. As we have seen, these competing factors may lead to the masking of strong entropic trapping effects. Entropy effects (both conformational and translational) need to be analyzed with concentration effects in mind, especially when the polymer number concentration approaches that of the pore sites.

This raises further issues regarding the interpretation of experimental data. For instance, for a polydisperse polymer solution, an experimentalist would typically measure the average diffusion coefficient. But as this average is effectively the sum contribution from all the individual chains, varying both with the overall concentration and the exact composition (polydispersity index), the measured diffusion coefficient will vary with the total concentration as well as on the exact composition of constituents in solution because of preferential trapping effects (as shown). Moreover, these effects are certainly non-trivial, as seen in the simple bimodal example described herein.

Chapter 6
Conclusion

In the literature review, we chronicled some of the work in active areas pertinent to the field of polymer dynamics in disordered systems. This constitutes a broad class of problems that requires the efforts of many, using various approaches, before leading up to a cohesive understanding.

We have focused our attention on the study of linear self-avoiding-walk (SAW) polymeric chains diffusing in systems with fixed disorder on a lattice of obstacles using the Monte Carlo approach first proposed by Carmesin and Kremer (Carmesin 1988). We have also predicted the effective behaviours for several observables using scaling as well as analytical models (Chapter 2).

Our lattice system possesses an obstacle sub-lattice whereby we are able to control the porosity by randomly removing a pre-determined fraction (1-c) of the obstacles (deletion disorder). Thus, we induce varying degrees of disorder while probing the static and dynamic properties of our probe chains in Chapter 3. Regular checks were also made to ensure that the model conformed to established theories in the appropriate limits.

Curiously, in the way of static properties, we characterized the degree of polymer collapse in strong entropic trapping systems as being rather small for our SAW chains. We demonstrated that the molecular size exponent (Flory exponent) is not affected for isolated chains, despite the advent of strong disorder ET regimes. Next we characterized the shape of the distribution functions for several observables, including the mean square radius of gyration, the mean square end-to-end distance, and the conformational compactness. There, surprisingly, we find that disorder and entropic trapping have little overall effect on the distribution of conformational states. This contrasts greatly with the large effects often reported for the dynamical properties. Moreover, the literature is replete with claims that the static properties govern the bulk transport of polymeric chains in fixed disordered media (as in the case of oil recovery applications, separation applications, etc.). Interestingly, but to our surprise, we do not find any clear evidence which supports this assertion.

Next, we investigated the steady-state diffusion properties of our linear chains, characterizing the "effective" molecular weight scaling for which we actually predicted an exponential functional-dependence using our derived ET model (sect. 2.5). In the case of intermediate obstacle concentrations (i.e., neither Rouse nor reptation), the steady-state diffusion regimes were shown to be preceded by very long transient regimes for which the mean square displacement of the centre-of-

mass (CM) increases with time to a power less than unity (subdiffusion). Not unexpectedly, the longest such transients were seen to occur in regimes where entropic trapping was very strong.

We established the existence of stretched-exponential conformational relaxation for disordered systems and characterized the effective scaling of the relaxation times with molecular size, mode number, and obstacle concentration c. Moreover, we also characterized the degree of non-exponentiality (the stretching exponents) as a function of obstacle concentration for various molecular sizes. Having clearly established that the conformational relaxation processes were occurring on time scales that were often much shorter (by up to 2 orders of magnitude) than those for steady-state diffusion, we looked for a relationship between the long anomalous diffusion regimes and the overall conformational relaxation process. There, we found that both processes were characterized by time exponents to powers less than unity. Moreover, when one removes the time-dependence of the autocorrelation function and instead plots the relaxation as a function of diffused distance, one finds that there is a unique length scale for which this occurs. In this way, we introduced the conformation relaxation length scale. We then went on to characterize these length scales in terms of the effective dependence on obstacle concentration and the effective molecular–size scaling. While we perceive that such length scales may be distinct from those characterizing the various static properties (like the radius of gyration), our data exhibited effective molecular-size scaling that did not substantively differ from that of the radius of gyration with its Flory exponent. So the question as to the relevance of such length scales remains an open one, although one will soon be able to conclusively establish the relevance or irrelevance of these relaxation length scales as the level of common computational power continues to rise at a rapid rate. One would have to perform a systematic study covering a much broader range of molecular sizes, however.

Throughout the analysis, the strong ET regime consistently yielded key signatures for exponents, such as non-monotonic behaviours (for the effective molecular size scaling, the anomalous subdiffusion time exponent, and hence also for the conformation relaxation time exponent), which, when these are plotted against the concentration of obstacles, is characterized by a drastic increase or decrease when adding only slight disorder to an otherwise perfectly-periodic system. The only exceptions noted in this regard were in the case of static conformational properties and in the case of the conformational relaxation length scale. Moreover, the exponents always yielded dynamics that exhibited stronger effective molecular-size scaling than could be expected for either the classical Rouse or reptation models, despite the fact that the volume fraction of the solvent space is less in the

reptation limit. Not surprisingly, such observations have led some groups to explore the possibility of constructing separation devices that exploit such properties.

The last two chapters focused on the topic of the strong entropic trapping of polymeric chains in imprinted hydrogels with mesoscopic voids, a very recent topic in the literature that is touted to be the first direct experimental confirmation of the entropic trapping phenomenon (Liu 1999). We adapted our 2D model to create imprinted gels and to simulate many chains up to reasonably large numbers (with very-high local monomer concentrations). With this model, we were able to mimic some of the qualitative features of the 3D systems as well as delve deeper into the subject by also considering the diffusion dynamics over a broad polymer solution concentration range that spanned well beyond the pore saturation threshold. Nontrivial behaviours were described, including trapping-assisted translational diffusion whereby polymers are squeezed-out of the entropic traps in order to gain translational entropy.

In our last chapter, we further investigated concentration effects, but this time for a bimodal polymer solution (the simplest form of polydispersity). There, we reported even more complex but novel dynamics as a competition between conformational entropy, translational entropy, and excluded volume effects led to non-trivial dynamical regimes that we qualitatively examined and characterized. There have been no dynamical studies to date that have addressed issues such as the competition between conformational and translational entropy in polydisperse solutions as a function of concentration of the constituent species. Our data, however, support the speculation that this interplay may be crucial to our understanding of the behaviour of polydisperse solutions in fixed obstacle networks such as gels. As such, several of these competing factors may lead to the masking of strong entropic trapping effects.

Recently, Reguera and Rubi (Reguera and Rubi 2001) have made good progress in deriving fairly general kinetic equations to describe the evolution of systems whose particle dynamics is influenced by entropic barriers. The extension of such theoretical schemes to more complex molecules, such as polymers, as well as to cases where the geometry is more complex, will prove very challenging. In the meantime, Monte Carlo studies will continue to serve as a valuable tool for exploring and deriving scaling laws and qualitative behaviours of polymers, including in the case of novel, specially engineered, separation systems.

Appendix A – Useful information for experimentalists

This appendix was drafted at the request of some examiners of the dissertation. It was felt that the inclusion of an appendix to help bridge the gap between simulation and the experimental world would prove useful for consultation purposes. To this end, we will use double-stranded DNA (dsDNA) as a particular polymer chain of reference from which one we will extract the experimentally relevant length and time scales. It is to be understood that our simulation polymers are SAW chains diffusing in 2D configurational space. The Rouse dynamical theory was derived for unperturbed RW chains, in the absence of hydrodynamic interactions between monomers whereas the reptation theory was derived for the special case where the SEV effects of the SAW chains, as well as the hydrodynamic interactions between monomers, are screened, as one has in a melt. Consequently, the links drawn herein, between theory and experiment, are somewhat approximate at the quantitative level but should suffice as order-of-magnitude estimates for the derived quantities.

A.1 Typical length and time scales

The contour length of a linear chain may be written as $L_c=(M-1)b_0$ where $b_0\approx2.89$ is the average bond length for the four-site-model of the BFA (Carmesin, 1988). An effective bond length b may also be defined implicitly via the relation $h^2=(M-1)b^2$ which, in-turn, may be related to the persistence length, l_p, via the Kratky-Porod equation $h^2=2l_pL_c$ in the limit $M\to\infty$ for a worm-like chain (WLC) (Kratky 1949). Thus, $b=[h^2/[(M-1)]^{1/2}$ and for M=25 chains (see Table 1), we have $l_p=h^2/[2(M-1)b_0]\approx746/[2(24)(2.89)]\approx5$ lattice spacings, l, with l being the natural unit of length for our system.

As the persistence length for double-stranded DNA (dsDNA) in physiological salt (solution) is $l_p\approx53$ nm (Bustamante 2000) with each base-pair having a length $bp\approx0.338$ nm, we have

$$l \approx 30\,bp \approx 10\,nm \tag{57}$$

from which follows that the contour length for an M=25 chain is $L_c \approx (24)(2.89) \approx 70l \approx 14l_p \approx 2100\text{bp} \approx 700$ nm.

As per Table 1 (p. 47), the mean-square radius of gyration of a SAW (but unperturbed c=0) M=25 monomer bead chain is $R_g^2(M=25) \approx 100l^2$ and so $R_g(M=25) \approx 10l \approx 100\text{nm} = 0.1\mu\text{m}$. As $R_g \sim (M-1)^{\nu}$ with $\nu=3/4$ (for d=2), we can also write

$$R_g \approx 10(\text{M}-1)^{3/4}\ nm \tag{58}$$

In dilute solution, one has to take into account hydrodynamic interactions, as described by the Zimm model. Each monomer along the chain creates drag forces on the others such that a group of monomers moves more easily than monomers in isolation under the same total force. Considering a polymer coil as such a group of monomers, the coil (along with solvent molecules) moves as a non-draining coil whose friction coefficient may be approximated by that of a hard sphere with an effective hydrodynamic radius $R_h \approx 2R_g/3$. Using the well-known hydrodynamic friction constant, $\zeta = 6\pi\eta_s R$, for a sphere of radius R for a solution viscosity η_s [(Doi 1986), Eq. (3.6)] together with the Einstein relation $D = k_B T/\zeta$ [(Doi 1986), Eq. (3.10)], one yields

$$D \approx \frac{k_B T}{4\pi\,\eta_s R_g} \approx \frac{(29/21\times10^{-23})(17/58\times10^{3})}{4(22/7)(10^{-3})\times10^{-8}(M-1)^{3/4}} \approx \frac{32}{(M-1)^{3/4}}\left(\frac{\mu m^2}{s}\right) \tag{59}$$

where $k_B \approx 1.381\times10^{-23}$ J/K is Boltzmann's constant, T=293.15 K is the room (i.e., 20°C) temperature in absolute Kelvin units, M is the number of monomer beads (molecular size), and $\eta_s \approx 10^{-3}$ N/(m^2/s) is a typical solution viscosity.

Using Eqs. (58) and (59), the conformational relaxation time may be approximated using simple scaling (p. 30) viz.

$$\tau \approx \frac{R_g^2}{D} \approx \frac{10^{-4}(M-1)^{3/2}}{32(M-1)^{-3/4}} \approx 3(M-1)^{9/4}\ \mu\text{s} \tag{60}$$

As such, we have $\tau \approx 4$ ms for a free M=25 monomer (≈2100 bp dsDNA) chain. From Fig. (27) and Fig. (33), we remark that the conformational relaxation time for a free (c=0, no gel) M=25 chain is given approximately by $\tau \approx 15000$ Monte Carlo Steps (MCS). From this, it follows that

$$1\,MCS \approx \frac{1}{4}\,\mu s \tag{61}$$

This completes our rudimentary analysis, in the special case of dsDNA molecules, relating our 2D MC simulation length and time scales with those of the experimental world.

Appendix B – Simulation performance and statistical sampling

This section briefly describes the information most pertinent to generating simulation results for our model systems. In particular, we will characterize the performance of some of the computers used in the simulation and provide a brief discussion on the method of statistical sampling in our Monte Carlo systems.

B.1 Typical performance characteristics of some host machines

We will now perform a short analysis of typical performance characteristics for much of the work in the thesis. Table 2 shows simulation data taken from a simulation logbook.

Table 2. Sample simulation performance characteristics for three host machines simulating the disordered point-defect void systems of Chapter 3.

Host machine	Input file / Pid	*M*	*Simul Start*	*Simul End*	*Total Run time*	*CPU time*	Simul Time (MCS)	=(M-1) MCS	= r/s0 times	*Machine Speed (Mon. moves / CPUs)*
Feynman	N25c0.9.in 23120	25	1997 Mar 22 18:22:45	1997 Apr 16 14:12:20	24d19h49m35s =2,144,975s (48.4% duty)	17313m,18s =1,038,798s 12d33m18s	4.226×10^{10}	6.75×10^{5}	62600	1.02×10^{6}
	n60c100.in 25972	60	1997 May 20 10:29:28	1997 June 16 18:18:56	27d7h49m28s 2,360,968s (20.6% duty)	8,090m15s 485,415s 5d14h50m15s	7.71×10^{9}	1.20×10^{7}	700	9.53×10^{5}
kikilfus	n100c00A.in 18372	100		1997 Oct 26 17:28:01		3,889m55s 233,395s 2d16h49m55s	2.6×10^{9}	5.26×10^{5}	4900	1.11×10^{6}
Taxensus	n50c90Bf2.in 30770	50	1997 Oct 03 19:31:43	1997 Nov 12 11:50:03	41d,7h,41m,40s =3,570,100s (29.2% duty)	17,383min,5s =1,042,985s =12d1h43m5s	1.9×10^{10}	1.15×10^{7}	1700	9.19×10^{5}
	n120c100f2.in	120	1998 Jan 29 22:54:56	1998 Feb 20 19:13:57	21d21h40m59s =1,892,459s (36.4% duty)	11,496min,32s =689,792s =7d23h36m32s	1.58×10^{10}	1.20×10^{8}	132	1.00×10^{6}

In Table 2, we have listed various columns: The host machine, the input filename and process identification number (pid), the number of monomers in the chain, the simulation start and end times, the total run time, the computer time as measured by the central processing unit (CPU), the simulation time in Monte Carlo Steps (MCS), the conformational relaxation time of Eq. (26), the simulation time measured in units of the conformational relaxation time (#rlxn times), and finally, the effective machine simulation speed in monomer moves per CPU second.

For the host machines listed, the inferred machine speed was similar for the same level of optimization. In fact, the generalized equation for the effective intrinsic speed for these host machines can be seen to be

$$t(MCS) \approx \frac{10^6 (MCS/s)}{M} \times \mathrm{t_{CPU}(s)} \tag{62}$$

where t_{CPU} is the net computing time measured in CPU seconds and M is the number of monomers in the chain. Knowing that excellent single-chain statistics were achieved for ~2×10^{10} MCS, we derived a convenient rule-of-thumb for the required run time for a typical 25% CPU duty cycle:

$$\text{RULE - OF - THUMB :} \quad \text{simulation run time} \approx M \text{ days at 25\% CPU duty cycle} \tag{63}$$

For many-chain systems, to first-order, the required simulation run time is essentially independent of the number of chains simulated, so long as M is taken to be the number of monomers in the largest chain.

B.2 Monte Carlo sampling and statistical uncertainties

If s represents the uncertainty of a single observation (i.e., the sample standard deviation) for observable Q and if the mean $\langle Q \rangle$ is obtained from n independent observations, then the uncertainty of the mean s_m is smaller than s by a factor $1/n^{1/2}$, that is:

$$\mathrm{s_m} = \frac{s}{\sqrt{n}} = \sqrt{\frac{\sum_{i=1}^{n} \left(Q_i - \langle Q \rangle\right)^2}{n(n-1)}} \tag{64}$$

In the case of time-averaged Monte Carlo sampling, one often performs a series of n successive observations over a total observation time $t_{obs}=n\Delta t$ with Δt ($\ll\tau$) being the number of MCS between observations and with τ being the integrated relaxation time, as derived from integrating the auto-

correlation (or normalized relaxation) function, as done in Eq. (26). Then, when one considers the time-averaged physical quantity Q, the mean square statistical uncertainty in the averaged quantity may be expressed as [see, e.g., (Binder 1988), Eq. (2.2.12)]

$$s_m = \sqrt{1 + \frac{2\tau}{\Delta t}} \times \frac{s}{\sqrt{n}} = \frac{s}{\sqrt{n_{eff}}} \tag{65}$$

where the *effective ensemble size* is given by

$$\begin{aligned} n_{eff} &= \frac{n}{1 + 2\tau/\Delta t} = \frac{t_{obs}}{\Delta t + 2\tau} \\ &\approx t_{obs}/2\tau, \quad (\Delta t << \tau) \\ &\approx n, \quad (\Delta t >> \tau) \end{aligned} \tag{66}$$

We see that the effective ensemble size is decreased relative to the total number of sampled observations, n, so long as the time interval, Δt, between observations is not large compared with the relaxation time, τ, of the physical quantity being sampled. Interestingly, in the special case where Δt is very small relative to τ, the statistical uncertainty is then independent of the particular choice of time interval Δt (i.e., so long as $\Delta t \ll \tau$) and depends only on the averaging time.

We note, in particular, that the statistical uncertainties in the mean square end-to-end distance $\langle h^2 \rangle$ and the mean square radius of gyration $\langle R_g^2 \rangle$, as listed in Table 1, were derived through the use of Eq. (65) and Eq. (66), along with the conformational relaxation time of Eq. (26) for k=1.

Glossary of Principal Symbols, Conventions, and Acronyms

1. Mathematical Conventions

$\langle\ \rangle$	The statistical mechanical (time-weighted) average of the quantity enclosed, taken over all configurations of the chain and, as appropriate, over all chains
$\langle x_0 \rangle$	The corresponding average for observable x unperturbed by interactions or external constraints
{a,b, ...c}	Explicit enumeration of a set of values a, b, ...c
$\equiv$	Equal by definition
$\forall$	For all
$\in$ [a,b)	Is an element of the set [a,b) where a is included and b is excluded from the set.
$\exists$	There exists
$\sim$	Scales as
$\approx$	Approximately equal to
$\cong$	Dimensionally equal to
$\ll$	Much smaller than
$\gg$	Much greater than
$\rightarrow$	Tends towards
$\propto$	Proportional to

2. English and German Letter Symbols

$a=\sqrt{(93/\pi)}$	Effective pore radius of our mesoscopic voids
Å	Angström unit, 10^{-10} m
$b=h^2/(M-1)$	The effective segment length between monomer beads

$b_0 \approx 2.89$	The average bond length (in units of l) between monomer beads for large chains
b_k	Effective scaling exponent of the k-dependence of time τ_k
$1+b_M$	Effective scaling exponent of the M-dependence of τ_k
B_1	Model-dependent proportionality constant in expression for τ_k (reptation)
B_2	Model-dependent topological constant in reptation time expression for τ_k (reptation)
c	Obstacle volume fraction (number concentration) on the obstacle sublattice
(1-c)	Volume fraction of randomly-placed voids or randomly-removed obstacles
$C_h(t)$, $C_k(t)$	Auto-correlation function of the end-to-end vector $\vec{h} = \vec{r}_M - \vec{r}_1$ and Fourier coordinate $\vec{X}_k(t)$, respectively
d	Dimensionality of the space under consideration
d_T	Effective reptation tube diameter
D	Diffusion coefficient of the CM (at SS)
$D_{10}(N_{20})$	D for M=10 chains for a particular number N_{20}=N-N_{10} of M=20 chains
$D_{20}(N_{10})$	D for M=20 chains for a particular number N_{10}=N-N_{20} of M=10 chains
D^*	Anomalous diffusion coefficient of the CM
D_T	1D Diffusion coefficient of the chain inside a curvilinear reptation tube
f(x)	Function of variable x (used when speaking of the SED)
$f_p(h/h_0)$	Reduced probability distribution function of the end-to-end distance amplitude h
$g=(\gamma-1)/\nu$	Critical exponent describing the general static features of isolated SAW chains on a lattice
$g_1(t)$	Mean-square displacement of the CB position after t MCS
$g_3(t)$	Mean-square displacement of the CM position after t MCS
$\vec{h} = \vec{r}_M - \vec{r}_1$	End-to-end vector
H	End-to-end distance scaled according to the root mean square end-to-end distance

k	Mode number of Fourier Coordinate $\vec{X}_k(t)$ and of conformational relaxation time τ_k
K	Partition coefficient or ratio of the number of chains in gel phase to that in the traps
k_B	Boltzmann's constant
l	Lattice spacing, the natural length scale of the system, incremental step distance for all successful monomer moves
L_c	Contour length of a linear chain
l_p	Persistence length, equivalent to one half the Kuhn statistical segment length b
L	Curvilinear length of the primitive chain (reptation tube length)
M	Molecular size in monomer "beads"
$M^{m_\eta} \approx M^{3.4}$	Experimentally-determined (effective) M-scaling for τ_D and η in the case of melts
M_p	Number of chain segments forming the 'blobs' inside the effective reptation tube (c.f., entanglements in the case of melts)
n	Ensemble size of a sampled observable
n_{eff}	Effective ensemble size of a sampled observable, relaxation processes taken into account
N	Total number of chains in the system (on the lattice)
N_{MAX}	Number of chains for which D is a maximum
N_{sat}	Number of chains for which the pores in the system are saturated with monomers
N_{traps}	The number of mesoscopic voids (entropic traps) in the system
p	Distance between obstacle sites (=4 lattice units)
P	Periodicity or number of lattice spacings between mesoscopic pores
p(H,c)	Probability distribution function of the reduced end-to-end distance H at obstacle lattice number concentration c
P(r)	Cumulative occupational probability density function for radial distance r

from the pore centre (on a unit cell centred on pore)

$P_{pore}=P(r=a)$ Pore-site occupation probability of the chain CM

$P_{10}=P_{pore}(M=10)$ Pore-site occupation probability of the chain CM for M=10 chains

$P_{20}=P_{pore}(M=20)$ Pore-site occupation probability of the chain CM for M=20 chains

$p(x)$ Probability of event x

$p(\tau_K)$ Probability density function for hopping time τ_K

$P(x,y)$ Probability of occupation of site (x,y) on the square lattice

r Radial distance from the centre of a mesoscopic void

r_{pore} Effective pore radius

$\vec{R}_{CM}$ Vector position of the CM

R_g Radius of gyration

R_h Hydrodynamic radius

R_{SS} Steady-State (SS) distance for the onset of normal (SS) CM diffusion

$\vec{r}_1$, $\vec{r}_{CB}$, and $\vec{r}_M$ Vector positions of the first (1), central (CB), and last (M) monomer beads, respectively

s Uncertainty (standard deviation) of the distribution of a sampled observable

s_m Uncertainty in the mean of a distribution of a sampled observable

$S^2=h^2/R_g^2$ Span of the conformation or conformational compactness

t MC time, as measured in MCS

t_{sim} The total simulation time, as measured in MCS

T	Absolute temperature (in Kelvins)
U'(x,y)	Effective potential energy of site position (x,y)
U	Dimensionless effective potential energy (Kelvin units)
w	Effective scaling exponent of the t-dependence of $g_1(t)\sim t^w$
$\vec{X}_k(t)$	Fourier coordinate for mode k at t MCS
z_{eff}	Effective coordination number (connectivity constant) of the lattice space
1D, 2D, 3D	One-, Two-, Three-dimension(s)(al), as appropriate

3. Greek Letter Symbols

α	KWW stretched-exponential exponent
α_h, α_k	KWW exponent for the decay of the auto-correlation functions for the end-to-end distance h and for the Fourier coordinate $\vec{X}_k(t)$, respectively
β	Effective CM anomalous diffusion temporal/time exponent of $g_3(t)$
$\chi\geq 0$	Entropic strength (or ET attrition) parameter for the system
δ	Molecular-size exponent for the (effective) M-scaling of D
Δ_α	Relative width of the SED, for fixed parameter value α, to its mean
Δt	Time interval between sampled observations of an observable
ϕ	Volume fraction
γ	Critical exponent such that γ-1=power law governing the scaling of Ω with M
η	Viscosity
$\kappa=(1-\nu)^{-1}$	Universal critical exponent responsible for most of the chain properties for large extensions
λ	Conformational relaxation length scale.

μ Effective molecular-size scaling exponent of the mean square conformational relaxation length scale λ.

μ_n Moment n of the distribution under consideration

Ω Total number of available polymer chain conformations

ν Universal critical molecular-size exponent (excluded volume interaction parameter) of the polymer mean square sizes of R_g and h

$\nu_F=3/(2+d)$ Flory's exponent, as generalized by Fisher into a hyperscaling relation

$\rho=N/N_{traps}$ Number density where N represents the number of chains and N_{traps} the number of entropic traps

$\rho_{sat}=N_{sat}/N_{traps}$ Number density ρ for which N_{traps} mesoscopic voids (ETs) are monomer saturated

$\sigma(r_i)$ Discrete radial site occupational probability density function for radial distance r_i from the pore centre (on a unit cell centred on pore)

$\sigma_\tau=\tau_{SS}$ Standard deviation of the Poisson distribution of hopping times between traps, as measured in MCS

$\sigma_x(\alpha)$ Standard deviation of SED function of x for fixed parameter value α

τ Simulation time, as measured in MCS

τ_h Conformational relaxation time of h, as measured in MCS

$\tau_h^* \approx \tau_h \times \Gamma(1/\alpha_h)/\alpha_h$ Time-integrated version of the conformational relaxation time of h, as measured in MCS

τ_k Conformational relaxation time of the Fourier mode k ($\tau_{k=1}=\tau_R$, the Rouse time), as measured in MCS

$\tau_k^* \approx \tau_k \times \Gamma(1/\alpha_k)/\alpha_k$ Time-integrated version of the conformational relaxation time of the Fourier coordinate $\vec{X}_k(t)$ ($\tau_{k=1}=\tau_R$, the Rouse time), as measured in MCS

$\tau_D=\tau_{k=1}(c=1)$ Tube disengagement time, or reptation time, as measured in MCS

$\tau_R(M_p)$	Relaxation time of a "reptation blob" comprised of M_p monomer blobs, as measured in MCS
$\tau_R=\tau_{k=1}(c=0)$	Rouse time, as measured in MCS
τ_{relax}	Effective relaxation time between de-trapping attempts within an entropic trap, as measured in MCS
τ_{SS}	Steady-State (SS) time for the onset of normal (SS) CM diffusion, as measured in MCS
ξ	Correlation length

4. List of Acronyms

BFA	Bond Fluctuation Algorithm of Carmesin and Kremer
CB	Centre Bead
CC	Chain Connectivity
CM	Centre of Mass
DNA	deoxyribonucleic acid
DSAW	Directed Self-Avoiding-Walk
dsDNA	double-stranded DNA
ET	Entropic Trapping or Entropic Trap, as appropriate
EV	Excluded Volume
KWW	Kaulrauch-Williams-Watts
MC	Monte Carlo
MCS	Monte Carlo time Steps (natural simulation time unit)
MFT	Mean Field Theory
PDF	Probability Density Function
RW	Random Walk
SAW	Self-Avoiding-Walk
SD	Sub-Diffusion
SED	(Un-normalized) simple Stretched-Exponential Distribution (function)
SEV	Self-Excluded-Volume
SS	Steady-State
VS	Verdier-Stockmayer
WLC	Worm-Like Chain

References

Bakajin, O. B., T. A. Duke, et al. (1998). "Electrohydrodynamic Stretching of DNA in Confined Environments." Phys. Rev. Lett. **80**(12): 2737-2740.

Baumgärtner, A. (1998). "Polymer localization in attractive random media." J. Chem. Phys. **109**(22): 10011-10014.

Baumgärtner, A. and B. K. Chakrabarti (1990). "Polymer chain in annealed random media." J. Phys. France **51**(16): 1679-1682.

Baumgärtner, A. and M. Moon (1989). "Anomalous Polymer Diffusion between Long Rods." Europhys. Lett. **9**(3): 203-208.

Baumgärtner, A. and M. Muthukumar (1987). "A trapped polymer chain in random porous media." J. Chem. Phys. **87**(5): 3082.

Baumgärtner, A. and M. Muthukumar (1996). Polymers in Disordered Media. New York, John Wiley & Sons.

Briber, R. M., X. Liu, et al. (1995). "The Collapse of Free Polymer Chains in a Network." Science **268**: 395-397.

Bustamante, C., S. B. Smith, et al. (2000). "Single-molecule studies of DNA mechanics." Current Opinion in Structural Biology **10**: 279-285.

Carmesin, I. and K. Kremer (1988). "The Bond Fluctuation Method: A New Effective Algorithm for the Dynamics of Polymers in All Spatial Dimensions." Macromolecules **21**: 2819-2823.

Casassa, E. (1967). Polym. Lett. **5**: 773.

Chen, Z. and F. A. Escobedo (2001). "Conformational Properties and Entropic Partitioning of Topologically Complex Polymers under Confinement." Macromolecules **34**: 8802-8810.

Crabb, C. C., D. F. Hoffman Jr., et al. (1988). "Effect of Lattice Coordination Number on the Dynamics of Models of Dense Polymer Systems." Macromolecules **21**(7): 2230-2235.

Cule, D. and T. Hwa (1998). "Polymer Reptation in Disordered Media." Phys. Rev.Lett. **80**(14): 3145-3148.

de Gennes, P. G. (1978). Solid State Phys. Suppl. **14**: 1.

de Gennes, P. G. (1979). Scaling Concepts in Polymer Physics. Ithaca, Cornell University Press.

de Gennes, P. G. (1990). Introduction to Polymer Dynamics. Cambridge, Cambridge University Press.

des Cloizeaux, J. (1976). J. Physique **37**: 431.

des Cloizeaux, J. and G. Jannink (1990). Polymer Solutions, their modelling and Structure, Clarendon Press.

Doi, M. and S. K. Edwards (1986). The Theory of Polymer Dynamics. Oxford, Oxford University Press.

Downey, J. P. (1994). "Static and Dynamic Scaling Properties of Single, Self-Avoiding Polymer Chains in Two Dimensions via the Bond Fluctuation Method of Monte Carlo Simulation." Macromolecules **27**: 2929-2932.

Downey, J. P., C. C. Crabb, et al. (1986). "Dynamics of a Face-Centered Cubic Lattice Model for Polymer Chains." Macromolecules **19**(8): 2202-2206.

Fisher, M. E. (1969). J. Phys. Soc. Japan **26** (Suppl.): 44.

Flory, P. J. (1953). Principles of Polymer Chemistry. Ithaca, Cornell University Press.

Flory, P. J. (1969). Statistical Mechanics of Chain Molecules. New York, Interscience.

Hilhorst, H. J. and J. M. Deutch (1975). "Analysis of Monte Carlo results on the kinetics of lattice polymer chains with excluded volume." J. Chem. Phys. **63**(12): 5153-5161.

Kramers, H. A. (1940). Physica (Utrecht) **7**: 284.

Kranbuehl, D. E., D. Eichinger, et al. (1991). "Simulation Studies of Excluded Volume Effects on Polymer Chain Dynamics in Several Nonlattice Models." Macromolecules **24**(9): 2419-2427.

Kranbuehl, D. E. and P. H. Verdier (1996). "Separating connectivity and expansion effects in polymer single chain dynamics." J. Chem. Phys. **106**(11): 4788-4796.

Kratky, O. and G. Porod (1949), Rec. Trav. Chim. Pays-Bas Belg., **68**: 1106.

Kremer, K., A. Baumgartner, et al. (1981). "Collapse transition and crossover scaling for self-avoiding walks on the diamond lattice." J. Phys. A: Math. Gen. **15**: 2879-2897.

Lee, J. Y. and R. F. Loring (2001). "Driven Diffusion of Confined Polymers." Macromolecules **34**(16): 5727-5729.

Liu, L., P. Li, et al. (1999). "Crystalline Colloidal Array of Water Voids in Hydrogels: Direct Evidence for Entropic Trappig of Flexible Polymers." J. Am. Chem. Soc. **121**(16): 4040-4046.

Liu, L., P. Li, et al. (1999). "Entropic trapping of mesoscopic periodic voids in a polymer hydrogel." Nature (London) **397**: 141-146.

Machta, J. (1989). "Static and Dynamic properties of polymers in random media." Phys. Rev. A **40**(3): 1720-1722.

Maier, B. and J. O. Rädler (1999). "Conformation and Self-Diffusion of Single DNA Molecules Confined to Two Dimensions." Phys. Rev. Lett. **82**(9): 1911-1914.

Maier, B. and J. O. Rädler (2000). "DNA on Fluid Membranes: A Model Polymer in Two Dimensions." Macromolecules **33**(19): 7185-7194.

Maier, B. and J. O. Rädler (2001). "Shape of Self-Avoiding Walks in Two Dimensions." Macromolecules **34**(16): 5723-5724.

Muthukumar, M. and A. Baumgärtner (1989). "Diffusion of a Polymer Chain in Random Media." Macromolecules **22**: 1941-1946.

Muthukumar, M. and A. Baumgärtner (1989). "Effects of Entropic Barriers on Polymer Dynamics." Macromolecules **22**: 1937-1941.

Naghizadeh, J. and J. Kovac (1985). "Cubic lattice model simulation of an entangled polymer system." J. Chem. Phys. **84**(6): 3559-3566.

Nienhuis, B. (1984) J. Stat. Phys. **34**, 731.

Nixon, G. I. (1994). A Brownian Dynamics Algorithm for the Simulation of Polymers in Confined Media. Department of Physics. Ottawa, University of Ottawa**:** 146.

Nixon, G. I. and G. W. Slater (1996). "Entropic trapping and electrophoretic drift of a polyelectrolyte down a channel with a periodically oscillating width." Phys. Rev. E **53**(5): 4969-4980.

Nixon, G. I. and G. W. Slater (1999). "Relaxation length of a polymer chain in a quenched disordered medium." Phys. Rev. E **60**(3): 3170-3173.

Nixon, G. I. and G. W. Slater (2002). "Saturation and entropic trapping of monodisperse polymers in porous media." J. Chem. Phys. **117**(8): 4042-4046.

Okun, K., M. Wolfgardt, et al. (1997). "Dynamics of Polymer Melts above the Glass Transition: Monte Carlo Studies of the Bond Fluctuation Model." Macromolecules **30**: 3075-3085.

Pereira, G. G. (1996). "Mean Field theory for long chain molecules." J. Chem. Phys. **104**(22): 9142-9153.

Reguera, D. and J. M. Rubi (2001). "Kinetic equations for diffusion in the presence of entropic barriers." Phys. Rev. E **64**: 061106-1 to 061106-8.

Romiszowski, P. and W. H. Stockmayer (1984). "Effect of variable excluded volume on dynamics of lattice chains." J. Chem. Phys. **80**(1): 485-490.

Rotstein, N. A. and T. P. Lodge (1992). "Tracer Diffusion of Linear olystyrenes in Poly(vinyl methyl ether) Gels." Macromolecules **25**(4): 1316-1325.

Simon, A. and A. Libchaber (1992). "Escape and Synchronization of a Brownian Particle." Phys. Rev. Lett. **68**(23): 3375-3378.

Slater, G. W., H. L. Guo, et al. (1997). "Bidirectional Transport of Polyelectrolytes Using Self-Modulating Entropic Trapping." Phys. Rev. Lett. **78**(6): 1170-1173.

Slater, G. W. and G. I. Nixon (1997). "Polymer Dynamics in Random Media." Phys. Canada **53**: 177-183.

Slater, G. W. and G. I. Nixon (1997). "The size of a polymer chain in an imperfect array of obstacles: Monte Carlo results." J. Chem. Phys. **108**(8): 3310-3312.

Slater, G. W. and S. Y. Wu (1995). "Reptation, Entropic Trapping, Percolation, and Rouse Dynamics of Polymers in "Random" Environments." Phys. Rev. Lett. **75**(1): 164-167.

Smith, D. E., T. T. Perkins, et al. (1995). "Self-DIffusion of an Entangled DNA Molecule by Reptation." Phy. Rev. Lett. **75**(22): 4146-4149.

Sokal, A. D. (1995). Monte Carlo and Molecular Dynamics Simulations in Polymer Science. New York, Oxford University Press.

Sommer, J.-U. and A. Blumen (1996). "Polymers in periodic and aperiodic potentials: localization effects." J. Chem. Phys. **105**(14): 6008-6017.

Sornette, D. (2000). Critical Phenomena in Natural Sciences: Chaos, Fractals, Selforganization and Disorder: Concepts and Tools. Berlin, Springer.

Stauffer, D. and A. Aharony (1992). Introduction to Percolation Theory, Taylor & Francis.

Van Oudenaarden, A. and S. Boxer (1999). "Brownian Ratchets: Molecular Separations in Lipid Bilayers Supported on Patterned Arrays." Science **285**(5430): 1046.

Verdier, P. H. (1966). J. Chem. Phys. **45**: 2118.

Verdier, P. H. and D. E. Kranbuehl (1987). "Simulation of Polymer Chain Dynamics by Lattice Models with Excluded Volume: Lattice Dependence." Macromolecules **20**(6): 1362-1368.

Verdier, P. H. and W. H. Stockmayer (1962). J. Chem. Phys. **36**: 227.

Zimm, B. H. and O. Lumpkin (1993). "Reptation of a Polymer Chain in an Irregular Matrix: Diffusion and Electrophoresis." Macromolecules **26**: 226-234.